République Algérienne démocratique et populaire

Ministère de l'Enseignement Supérieur et de la Recherche Scientifique

Université de Hamma Lakhdar –El Oued

Faculté de Technologie

Département de génie électrique

Mémoire présenté par:

HAMIDANI Bilal

En vue de l'obtention du diplôme de doctorat en LMD

Filière: **Electrotechnique**

Option: **Optimisation et gestion d'énergie**

Techniques avancées de commande, d'observation et de diagnostic robustes dédiées à la machine synchrone basée sur le modèle Takagi-Sugeno

Soutenu le : 18/09/2019

Devant le jury composé de:

Nom et Prénom	*Grade*	*Affiliation*	*Position*
BEN ATTOUS Djilani	***Professeur***	***Université d'El Oued***	***Président***
ALLAG Abdelkrim	***Professeur***	***Université d'El Oued***	***Encadreur***
BETKA Achour	***Professeur***	***Université de Biskra***	***Examinateur***
ALLOUI Lotfi	***Professeur***	***Université de Biskra***	***Examinateur***
KHENE Mohamed Lotfi	***Professeur***	***Université de Biskra***	***Examinateur***
CHEMSA Ali	***MCA***	***Université d'El Oued***	***Examinateur***

2018/2019

People's Democratic Republic of Algeria

Ministry of Higher Education and Scientific Research

University of Hamma Lakhdar –El Oued

Faculty of Sciences and Technology

Department of Electrical Engineering

Thesis presented by:

HAMIDANI Bilal

For the purpose of obtaining a doctorate degree in LMD

Sector: **Electrical Engineering**

Option: **Optimization and energy management**

Robust advanced control, observation and diagnostic techniques for the synchronous machine based on the Takagi-Sugeno model

Defensed the : 18/09/2019

In front of the Jury composed of:

Full name	*Grade*	*Affiliation*	*Position*
BEN ATTOUS Djilani	***Professor***	***El Oued University***	***President***
ALLAG Abdelkrim	***Professor***	***El Oued University***	***Supervisor***
BETKA Achour	***Professor***	***Biskra University***	***Examiner***
ALLOUI Lotfi	***Professor***	***Biskra University***	***Examiner***
KHENE Mohamed Lotfi	***Professor***	***Biskra University***	***Examiner***
CHEMSA Ali	***MCA***	***El Oued University***	***Examiner***

2018/2019

Abstract

The objective of the work presented in this thesis is to propose a methodology for the control and observation of the permanent magnet synchronous machine (PMSM). These algorithms are based on the mean value theorem (MVT) and the sector non-linearity transformations approach, with employing a linear parameter varying (LPV) systems, linear matrix inequalities (LMIs) and Lyapunov theory. Firstly, generalization on the Takagi-Seguno (T-S) model and the fuzzy control based on a parallel distributed control (PDC) approach are presented.

Using the MVT and the sector non-linearity approaches and the previously mathematics theories, we developed deferent technics for designing the controller and the observer for PMSM application like: MVT controller, MVT observer, PI-MVT controller, MVT_H_∞ controller and observer, extended MVT observer and observer based-controller (sensorless control) …, all these algorithms have been validated through the numerical simulation in MATLAB/SIMULINK for confirming the effectiveness of developed algorithms, and some of its affirmed by experimental tests.

Finally, application of extended MVT observer for the detection and diagnosis of inter turns short-circuit fault in PMSM has been presented, this using for an estimate all the parameters of the faulty model of PMSM as an indicator of fault. This algorithm also validated through the numerical simulation in MATLAB/SIMULINK to confirming the effectiveness of algorithms.

Keywords:

Permanent Magnet Synchronous Machine, Mean Value Theorem, Sector Non-Linearity Approach, Parallel Distributed Control, MVT Observer, MVT Controller, Takagi-Sugeno Model, Fault Detection And Diagnosis, Linear Parameter Varying systems, Linear Matrix Inequalities, Lyapunov Theory.

ملخص

الهدف من العمل المقدم في هذه الرسالة هو اقتراح منهجية لتحكم ومراقبة المحرك المتزامن ذو المغناطيس الدائم (PMSM). وتستند هذه الخوارزميات إلى نظرية القيمة المتوسطة (MVT) ونهج تحويلات لاخطية في القطاع ، مع استخدام أنظمة خطية ذات معلمات متغيرة (LPV), المتراجحات الخطية المصفوفية (LMIs) ونظرية Lyapunov. أولاً ، تم تقديم عموميات على نموذج Takagi-Seguno (T-S) والتحكم الغامض القائم على نهج التحكم الموزع المتوازي (PDC).

باستخدام MVT ونهج تحويلات لاخطية في القطاع والنظريات الرياضيات السابقة ، قمنا بتطوير مختلف التقنيات لتصميم متحكم ومراقب لتطبيق PMSM مثل: متحكم MVT، مراقب MVT، متحكم PI-MVT، متحكم و مراقب MVT_H_∞، مراقب MVT ممتد و متحكم معتمد على المراقب (تحكم بدون استشعار) ... ، تم التحقق من صحة كل هذه الخوارزميات من خلال المحاكاة العددية في MATLAB/SIMULINK لتأكيد فعالية الخوارزميات المتقدمة ، وبعضها مؤكد من خلال الاختبارات التجريبية.

خيرًا ، تم تقديم تطبيق مراقب MVT ممتد لإكتشاف وتشخيص خطئ دارة قصيرة بين اللفات في PMSM ، وهذا يستخدم لتقدير جميع معلمات النموذج الخاطئ من PMSM كمؤشر للخطأ. تم التحقق من هذه الخوارزمية أيضًا من خلال المحاكاة العددية في MATLAB / SIMULINK لتأكيد فعالية الخوارزميات.

الكلمات المفتاحية:

المحرك المتزامن ذو المغناطيس الدائم، نظرية القيمة المتوسطة، نهج تحويلات لاخطية في القطاع، التحكم الموزع المتوازي، مراقب MVT، متحكم MVT، نموذج Takagi-Sugeno، اكتشاف و تشخيص الأعطال، أنظمة خطية ذات معلمات متغيرة، المتراجحات الخطية المصفوفية، نظرية Lyapunov.

Résumé

L'objectif du travail présenté dans cette thèse est de proposer une méthodologie pour le contrôle et l'observation de la machine synchrone à aimant permanent (PMSM). Ces algorithmes sont basés sur le théorème de la valeur moyenne (MVT) et sur l'approche des transformations de secteur non-linéarité, en utilisant les systèmes linéaire à paramètre variation (LPV), les inégalités matricielles linéaires (LMI) et la théorie de Lyapunov. Premièrement, on présente la généralisation sur le modèle Takagi-Seguno (T-S) et le contrôle flou basé sur l'approche de contrôle distribué parallèle (PDC).

En utilisant les approches, MVT et secteur non-linéarité et les théories mathématiques antérieures, nous avons développé des techniques déférentes pour la conception du contrôleur et de l'observateur d'applications PMSM telles que : contrôleur MVT, observateur MVT, contrôleur PI-MVT, contrôleur et observateur MVT_H_∞, observateur MVT étendu et contrôleur basé sur l'observateur (contrôle sans capteur)…, tous ces algorithmes ont été validés par la simulation numérique dans MATLAB / SIMULINK afin de confirmer l'efficacité des algorithmes développés, dont certains ont été confirmés par des tests expérimentaux.

Enfin, l'application de l'observateur MVT étendu pour la détection et le diagnostic des défauts de court-circuit entre spires dans le PMSM a été présentée, ce qui permet d'estimer tous les paramètres du modèle défaillant de PMSM en tant qu'indicateur de défaut. Cet algorithme a également été validé par la simulation numérique dans MATLAB / SIMULINK pour confirmer l'efficacité des algorithmes.

Mots clés:

Machine synchrone à aimants permanents, théorème de valeur moyenne, approche de secteur non linéaire, contrôle distribué parallèle, observateur MVT, contrôleur MVT, modèle de Takagi-Sugeno, détection et diagnostic des défauts, system linéaire à paramètre variable, inégalités matricielles linéaires, théorie de Lyapunov.

Acknowledgment

I first want to prostrate thanking **ALLAH** Almighty for giving me the courage and the patience to complete this work in good conditions.

This thesis is the result of several years of hard and team work. Therefore there is a large number of people to whom I owe my utmost thanks and gratitude.

I would like to express my sincere gratitude to my supervisor Prof. **Dr. Allag Abdelkrim** for his encouragement and guidance throughout the study. I also thank him not only for his technical assists but for his friendship in due course of development of the thesis.

Also, I would like to thank the PhD student **Mr. Zeghib Okba** for their help and continuous sensory and moral support during my work.

Also, I would like to thanks Prof. **Dr. Betka Achour,** Prof. **Dr. ZOUZOU Salah Eddine** and the PhD student **Mr. Sellali Mehdi** for their help during the experimental tests in the **LGEB** Laboratory University of Biskra.

Finally, my special thanks go to **Dr. Nik Rumzi bin Nik Idris**, **Prof. Dr. Zainal bin Salem**, and **Mr. Kermadi Mostafa** for their help during the experimental stage of this work.

A big thank goes to the Department of Electrical Engineering and the College of Engineering at the University of **Hamma Lakhdar** in El Oued for offering me the opportunity to pursue this Doctoral study.

Dedication

To my dear parents,

To my brothers and sisters,

In memory of my grandparents,

To my uncles, aunts, and cousins,

And to all who count for me.

Table of contents

CHAPTER I

General Introduction

CHAPTER II

Controllers and Observers Design Based on MVT and T-S Fuzzy Models

CHAPTER III

Permanent Magnet Synchronous Machines

CHAPTER IV

Advanced Control and Observation Techniques Based on the MVT Applied to the PMSM Drives

CHAPTER V

Robust Extended H_∞ Observer and Controller Based on the MVT Approach Applied to the PMSM Drive

CHAPTER VI

Fault Detection and Diagnosis Based on Extended MVT Observer Applied to the PMSM

CHAPTER VII

General Conclusion

Appendixes

List of Figures

CHAPTER II

Controllers and Observers Design Based on MVT and T-S Fuzzy Models

CHAPTER III

Permanent Magnet Synchronous Machines

CHAPTER IV

Advanced Control and Observation Techniques Based on the MVT Applied to the PMSM Drives

CHAPTER V

Robust Extended H_∞ Observer and Controller Based on the MVT Approach Applied to the PMSM Drive

CHAPTER VI

Fault Detection and Diagnosis Based on Extended MVT Observer Applied to the PMSM

Appendixes

Nomenclatures and Abbreviations

1. Nomenclatures

$x(t)$	State vector
$\hat{x}(t)$	Estimated state vector
$e_o(t)$	Estimation error
$e(t)$	Control error
$u(t)$	Input vector
$y(t)$	Output vector
w_r	Rotor speed
θ	Rotor position
Φ_f	Permeant magnets flux
I_d, I_q	The (d,q) stator currents
u_d, u_q	The (d,q) stator voltages
L_d, L_q	The (d,q) stator inductances
R_s	Stator resistance
J	Moment of inertia
f	Friction coefficient
p	Pole pair number
T_e	Electromagnetic torque
T_L	Load torque
T_e	Electromagnetic torque
L_0	Observer gain
K_0	Controller gain
L_∞	Robust Observer gain

K_∞	Robust controller gain
$\overline{K}$	Augmented controller gain
K_i	Fuzzy controller gain
L_i	Fuzzy observer gain
E	Force electro mortice (fem)
K_e	Constant of fem
$\theta_{s/c}$	Angle of localization of the fault
$n_{s/c}$	Percentage of turns in short circuit
θ_e	Electrical position angle
$R_{S\_healthy}$	Healthy resistance
R_{s_faulty}	Faulty resistance
$L_{p\_healthy}$	Healthy inductance
L_{p_faulty}	Faulty inductance
$T_{s/c}$	Short-circuit matrix
$I_{s/c}$	Short-circuit current
$V_{s/c}$	Short-circuit voltage
$Z_{s/c}$	Short-circuit impedance
$h_i\big(z(t)\big)$	the weight of the i_{th} rule
V	Lyapunov function
P_{in}	Input power
P_{out}	Output power

2. Abbreviations

MVT	Mean Value Theorem
PMSM	Permanent Magnet Synchronous Machine
LPV	Linear Parameter Varying
LMIs	Linear Matrix Inequalities
FOC	Field Oriented Control
SDRE	State Dependent Ricatti Equation
PWM	Pulse Width Modulation
SMPM	Surface Mounted Permanent Magnet
IPM	Interior Permanent Magnet
P	Proportional
PI	Proportional Integral
T-S	Takagi-Sugeno
PDC	Parallel distributed compensator
LTI	Linear time invariant
DTC	Direct torque control
FDD	Fault detection and diagnosis
IM	Induction machine
OL-FOC	Open Loop Field Oriented Control
CFS	Continuous Fuzzy System

CHAPTER I

1.1. General Introduction

Nowadays, electric motors are widely used. According to [1], more than 60% of the electricity is used to run electric machines. The Permanent Magnet Synchronous Motor (PMSM) is an important type of electric motor which is increasingly used in recent years. The main features of a PMSM motor are its high power and torque density, low energy consumption (high power factor) and good dynamic behaviour. Thus, PMSM is replacing asynchronous motors in many types of applications. Besides, the fast development of power electronics components and the fast increasing of signal processing speed are also behind the increased use of these motors.

PMSMs are used in multiple applications as electric vehicles and washing machines (which need high power density). They are also used for high precision devices like the electric printer, manufacture tools, high precision medical equipment (medical pumps, blowers and compressors) and many other domains [2-4].

In general, an electric drive is used to control electric motors and in particular PMSMs. It is a power electronic device which generates a variable frequency and variable amplitude voltage using a voltage source with fixed frequency and amplitude. There are many advantages of using an electric drive rather than plugging the motor directly into a fixed frequency and amplitude voltage source. Indeed, an electric drive is used to vary the motor speed and to save the electric energy where 50% of the energy consumed by the motor can be reduced.

Sensorless field oriented control becomes a major issue in the PMSM control. This research field has been highlighted extensively in the previous few decades due to increasing demand in the industry for high-performance sensorless control, in order to overcome the drawbacks of sensor implementation within the machine [5]. Unfortunately, the use of sensors increases the weight, the cost, and the electrical sensibility, as well as having an undesirable influence on system reliability. Indeed, much research has focused on the improvement of the sensorless control's performance by using intelligent and sophisticated approaches like the model reference adaptive system observer [6], Kalman filtering [7, 8], neural networks [9, 10], the sliding mode observer [11-13], and the Luenberger adaptive observer [14].

Nowadays, a wide range of research activities is affected by the problem of application of the observer-based controller for nonlinear systems. This is also a proof of the increased interest

in the utilisation of the control theory. The basis for making a precise choice of the controller is the specific performance, which requires having knowledge of all the variables for the states of the dynamic system. As a matter of fact, the observers were able to incorporate a filter that provides an estimate for all the state vectors or even just the unmeasured part. It is considered one of the major reasons for why the observers design problem has been extensively examined in numerous papers of late [15-17]. The main motivations lie in the fact that state estimation may be used for control design, diagnosis or supervision. More recently, other applications like synchronization and input recovery, in communication systems, become one of the emerging and interesting research areas

Until now, the issue of observer-based controls (sensorless controls) for nonlinear systems is still a research subject. It is a difficult challenge to obtain a systematic observer-based control method that can be utilised for nonlinear systems given the conditions of the LMIs. As we well know, PMSM are considered to be non-linear multivariable dynamic systems. Thus, in the absence of speed sensors and parameter, and under load perturbations, controlling motor variables with high performance can be difficult when using conventional control strategies, like a sliding mode control [18], backstepping control [19], and adaptive State Dependent Ricatti Equation control (SDRE) [20], and methods used for the observer-based control problem for nonlinear systems include the adaptive method and the sliding mode, as presented by the authors in [6, 12, 21, 22]. All the methods presented previously is difficult to reach a proof of the stability of all the system (observer and controller), this because the conditions become very hard, this due to no separation principle was proven in the determination of the observer and the controller gains.

This thesis will focus on the advanced techniques of controls and observers, this based on the mean value theorem (MVT) and sector nonlinearity transformation for a class of Lipchitz nonlinear systems. These techniques will be apply for the control, the observation and diagnosis of PMSM drive. First appearance of MVT approach dates back to 2005 where it was applied on the observer design for nonlinear system[23], in 2011 an author it was applied also to the nonlinear observer for bounded Jacobian systems for application to automotive slip angle estimation [15], in [24] the researcher was used the MVT on observer for Lipchitz nonlinear systems this in 2012, in 2014 first application of MVT observer on Induction Machine (IM) [25], and first controller design was applied to the PMSM drive in 2015. Approximately these all researches use the MVT approach.

This thesis examines the problems of the observer and the control theory, based on the MVT and sector nonlinearity approaches for a class of Lipschitz nonlinear systems, for designing a controllers and observers for a PMSM drive application. Furthermore, we will use an extended MVT Observer for a Fault Detection and Diagnosis theory (FDD). Where we can transfer the nonlinear model of the PMSM into the Lipschitz form, and use the MVT and sector non-linearity approaches to express the nonlinear error dynamics of the combined system, controller or observer as a convex combination of known matrices with time-varying coefficients as linear parameter varying systems (LPV). These kinds of problems have been solved by using MVT and sector nonlinearity to nonlinear terms in the state error controller or observer equation. The controller and the observer gains can be designed based on the results for that class of nonlinear systems by using the Lyapunov theory, so, stability conditions are obtained and expressed in terms of linear matrix inequalities (LMIs), That are solved through the YALMIP software in order to obtain the observer and the controller gains separately based on the separation property [26]. The important idea of this work is to find the observer and the controller gains and so as that the nonlinear and coupling model of the PMSM drive makes as in linear model feedback control theory. The main advantage of the MVT approach is to obtain the observer and the controller parameters gain separately to each other with a proven methodology that stabilize the estimation and the control errors of the PMSM, and doesn't depend on the states of it, contrarily as in other technics for the control and the estimation of the states of the nonlinear systems.

1.2. Outline

The thesis report is organized as follows.

Chapter 2: Controllers and observers design based on MVT and T-S fuzzy models; this chapter starts with the introduction of the Takagi-Sugeno fuzzy model (T-S fuzzy model) followed by construction procedures of such models. Then a model-based fuzzy controller design utilizing the concept of "parallel distributed compensation (PDC)" is described. The main idea of the controller design is to derive each control rule so as to compensate each rule of a fuzzy system. The design procedure is conceptually simple and natural. Moreover, it is shown in this chapter that the stability analysis and control design problems can be reduced to linear matrix inequality LMI problems. Secondly, the designs of observers and controllers based

on MVT are presented, such as, we shown the basic mathematic tools used in the MVT and sector nonlinearity approaches. The stability analysis expressed in term of LMIs and solved by the YALMIP software in MATLAB are presented.

Chapter 3: Modeling of Permanent Magnet Synchronous Machines; this chapter presents a generalized dynamic mathematical model of the PMSM which can be used to construct various equivalent circuit models in the d-q rotating reference frame.

Chapter 4: Advanced Control and Observation Techniques Based on the MVT Applied to the PMSM Drives; the focus of this chapter is on the notion of an extended observer based-controller. The MVT and sector non-linearity approaches have been implemented for a class of the Lipchitz model of PMSM. The MVT is applied to the nonlinear error dynamic of the controller and observer. It is then can be considered as a convex combination of LPV system. In order to obtain zero steady state error, an integrator is added, thus making the structure of the proposed controller similar to that of the PI controller. By using Lyapunov stability conditions, the linear matrix inequalities (LMI) is obtained. Subsequently, the gains of the controller and observer are obtained by solving the LMI. This chapter demonstrate the feasibility and effectiveness of the proposed approach, despite of its simple implementation. The extended observer and the controller gains are separately determined based on the separation principles and have gotten by the exploitation of YALMIP software computer. Furthermore, these gains have completely independent from the PMSM states. As a proof of the efficacy of the proposed approach, one applies an illustrative simulation to the sensorless FOC of the PMSM drive by utilizing the MATLAB/SIMULINK environment.

Chapter 5: Robust Extended H_∞ Observer and Controller Based on the MVT Approach Applied to the PMSM Drive; in this chapter, we will focus on the synthesis of an extended H_∞ observer and H_∞ controller. The observer and controller are based on the MVT approach applied to the PMSM drive, the extended observer is under the Open Loop Field Oriented Control (OL-FOC). The robust extended observer and controller design are based on the MVT combined with the sector nonlinearity approach to stabilizing the observer and controller dynamic errors of PMSM drive

and ensured a minimum disturbance attenuation level to the error. The dynamics of the error are exhibited as LPV system after representing the nonlinear system of the PMSM as a Lipschitz form. Using the Lyapunov theory, the stability terms are obtained and expressed in form of LMIs, the extended observer gain and the controller gain are calculated offline by solving the LMIs. With two line currents are measured, the extended observer estimates all PMSM drive states and moreover the rotor position. At the end, the suggested approach is applied to PMSM machine under OL-FOC through an illustrative simulation to affirm the effectiveness of the concept.

Chapter 6: Fault Detection and Diagnosis Based on Extended MVT Observer Applied to the PMSM; this chapter present the concept of a special extended MVT observers, using for the detection and diagnosis of fault in the PMSM. Firstly, general diagnosis and deferent fault exist in the motor drive have been presented, such as, in this chapter we will concentrate on the inter turns short-circuit fault. Secondly, modeling of the PMSM machine in the presence of stator faults have been presented. Finally, the application of the extended MVT observer on the "Healthy" and "Faulty" PMSM model for estimate all its parameters, which we are used as an indicators of the fault have been also presented. As a proof of the efficacy of the proposed approach, one applies an illustrative simulation by utilizing the MATLAB/SIMULINK environment.

1.3. List of Publications

A. International Publications

1- B. Hamidani, A. Allag, A. Allag, and O. Zeghib, "Sensorless Non-linear Control Applied to a PMSM Machine Based on New Extended MVT Observer," *Journal of Electrical Engineering & Technology*, pp. 1-9, 2019.

2- O. Zeghib, A. Allag, M. Allag, and B. Hamidani, "An Extended MVT Observer Designed for Induction Motor Drive," *Mediterranean Journal of Measurement and Control*, vol. 13, pp. 805-811, 2017.

3- O. Zeghib, A. Allag, M. Allag, and B. Hamidani, "A robust extended H∞ observer based on the mean value theorem designed for induction motor drives," *International Journal of System Assurance Engineering and Management*, February 08 2019.

B. International Conferences

1- B. Hamidani, A. Allag, O. Zeghib and A. Allag, "An extended H∞ observer based on the mean value theorem approach applied to open loop FOC of PMSM drive," *2018 International Conference on Communications and Electrical Engineering (ICCEE)*, El Oued, Algeria, 2018, pp. 1-8.

2- B. Hamidani, A. Allag, O. Zeghib and A. Allag, " Design of an extended observer for non-linear Lipchitz systems based on the MVT approach under open loop FOC applied to the PMSM " Second International Conference on Electrical Engineering (ICEEB), Biskra, *Algeria, 2018, pp. 1-7*

3- O. ZEGHIB, A. ALLAG, B. HAMIDANI and M. ALLAG, "Input-output linearizing control of Induction Motor based on a newly extended MVT Observer Design," *2018 International Conference on Communications and Electrical Engineering (ICCEE)*, El Oued, Algeria, 2018, pp. 1-6.

References of Chapter I

[1] S.-K. Sul, *Control of electric machine drive systems* vol. 88: John Wiley & Sons, 2011.

[2] R. Molavi and D. Khaburi, "Optimal control strategies for speed control of permanent-magnet synchronous motor drives," in *Proceedings of World Academy of Science, Engineering and Technology*, 2008, pp. 428-432.

[3] R. Krishnan, *Electric motor drives: modeling, analysis, and control* vol. 626: Prentice Hall New Jersey, 2001.

[4] B. S. Guru and H. R. Hiziroglu, *Electric machinery and transformers* vol. 3: Oxford University Press New York, 2001.

[5] D. A. Dominic and T. R. Chelliah, "Analysis of field-oriented controlled induction motor drives under sensor faults and an overview of sensorless schemes," *ISA transactions*, vol. 53, pp. 1680-1694, 2014.

[6] D. Liang, J. Li, R. Qu, and W. Kong, "Adaptive second-order sliding-mode observer for PMSM sensorless control considering VSI nonlinearity," *IEEE Transactions on Power Electronics*, vol. 33, pp. 8994-9004, 2018.

[7] N. K. Quang, N. T. Hieu, and Q. Ha, "FPGA-based sensorless PMSM speed control using reduced-order extended Kalman filters," *IEEE Transactions on Industrial Electronics,* vol. 61, pp. 6574-6582, 2014.

[8] S. Bolognani, L. Tubiana, and M. Zigliotto, "Extended Kalman filter tuning in sensorless PMSM drives," *IEEE Transactions on Industry Applications,* vol. 39, pp. 1741-1747, 2003.

[9] H.-r. LI and S.-s. GU, "Neural-network-based adaptive observer of position and speed of PMSM [J]," *Proceedings of the Csee,* vol. 12, 2002.

[10] A. Accetta, M. Cirrincione, M. Pucci, and G. Vitale, "Sensorless control of PMSM fractional horsepower drives by signal injection and neural adaptive-band filtering," *IEEE Transactions on Industrial Electronics,* vol. 59, pp. 1355-1366, 2012.

[11] C.-X. Chen, Y.-X. Xie, and Y.-H. Lan, "Backstepping control of speed sensorless permanent magnet synchronous motor based on slide model observer," *International Journal of Automation and Computing,* vol. 12, pp. 149-155, 2015.

[12] X. Zhu, "Research on Sensorless Control of PMSM Based on a Novel Sliding Mode Observer," in *Chinese Intelligent Automation Conference*, 2017, pp. 193-199.

[13] J.-J. Ren, Y.-C. Liu, N. Wang, and S.-Y. Liu, "Sensorless control of ship propulsion interior permanent magnet synchronous motor based on a new sliding mode observer," *ISA transactions,* vol. 54, pp. 15-26, 2015.

[14] I. Vicente, A. Endemano, X. Garin, and M. Brown, "Comparative study of stabilising methods for adaptive speed sensorless full-order observers with stator resistance estimation," *IET control theory & applications,* vol. 4, pp. 993-1004, 2010.

[15] G. Phanomchoeng, R. Rajamani, and D. Piyabongkarn, "Nonlinear observer for bounded Jacobian systems, with applications to automotive slip angle estimation," *IEEE Transactions on Automatic Control,* vol. 56, pp. 1163-1170, 2011.

[16] S. Zhou, D. Zhu, and Z. Hu, "Based on an Improved Sliding Mode Observer for Position Estimation of PMSM," in *Society of Automotive Engineers (SAE)-China Congress*, 2016, pp. 99-109.

[17] D. Ichalal, H. Arioui, and S. Mammar, "Observer design for two-wheeled vehicle: A takagi-sugeno approach with unmeasurable premise variables," in *Control & Automation (MED), 2011 19th Mediterranean Conference on*, 2011, pp. 934-939.

[18] X. Zhang, L. Sun, K. Zhao, and L. Sun, "Nonlinear speed control for PMSM system using sliding-mode control and disturbance compensation techniques," *IEEE Transactions on Power Electronics,* vol. 28, pp. 1358-1365, 2013.

[19] J. Zhou and Y. Wang, "Adaptive backstepping speed controller design for a permanent magnet synchronous motor," *IEE Proceedings-Electric Power Applications,* vol. 149, pp. 165-172, 2002.

[20] P. V. Medagam, T. Yucelen, and F. Pourboghrat, "Adaptive SDRE-based nonlinear sensorless speed control for PMSM drives," in *Power Symposium, 2007. NAPS'07. 39th North American*, 2007, pp. 518-522.

[21] Y.-j. Wu and G.-f. Li, "Adaptive disturbance compensation finite control set optimal control for PMSM systems based on sliding mode extended state observer," *Mechanical Systems and Signal Processing,* vol. 98, pp. 402-414, 2018.

[22] X. Zhang and Z. Li, "Sliding-mode observer-based mechanical parameter estimation for permanent magnet synchronous motor," *IEEE Transactions on Power Electronics,* vol. 31, pp. 5732-5745, 2016.

[23] A. Zemouche, M. Boutayeb, and G. I. Bara, "Observer Design for Nonlinear Systems: An Approach Based on the Differential Mean Value Theorem," in *Decision and Control, 2005 and 2005 European Control Conference. CDC-ECC'05. 44th IEEE Conference on*, 2005, pp. 6353-6358.

[24] D. Ichalal, B. Marx, S. Mammar, D. Maquin, and J. Ragot, "Observer for Lipschitz nonlinear systems: mean value theorem and sector nonlinearity transformation," in *Intelligent Control (ISIC), 2012 IEEE International Symposium on*, 2012, pp. 264-269.

[25] M. Y. Hammoudi, A. Allag, M. Becherif, M. Benbouzid, and H. Alloui, "Observer design for induction motor: an approach based on the mean value theorem," *Frontiers in Energy,* vol. 8, pp. 426-433, 2014.

[26] J. Yoneyama, "Nonlinear control design based on generalized Takagi–Sugeno fuzzy systems," *Journal of the Franklin Institute,* vol. 351, pp. 3524-3535, 2014.

CHAPTER II

Controllers and Observers Design Based on MVT and T-S Fuzzy Models

2.1. Takagi-sugeno fuzzy model and parallel distributed compensation

Recent years have witnessed rapidly growing popularity of fuzzy control systems in engineering applications. The numerous successful applications of fuzzy control have sparked a flurry of activities in the analysis and design of fuzzy control systems. In this chapter, we introduce some of the analysis and design tools for fuzzy control systems to assist control researchers and engineers to solve engineering problems. The toolkit presented in this chapter is based on the framework of the Takagi-Sugeno fuzzy model and the so-called parallel distributed compensation, a controller structure devised in accordance with the fuzzy model. This chapter introduces the basic concepts, analysis, and design procedures of this approach [3].

This chapter starts with the introduction of the Takagi-Sugeno fuzzy model (T-S fuzzy model) followed by construction procedures of such models. Then a model-based fuzzy controller design utilizing the concept of "parallel distributed compensation" is described. The main idea of the controller design is to derive each control rule so as to compensate each rule of a fuzzy system. The design procedure is conceptually simple and natural. Moreover, it is shown in this chapter that the stability analysis and control design problems can be reduced to linear matrix inequality LMI problems.

2.1.1. Takagi-sugeno fuzzy model

The fuzzy model proposed by Takagi and Sugeno [4] is described by fuzzy IF-THEN rules which represent local linear input-output relations of a nonlinear system. The main feature of a Takagi-Sugeno fuzzy model is to express the local dynamics of each fuzzy implication (rule) by a linear system model. The overall fuzzy model of the system is achieved by fuzzy ''blending'' of the linear system models. In this chapter, the readers will find that many nonlinear dynamic systems can be represented by Takagi-Sugeno fuzzy models. In fact, it is proved that Takagi-Sugeno fuzzy models are universal approximators.

Continuous Fuzzy System: CFS

IF $z_1(t)$ is M_{i1} and … and $z_p(t)$ is M_{ip},

$$\textbf{\textit{THEN}} \begin{cases} \dot{x}(t) = A_i x(t) + B_i u(t), \\ y(t) = C_i x(t) \end{cases} \qquad i = 1,2,\dots,r. \tag{-1}$$

Here, M_{ip} is the fuzzy set and r is the number of model rules; $x(t) \in R^n$ is the state vector, $u(t) \in R^m$ is the input vector, $y(t) \in R^q$ is the output vector, $A_i \in R^{n\times n}$, $B_i \in R^{n\times m}$, and $C_i \in R^{q\times n}$; $z_1(t), \dots, z_p(t)$ are known premise variables that may be functions of the state variables, external disturbances, and / or time. We will use $z(t)$ to denote the vector containing all the individual elements $z_1(t), \dots, z_p(t)$. It is assumed in this book that the premise variables are not functions of the input variables $u(t)$. This assumption is needed to avoid a complicated defuzzification process of fuzzy controllers [3]. Note that stability conditions derived in this book can be applied even to the case that the premise variables are functions of the input variables $u(t)$. Each linear consequent equation represented by $A_i x(t) + B_i u(t)$ is called a ‘‘subsystem’’.

Given a pair of $\big(x(t),\ u(t)\big)$, the final outputs of the fuzzy systems are inferred as follows:

$$\dot{x}(t) = \frac{\sum_{i=1}^{r} w_i\big(z(t)\big)\{A_i x(t) + B_i u(t)\}}{\sum_{i=1}^{r} w_i\big(z(t)\big)}$$

$$= \sum_{i=1}^{r} h_i\big(z(t)\big)\{A_i x(t) + B_i u(t)\} \tag{-2}$$

$$y(t) = \frac{\sum_{i=1}^{r} w_i\big(z(t)\big)\, C_i x(t)}{\sum_{i=1}^{r} w_i\big(z(t)\big)}$$

$$= \sum_{i=1}^{r} h_i\big(z(t)\big)\, C_i x(t) \tag{-3}$$

Where

$$\big[z_1(t), z_2(t), \dots, z_p(t)\big],$$

$$w_i\big(z(t)\big) = \prod_{j=1}^{p} M_{ij}\left(z_j(t)\right),$$

$$h_i\big(z(t)\big) = \frac{w_i\big(z(t)\big)}{\sum_{i=1}^{r} w_i\big(z(t)\big)} \tag{-4}$$

For all *t*. The term $M_{ij}\left(z_j(t)\right)$ is the grade of membership of $z_j(t)$ in M_{ij}. Since

$$\begin{cases} \dot{x}(t) = \sum_{i=1}^{r} w_i\big(z(t)\big) > 0, \\ w_i\big(z(t)\big) \geq 0, \qquad\qquad i = 1,2,\dots,r. \end{cases} \tag{-5}$$

We have

$$\begin{cases} \dot{x}(t) = \sum_{i=1}^{r} h_i\big(z(t)\big) = 1, \\ h_i\big(z(t)\big) \geq 0, \qquad\qquad i = 1,2,\dots,r. \end{cases} \tag{-6}$$

For all *t*.

2.1.2. Construction of fuzzy model

Figure 2.1 illustrates the model-based fuzzy control design approach discussed in this chapter. To design a fuzzy controller, we need a Takagi-Sugeno fuzzy model for a nonlinear system. Therefore the construction of a fuzzy model represents an important and basic procedure in this approach. In this section we discuss the issue of how to construct such a fuzzy model. In general there are two approaches for constructing fuzzy models:

a) Identification fuzzy modeling using input-output data.
b) Derivation from given nonlinear system equations.

There has been an extensive literature on fuzzy modeling using input-output data following Takagi's, Sugeno's, and Kang's excellent work [5, 6]. The procedure mainly consists of two parts: structure identification and parameter identification. The identification approach to fuzzy modeling is suitable

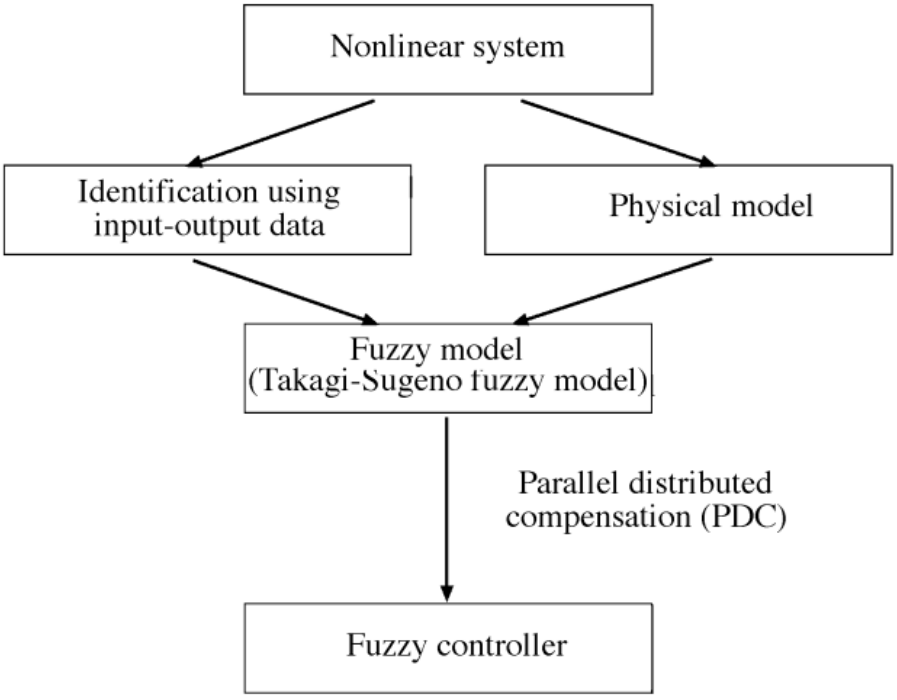

Figure 2.1 Model-based fuzzy control design[4].

for plants that are unable or too difficult to be represented by analytical and/or physical models. On the other hand, nonlinear dynamic models for mechanical systems can be readily obtained by, for example, the Lagrange method and the Newton-Euler method. In such cases, the second approach, which derives a fuzzy model from given nonlinear dynamical models, is more appropriate. This section focuses on this second approach. This approach utilizes the idea of ‘‘sector nonlinearity,’’ ‘‘local approximation,’’ or a combination of them to construct fuzzy models.

2.1.2.1. Sector nonlinearity

The idea of using sector nonlinearity in fuzzy model construction first appeared in [7]. Sector nonlinearity is based on the following idea. Consider a simple nonlinear system $\dot{x}(t) = f\big(x(t)\big)$, where $f(0) = 0$. The aim is to find the global sector such that $\dot{x}(t) = f\big(x(t)\big) \in [a_1 \;\; a_2]x(t)$. Figure 2.2 illustrates the sector nonlinearity approach. This approach guarantees an exact fuzzy model construction. However, it is sometimes difficult to find global sectors for general nonlinear systems. In this case, we can consider local sector nonlinearity. This is reasonable as variables of physical systems are always bounded. Figure 2.3 shows the local sector nonlinearity, where two

lines become the local sectors under $-d < x(t) < d$. The fuzzy model exactly represents the nonlinear system in the ‘‘local’’ region, that is $-d < x(t) < d$. The following example illustrate the concrete steps to construct fuzzy models.

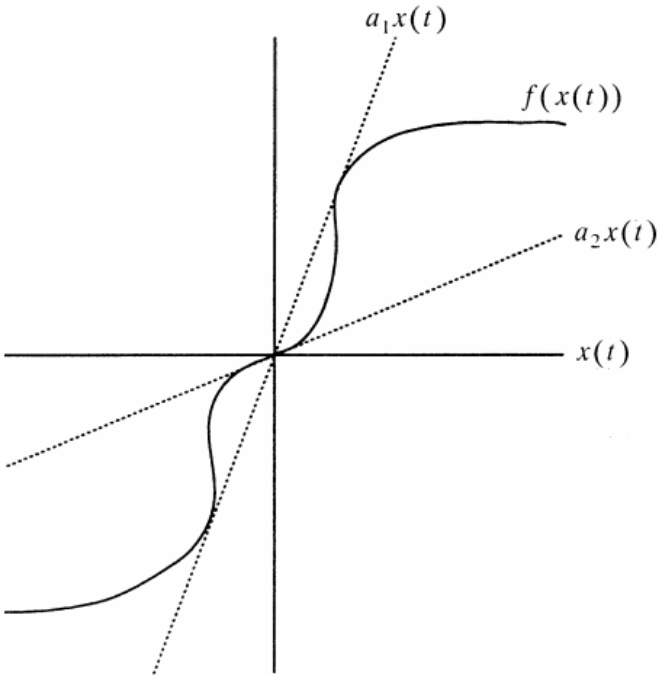

Figure 2.2 Global sector nonlinearity[4].

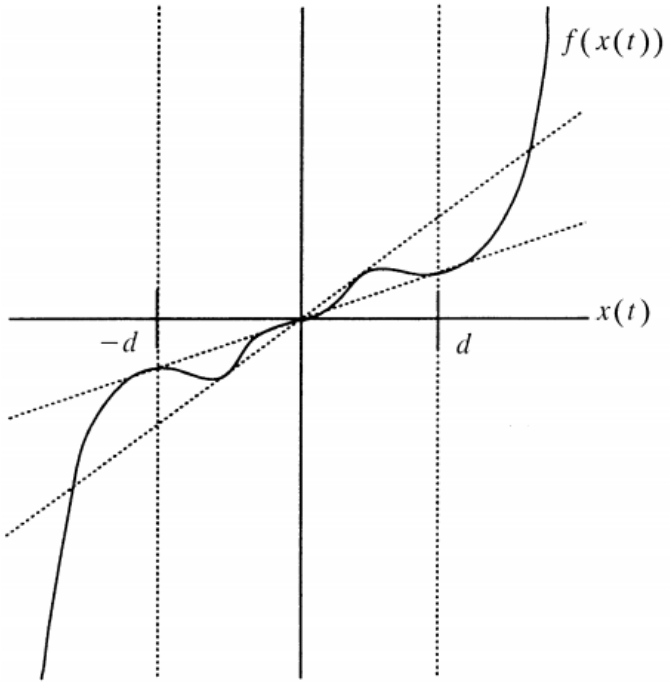

Figure 2.3 Local sector nonlinearity.

Example: consider the following nonlinear system:

$$\begin{pmatrix}\dot{x}_1(t)\\ \dot{x}_2(t)\end{pmatrix} = \begin{pmatrix}-x_1(t) + x_1(t){x_2}^3(t)\\ -x_2(t) + \big(3 + x_2(t)\big){x_1}^3(t)\end{pmatrix} \tag{2-7}$$

For simplicity, we assume that $x_1(t) \in [-1\ \ 1]$ and $x_2(t) \in [-1\ \ 1]$. Of course, we can assume any range for $x_1(t)$ and $x_2(t)$ to construct a fuzzy model.

Equation (2.7) can be written as

$$\dot{x}(t) = \begin{bmatrix}-1 & x_1(t){x_2}^2(t)\\ \big(3 + x_2(t)\big){x_1}^2(t) & -1\end{bmatrix} x(t), \tag{2-8}$$

Where $x(t) = [x_1(t) \quad x_2(t)]^T$ and $x_1(t){x_2}^2(t)$ and $\big(3 + x_2(t)\big){x_1}^2(t)$ are nonlinear terms. For the nonlinear terms, define $z_1(t) = x_1(t){x_2}^2(t)$ and $z_2(t) = \big(3 + x_2(t)\big){x_1}^2(t)$. Then, we have

$$\dot{x}(t) = \begin{bmatrix}-1 & z_1(t)\\ z_2(t) & -1\end{bmatrix} x(t). \tag{2-9}$$

Next, calculate the minimum and maximum values of $z_1(t)$ and $z_2(t)$ under $x_1(t) \in [-1\ \ 1]$ and $x_2(t) \in [-1\ \ 1]$. They are obtained as follows:

$$\underset{x_1(t), x_1(t)}{\boldsymbol{Max}}\ z_1(t) = 1, \qquad \underset{x_1(t), x_1(t)}{\boldsymbol{Min}}\ z_1(t) = -1,$$

$$\underset{x_1(t), x_1(t)}{\boldsymbol{Max}}\ z_2(t) = 4, \qquad \underset{x_1(t), x_1(t)}{\boldsymbol{Min}}\ z_2(t) = 0.$$

From the maximum and minimum values, $z_1(t)$ and $z_2(t)$ can be represented by

$$z_1(t) = x_1(t){x_2}^2(t) = M_1\big(z_1(t)\big) \times 1 + M_2\big(z_1(t)\big) \times (-1)$$

$$z_2(t) = \big(3 + x_2(t)\big){x_1}^2(t) = N_1\big(z_2(t)\big) \times 4 + N_2\big(z_2(t)\big) \times 0$$

Where

$$M_1\big(z_1(t)\big) + M_2\big(z_1(t)\big) = 1,$$

$$N_1\big(z_2(t)\big) + N_2\big(z_2(t)\big) = 1.$$

Therefore the membership functions can be calculated as

$$M_1\big(z_1(t)\big) = \frac{z_1(t)+1}{2}, \qquad M_2\big(z_1(t)\big) = \frac{1-z_1(t)}{2}$$

$$N_1\big(z_2(t)\big) = \frac{z_2(t)}{4}, \qquad N_2\big(z_2(t)\big) = \frac{4-z_2(t)}{4}$$

We name the membership functions "Positive", "Negative", "Big", and "Small" respectively. Then, the nonlinear system (2-7) is represented by the following fuzzy model.

Model Rule 1:

IF $z_1(t)$ is "Positive" and $z_2(t)$ is "Big",

THEN $\dot{x}(t) = A_1 x(t)$.

Model Rule 2:

IF $z_1(t)$ is "Positive" and $z_2(t)$ is "Small",

THEN $\dot{x}(t) = A_2 x(t)$.

Model Rule 3:

IF $z_1(t)$ is "Negative" and $z_2(t)$ is "Big",

THEN $\dot{x}(t) = A_3 x(t)$.

Model Rule 4:

IF $z_1(t)$ is "Negative" and $z_2(t)$ is "Small",

THEN $\dot{x}(t) = A_4 x(t)$.

Where

$$A_1 = \begin{bmatrix} -1 & 1 \\ 4 & -1 \end{bmatrix}, \qquad A_2 = \begin{bmatrix} -1 & 1 \\ 0 & -1 \end{bmatrix},$$

$$A_3 = \begin{bmatrix} -1 & -1 \\ 4 & -1 \end{bmatrix}, \qquad A_4 = \begin{bmatrix} -1 & -1 \\ 0 & -1 \end{bmatrix}.$$

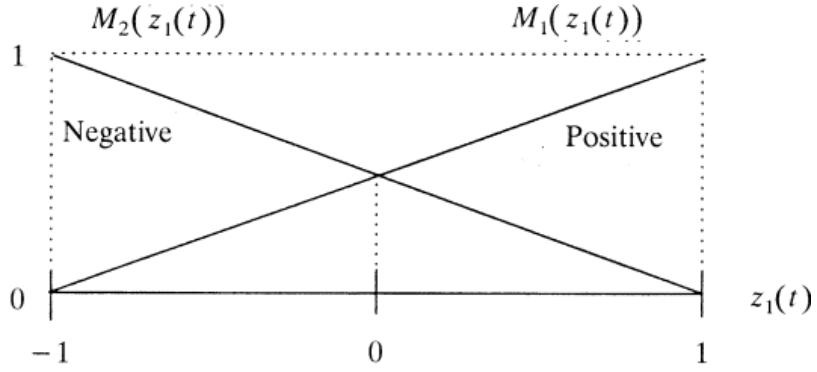

Figure 2.4 Membership functions $M_1(z_1(t))$ and $M_2(z_1(t))$ [4].

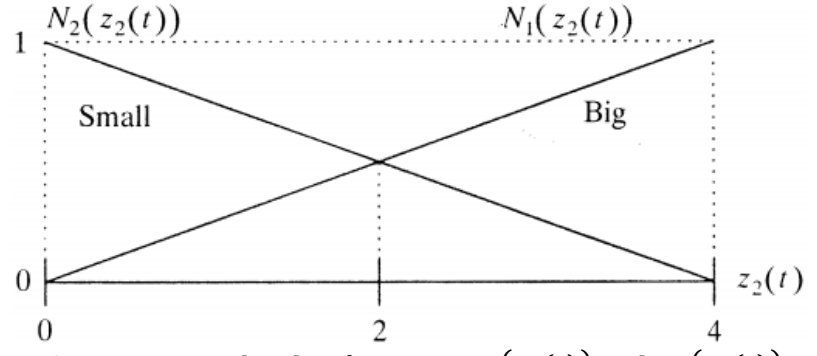

Figure 2.5 Membership functions $N_1(z_2(t))$ and $N_2(z_2(t))$

Figures 2.4 and 2.5 show the membership functions.

The defuzzification is carried out as

$$\dot{x}(t) = \sum_{i=1}^{4} h_i(z(t))\, A_i x(t), \tag{2-10}$$

Where

$$h_1(z(t)) = M_1(z_1(t)) \times N_1(z_2(t)),$$

$$h_2(z(t)) = M_1(z_1(t)) \times N_2(z_2(t)),$$

$$h_3(z(t)) = M_2(z_1(t)) \times N_1(z_2(t)),$$

$$h_4(z(t)) = M_2(z_1(t)) \times N_2(z_2(t)).$$

This fuzzy model exactly represents the nonlinear system in the region $[-1,1] \times [-1\ \ 1]$ on the $x_1 - x_1$ space.

2.1.2.2. Parallel distributed compensation

The history of the so-called parallel distributed compensation (PDC) began. with a model-based design procedure proposed by Kang and Sugeno (e.g., [8]). However, the stability of the control systems was not addressed in the. Design procedure. The design procedure was improved and the stability of the control systems was analyzed in [2]. The design procedure is named ‘‘parallel distributed compensation’’ in [9].

The PDC [2, 9, 10] offers a procedure to design a fuzzy controller from a given T-S fuzzy model. To realize the PDC, a controlled object (nonlinear system) is first represented by a T-S fuzzy model. We emphasize that many real systems, for example, mechanical systems and chaotic systems, can be and have been represented by T-S fuzzy models.

In the PDC design, each control rule is designed from the corresponding rule of a T-S fuzzy model. The designed fuzzy controller shares the same fuzzy sets with the fuzzy model in the premise parts. For the fuzzy model (2-1), we construct the following fuzzy controller via the PDC:

Control rule i:

IF $z_1(t)$ is M_{i1} and … and $z_p(t)$ is M_{ip},

THEN $u(t) = -K_i(t)x(t), \qquad i = 1,2,\dots,r.$

The fuzzy control rules have a linear controller state feedback laws in this case in the consequent parts.

The overall fuzzy controller is represented by

$$\dot{x}(t) = -\frac{\sum_{i=1}^{r} w_i\big(z(t)\big)\, K_i x(t)}{\sum_{i=1}^{r} w_i\big(z(t)\big)} = -\sum_{i=1}^{r} h_i\big(z(t)\big)\, K_i x(t) \tag{2-11}$$

The fuzzy controller design is to determine the local feedback gains K_i in the consequent parts. With PDC we have a simple and natural procedure to handle nonlinear control systems. Other nonlinear control techniques require special and rather involved knowledge.

Remark: Although the fuzzy controller (2.11) is constructed using the local design structure, the feedback gains K_i should be determined using global design conditions. The global design conditions are needed to guarantee the global stability and control performance. An interesting example will be presented in the next section.

The open-loop system of (2.3) is

$$\dot{x}(t) = \sum_{i=1}^{r} h_i\big(z(t)\big)\, A_i x(t) \tag{2-12}$$

A sufficient stability condition, derived by Tanaka and Sugeno [1, 2], for ensuring stability of (2.12) as follows.

Theorem 1: [1, 2] *the equilibrium of a fuzzy system* (2.12) *is globally asymptotically stable if there exists a common positive definite matrix* $\boldsymbol{P}$ *such that*

$$\boldsymbol{A_i^T P A_i - P < 0}, \qquad i = 1,2,\dots,r, \tag{2-13}$$

That is, a common $\boldsymbol{P}$ *has to exist for all subsystems.*

2.1.3. Stable controller design via iterative procedure

The PDC fuzzy controller is

$$\dot{x}(t) = -\sum_{j=1}^{r} h_j\big(z(t)\big) K_j x(t) \tag{2-14}$$

Note that the controller (2-14) is nonlinear in general.

Substituting (2-14) into (2-3) we obtain

$$\dot{x}(t) = \sum_{i=1}^{r}\sum_{j=1}^{r} h_i\big(z(t)\big) h_j\big(z(t)\big)\big\{A_i - B_i K_j\big\} x(t) \tag{2-15}$$

Applying Theorem 1, we have the following sufficient condition for quadratic Lyapunov stability.

Theorem 2: *the equilibrium of a fuzzy system* (2.15) *is globally asymptotically stable if there exists a common positive definite matrix* ***P*** *such that*

$$\{\boldsymbol{A_i} - \boldsymbol{B_i K_j}\}^{\boldsymbol{T}} \boldsymbol{P}\{\boldsymbol{A_i} - \boldsymbol{B_i K_j}\} - \boldsymbol{P} < \boldsymbol{0} \tag{2-16}$$

For $h_i(z(t)).h_j(z(t)) \neq 0, \forall\, t, i, j = 1,2,\dots,r.$

Note that system (2-15) can also be written as

$$\dot{x}(t) = \sum_{i=1}^{r} h_i(z(t))h_i(z(t))\{A_i - B_i K_i\}x(t) + 2\sum_{i=1}^{r}\sum_{i<j} h_i(z(t))h_j(z(t))G_{ij}x(t) \tag{2-17}$$

Where

$$G_{ij} = \frac{\{A_i - B_i K_j\} + \{A_j - B_j K_i\}}{2}, \quad i < j \;\; s.t. \;\; h_i \cap h_j \neq \phi$$

Therefore we have the following sufficient condition.

Theorem 3: *the equilibrium of a fuzzy system* (2.15) *is globally asymptotically stable if there exists a common positive definite matrix* ***P*** *such that the following tow conditions are satisfied:*

$$\{\boldsymbol{A_i} - \boldsymbol{B_i K_i}\}^{\boldsymbol{T}} \boldsymbol{P}\{\boldsymbol{A_i} - \boldsymbol{B_i K_i}\} - \boldsymbol{P} < \boldsymbol{0}, \qquad i = 1,2,\dots,r. \tag{2-18}$$

$$\boldsymbol{G_{ij}}^{\boldsymbol{T}} \boldsymbol{P G_{ij}} - \boldsymbol{P} < \boldsymbol{0}, \quad i < j \leq r \;\; s.t. \;\; h_i \cap h_j \neq \phi. \tag{2-19}$$

The meaning of the notation $< j \leq r \;\; s.t. \;\; h_i \cap h_j \neq \phi$. This means that the condition should be hold for all $i < j$ excepting $h_i \cap h_j = \phi$ [i.e., $h_i(z(t)) \times h_j(z(t)) = 0$ for all $z(t)$], where $h_i(z(t))$ denotes the weight of the *i*th rule calculated from membership functions in the premise parts and *r* denotes the number of IF-THEN rules. Note that $h_i \cap h_j = \phi$ if and only if the *i*th rule and *j*th rule have no overlap.

2.2. Fuzzy observer design

In practical applications, the state of a system is often not readily available. Under such circumstances, the question arises whether it is possible to determine the state from the system

response to some input over some period of time. For linear systems, a linear observer [3, 11] provides an affirmative answer if the system is observable. Likewise, a systematic design method of fuzzy regulators and fuzzy observers plays an important role for fuzzy control systems. This chapter presents the concept of fuzzy observers and two design procedures for fuzzy observer-based control [12, 13]. In linear system theory, one of the most important results on observer design is the so-called separation principle, that is, the controller and observer design can be carried out separately without compromising the stability of the overall closed-loop system. In this chapter, it is shown that a similar separation principle also holds for a large class of fuzzy control systems.

2.2.1. Fuzzy observer

Up to this point we have mainly dealt with LMI-based fuzzy control designs involving state feedback. In real-world control problems, however, it is often the case that the complete information of the states of a system is not always available. In such cases, one need to resort to output feedback design methods such as observer-based designs. This subchapter presents fuzzy observer design methodologies involving state estimation for T-S fuzzy models.

As in all observer designs, fuzzy observers [14] are required to satisfy

$$x(t) - \hat{x}(t) \to 0 \qquad \text{as } t \to \infty,$$

Where $x(t)$ denotes the state vector estimated by a fuzzy observer. This condition guarantees that the steady-state error between $x(t)$and $\hat{x}(t)$ converges to 0. As in the case of controller design, the PDC concept is employed to arrive at the following fuzzy observer structures:

Continuous Fuzzy System:

Observer rule i:

IF $z_1(t)$ is M_{i1} and … and $z_p(t)$ is M_{ip},

$$\textbf{\textit{THEN}} \begin{cases} \dot{\hat{x}}(t) = A_i\hat{x}(t) + B_i u(t) + L_i\big(y(t) - \hat{y}(t)\big), \\ \hat{y}(t) = C_i\hat{x}(t) \end{cases} \qquad i = 1,2,\dots,r. \tag{2-20}$$

The fuzzy observer has the linear state observer's laws in its consequent parts.

The fuzzy observer is represented as follows:

$$\hat{\dot{x}}(t) = \frac{\sum_{i=1}^{r} w_i\big(z(t)\big)\big\{A_i\hat{x}(t) + B_i u(t) + L_i\big(y(t) - \hat{y}(t)\big)\big\}}{\sum_{i=1}^{r} w_i\big(z(t)\big)}$$

$$= \sum_{i=1}^{r} h_i\big(z(t)\big)\big\{A_i\hat{x}(t) + B_i u(t) + L_i\big(y(t) - \hat{y}(t)\big)\big\} \tag{2-21}$$

$$\hat{y}(t) = \frac{\sum_{i=1}^{r} w_i\big(z(t)\big)\, C_i\hat{x}(t)}{\sum_{i=1}^{r} w_i\big(z(t)\big)}$$

$$= \sum_{i=1}^{r} h_i\big(z(t)\big)\, C_i\hat{x}(t) \tag{2-22}$$

We use the same weight $w_i\big(z(t)\big)$ as that of the *i*th rule of the fuzzy models (2-1) and (2-2), and (2-3) and (2-4). The fuzzy observer design is to determine the local gains L_i in the consequent parts.

The estimation error is $e(t) = x(t) - \hat{x}(t)$, we obtain the following system representations:

$$\dot{e}(t) = \sum_{i=1}^{r}\sum_{j=1}^{r} h_i\big(z(t)\big)h_j\big(z(t)\big)\big\{A_i - L_i C_j\big\}e(t) \tag{2-23}$$

We have the following sufficient condition for quadratic Lyapunov stability.

Theorem 4: *the equilibrium of a fuzzy system* (2.23) *is globally asymptotically stable if there exists a common positive definite matrix* $\boldsymbol{P}$ *such that*

$$\boldsymbol{\{A_i - L_i C_j\}^T P\{A_i - L_i C_j\} - P < 0} \tag{2-24}$$

For $h_i\big(z(t)\big).h_j\big(z(t)\big) \neq 0, \forall\, t, i, j = 1,2,\dots,r.$

2.3. Designs of observers and controller based on MVT

2.3.1. Problem statement

This section presents an efficient methodology for designing observers and controllers for the class of nonlinear systems described by[15]:

$$\begin{cases} \dot{x}(t) = f\big(x(t)\big) + g\big(x(t)\big)u(t) \\ y(t) = Cx(t) \end{cases} \tag{2-25}$$

Where $x(t) \in R^n$ is the state vector, $u(t) \in R^p$ is the input vector, and $y(t) \in R^m$ is the output measurement vector, are appropriate matrices. The functions $f\big(x(t)\big): R^n \to R^n$ and $g\big(x(t)\big): R^m \times R^P \to R^n$ are nonlinear. In addition $f\big(x(t)\big)$ is assumed to be differentiable.

The (2-25) can be transformed into Takagi-Sugeno form as follows[3]:

$$\begin{cases} \dot{x}(t) = \sum_{i=1}^{r} \mu_i\big(x(t)\big)\big(A_i x(t) + B_i u(t)\big) \\ y(t) = C_i x(t) \end{cases} \tag{2-26}$$

One can suppose the following matrixes:

$$A_0 = \frac{1}{r}\sum_{i=1}^{r} A_i \;; \quad B_0 = \frac{1}{r}\sum_{i=1}^{r} B_i \;; \quad \bar{A}_i = A_i - A_0 \;; \quad \bar{B}_i = B_i - B_0 \tag{2-27}$$

It's simple to rewrite (2-26) in the Lipchitz form based on (2-27) as follows:

$$\begin{cases} \dot{x}(t) = A_0 x(t) + B_0 u(t) + \sum_{i=1}^{r} \mu_i\big(x(t)\big)\big(\bar{A}_i x(t) + \bar{B}_i u(t)\big) \\ y(t) = Cx(t) \end{cases} \tag{2-28}$$

So

$$\begin{cases} \dot{x}(t) = A_0 x(t) + B_0 u(t) + \Phi\big(x(t)\big) \\ y(t) = Cx(t) \end{cases} \tag{2-29}$$

Where

$$\Phi\big(x(t)\big) = \sum_{i=1}^{r} \mu_i\big(x(t)\big)\big(\bar{A}_i x(t) + \bar{B}_i u(t)\big) \tag{2-30}$$

So, one can also present the observer in state space Lipchitz form as follows:

$$\begin{cases} \dot{\hat{x}}(t) = A_0 \hat{x}(t) + B_0 u(t) + \Phi\big(\hat{x}(t)\big) + L_0\big(y(t) - \hat{y}(t)\big) \\ \hat{y}(t) = C\hat{x}(t) \end{cases} \tag{2-31}$$

Where

$$\Phi\big(\hat{x}(t)\big) = \sum_{i=1}^{r} \mu_i\big(\hat{x}(t)\big)\big(\bar{A}_i \hat{x}(t) + \bar{B}_i u(t)\big) \tag{2-32}$$

2.3.2. MVT observers Design

The estimation error $e(t)$ is defined in such a way that

$$e(t) = x(t) - \hat{x}(t) \tag{2-33}$$

Using (2-33), one can obtain the dynamic of the estimation error as follows:

$$\dot{e}(t) = \dot{x}(t) - \hat{\dot{x}}(t) \tag{2-34}$$

So, the (2-29) and (2-31) are replaced in (2-34), one can obtain:

$$\dot{e}(t) = (A_0 - L_0 C)e(t) + \left(\Phi(x(t)) - \Phi\left(\hat{x}(t)\right)\right) \tag{2-35}$$

Before going to the stability analysis for the proposed observer, we will introduce some mathematical tools, which the mean value theorem and the sector nonlinearity transformations in the next subsection that will be applied it to the nonlinear part of equation (2-35).

2.3.2.1. Mean value theorem for bounded Jacobian systems

In this sub-section, we present a mathematical tools which are used subsequently to develop the observer gain in the next section. First, we present the scalar mean value theorem and the mean value theorem for vector functions. Then, we define the canonical basis for writing a vector function with a composition form. Lastly, we present a new modified form of the mean value theorem for vector functions[16].

2.3.2.2. Scalar MVT

Lemma 1: Let consider $f(x)$ be a function continuous on $[a, b]$ and differentiable on (a, b). There exist numbers $c \in (a, b)$ such as

$$f(a) - f(b) = \left.\frac{df}{dx}\right|_{x=c} \times (a - b) \tag{2-36}$$

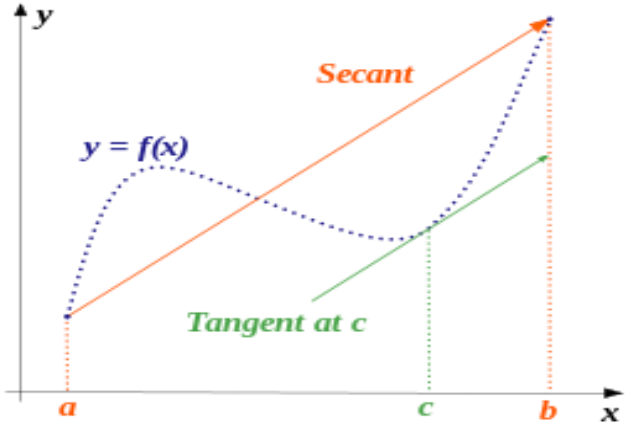

Figure 2.6 Mean Value Theorem

The equation (2-36) can also rewritten as

$$f(a)-f(b)=\left(\delta_1\frac{df}{dx}\Big|_{x=c_1}+\delta_2\frac{df}{dx}\Big|_{x=c_2}\right)\times(a-b) \qquad \delta_1,\delta_2>0, \quad \delta_1+\delta_2=1 \tag{2-37}$$

Where $c_1, c_2 \in (a,b)$ and δ_1, δ_2 are parameters depend on the value of a and b.

The proof of lemma 1 is presented in [17].

2.3.2.3. MVT for a vector function[18]

Lemma 2: Let consider $f(x)$ be a function continuous on $[a,b]$ and differentiable on convex hull of a set (a,b) with a Lipchitz continuous gradient ∇f . There exist numbers $c \in (a,b)$ such as

$$f(a)-f(b)=\nabla f(c)\times(a-b) \tag{2-38}$$

However, we cannot directly use the mean value theorem of equation (2-38), since is a varying parameter that continuously changes with the values of a and b. Thus $\nabla f(c)$ is an unknown and changing matrix. We need to modify the mean value theorem before it can be utilized.

canonical basis [19]

Lemma 3: Let's define the vector function as

$$f(x)=\left[f_1(x), f_2(x), \dots, f_q(x)\right]^T \tag{2-39}$$

Where $f_i(x)$ is the i^{th} component of $f(x)$

The function $f(x)$ can be written as

$$f(x) = \sum_{i=1}^{q} e_q(i) f_i(x) \tag{2-40}$$

Where

$$e_q(i) = (0, \dots, 0, 1, 0, \dots, 0), \qquad i = 1, 2, \dots, q \tag{2-41}$$

Now, we are ready to state and prove a modified form of the mean value theorem for a vector function.

2.3.2.4. modified MVT for a vector function (sector nonlinearity transformation) [18]

Theorem 1: Let consider $f(x)$ be a function continuous on $[a, b]$ and differentiable on convex hull of a set (a, b) with a Lipchitz continuous gradient ∇f . There exist ${\delta_{ij}}^{max}$ and ${\delta_{ij}}^{min}$ for $i, j = 1,2, \dots n$ such that:

$$f(a) - f(b) = \left[\left(\sum_{i,j=1}^{n,n} {Z_{ij}}^{max} {\delta_{ij}}^{max} \right) + \left(\sum_{i,j=1}^{n,n} {Z_{ij}}^{min} {\delta_{ij}}^{min} \right) \right] (a - b) \tag{2-42}$$

Where

${h_{ij}}^{max} \geq max\left(\frac{\partial f_i}{\partial x}\right)$ and ${h_{ij}}^{min} \leq min\left(\frac{\partial f_i}{\partial x}\right)$ $\forall x \in (a, b)$

And

${Z_{ij}}^{max} = e_n(i) {e_n}^T(j) {h_{ij}}^{max}$ and ${Z_{ij}}^{min} = e_n(i) {e_n}^T(j) {h_{ij}}^{min}$

Based on lemma 2, we have

$$f(a) - f(b) = \nabla f(c) \times (a - b) = \begin{bmatrix} \frac{\partial f_1}{\partial x_1} & \frac{\partial f_1}{\partial x_2} & \dots & \frac{\partial f_1}{\partial x_n} \\ \frac{\partial f_2}{\partial x_1} & \frac{\partial f_2}{\partial x_2} & \dots & \frac{\partial f_2}{\partial x_n} \\ \vdots & \vdots & \ddots & \vdots \\ \frac{\partial f_n}{\partial x_1} & \frac{\partial f_n}{\partial x_2} & \dots & \frac{\partial f_n}{\partial x_n} \end{bmatrix} [(a - b)] \tag{2-43}$$

Lemma 1 shows that each derivative function can be replaced with a convex combination of 2 values of the derivative of the function. Hence, the derivative function $\frac{\partial f_i(c)}{\partial x_j}$ can be replaced by

$$\begin{aligned} \frac{\partial f_i}{\partial x_j}(c) &= {\delta_{ij}}^{max}\frac{\partial f_i}{\partial x_j}(\gamma) + {\delta_{ij}}^{min}\frac{\partial f_i}{\partial x_j}(\varepsilon) \\ {\delta_{ij}}^{max}, {\delta_{ij}}^{min} &> 0, \qquad {\delta_{ij}}^{max} + {\delta_{ij}}^{min} = 1 \end{aligned} \tag{2-44}$$

Where

$\gamma = (\gamma_1, \gamma_2, \dots, \gamma_n)$ and $\varepsilon = (\varepsilon_1, \varepsilon_2, \dots, \varepsilon_n)$ with $\gamma, \varepsilon \in (a, b)$

The values of $\frac{\partial f_i}{\partial x_j}(\gamma)$ and $\frac{\partial f_i}{\partial x_j}(\varepsilon)$ need to be chosen as follows in order to satisfy lemma 1

$$\frac{\partial f_i}{\partial x_j}(\gamma) = {h_{ij}}^{max} \geq max\left(\frac{\partial f_i}{\partial x_j}\right), \qquad and \qquad \frac{\partial f_i}{\partial x_j}(\varepsilon) = {h_{ij}}^{min} \leq min\left(\frac{\partial f_i}{\partial x_j}\right) \tag{2-45}$$

Then the equation (2-45) can be rewritten as

$$\begin{aligned} \frac{\partial f_i}{\partial x_j}(c) &= {\delta_{ij}}^{max}{h_{ij}}^{max} + {\delta_{ij}}^{min}{h_{ij}}^{min} \\ {\delta_{ij}}^{max}, {\delta_{ij}}^{min} &> 0, \qquad {\delta_{ij}}^{max} + {\delta_{ij}}^{min} = 1 \end{aligned} \tag{2-46}$$

With ${\delta_{ij}}^{max}\ and\ {\delta_{ij}}^{min}$ are parameters that vary with the value of a and b. Subsequently, the equation (2-43) become as

$$\begin{aligned} f(a) - f(b) = &\begin{bmatrix} {\delta_{11}}^{max}{h_{11}}^{max} & {\delta_{12}}^{max}{h_{12}}^{max} & \dots & {\delta_{1n}}^{max}{h_{1n}}^{max} \\ {\delta_{21}}^{max}{h_{21}}^{max} & {\delta_{22}}^{max}{h_{22}}^{max} & \cdots & {\delta_{2n}}^{max}{h_{2n}}^{max} \\ \vdots & \vdots & \ddots & \vdots \\ {\delta_{n1}}^{max}{h_{n1}}^{max} & {\delta_{n2}}^{max}{h_{n2}}^{max} & \dots & {\delta_{nn}}^{max}{h_{nn}}^{max} \end{bmatrix}[(a-b)] \\ &+ \begin{bmatrix} {\delta_{11}}^{min}{h_{11}}^{min} & {\delta_{12}}^{min}{h_{12}}^{min} & \dots & {\delta_{1n}}^{min}{h_{1n}}^{min} \\ {\delta_{21}}^{min}{h_{21}}^{min} & {\delta_{22}}^{min}{h_{22}}^{min} & \cdots & {\delta_{2n}}^{min}{h_{2n}}^{min} \\ \vdots & \vdots & \ddots & \vdots \\ {\delta_{n1}}^{min}{h_{n1}}^{min} & {\delta_{n2}}^{min}{h_{n2}}^{min} & \dots & {\delta_{nn}}^{min}{h_{nn}}^{min} \end{bmatrix}[(a-b)] \end{aligned} \tag{2-47}$$

Use the canonical basis from lemma 3, then $f(a) - f(b)$ can be written as

$$f(a) - f(b) = \left[\left(\sum_{i,j=1}^{n,n} {Z_{ij}}^{max} {\delta_{ij}}^{max}\right) + \left(\sum_{i,j=1}^{n,n} {Z_{ij}}^{min} {\delta_{ij}}^{min}\right)\right](a - b) \tag{2-48}$$

Where ${Z_{ij}}^{max} = e_n(i){e_n}^T(j){h_{ij}}^{max}$ and ${Z_{ij}}^{min} = e_n(i){e_n}^T(j){h_{ij}}^{min}$

${h_{ij}}^{max} \geq max\left(\frac{\partial f_i}{\partial x_j}\right)$ and ${h_{ij}}^{min} \leq min\left(\frac{\partial f_i}{\partial x_j}\right)$

The equation (2-48) can be modified as

$$f(a) - f(b) = \left(\sum_{r=1}^{r} {\delta_{ij}}^{r} \mathcal{A}_i\right)(a - b) \tag{2-49}$$

With

$r = 1,2$ ${\delta_{ij}}^{1} = {\delta_{ij}}^{max}$ and ${\delta_{ij}}^{2} = {\delta_{ij}}^{min}$

And

$$\mathcal{A}_i = \sum_{i,j,r=1}^{n,n,r} {Z_{ij}}^{r}$$

$r = 1,2$ ${Z_{ij}}^{1} = {Z_{ij}}^{max}$ and ${Z_{ij}}^{2} = {Z_{ij}}^{min}$

So, based on the equation (2-49) the dynamics of the estimation error (2-35) can be expressed as

$$\dot{e}(t) = (A - L_0C)e(t) + \left(\sum_{r=1}^{2} {\delta_{ij}}^{r} \mathcal{A}_i\right)\left(x(t) - \hat{x}(t)\right) \tag{2-50}$$

Then the dynamics of the estimation error can be expressed as follows

$$\dot{e}(t) = \left(A_0 - L_0C + \sum_{r=1}^{2} {\delta_{ij}}^{r} \mathcal{A}_i\right)e(t) \tag{2-51}$$

Due

$$\sum_{r=1}^{2} {\delta_{ij}}^{r} = {\delta_{ij}}^{max} + {\delta_{ij}}^{min} = 1$$

It's possible to rewrite the dynamics of the estimation error as the next final form

$$\dot{e}(t) = \sum_{r=1}^{2} {\delta_{ij}}^{r} (A_0 - L_0 C + \mathcal{A}_i) e(t) \tag{2-52}$$

2.3.3. Stability analysis

The stability analysis of the dynamic of the estimation error represented in (2-52) will study by the quadratic Lyapunov function with common matrix as follows:

$$V\big(e(t)\big) = e^T(t) P e(t)\,, \qquad P = P^T > 0 \tag{2-53}$$

The stability is checked when the derivative of the Lyapunov function (2-54) is lower than zero

$$\dot{V}\big(e(t)\big) \leq 0 \tag{2-54}$$

The stability is related to the derivative of (2-53), so:

$$\dot{V}\big(e(t)\big) = e^T(t) \Big((A_0^T P + P A_0 - C^T L_0^T P - P L_0 C) + \mathcal{A}_i^T P + P \mathcal{A}_i \Big) e(t) \tag{2-55}$$

The stability of the estimation error dynamic is ensured if the time derivative of the Lyapunov equation (2-55) is negative definite, such that the following LMIs is with time-independent

$$A_0^T P + P A_0 - C^T L_0^T P - P L_0 C + \mathcal{A}_i^T P + P \mathcal{A}_i < 0 \tag{2-56}$$

To express the inequality (2-56) in term of LMI, the change of variables $N = P L_0$ is used and the LMIs conditions are obtained as follows, with the addition of α representing the rate of convergence.

Theorem 5: *The dynamics of system (2-52) is asymptotically stable, if there exist $P = P^T > 0$, such that:*

$$A_0^T P + P A_0 + \mathcal{A}_i^T P + P \mathcal{A}_i - C^T N^T - N C + \alpha P < 0 \tag{2-57}$$

For $i = 1, \dots, r$,
The observer gain is $L_0 = P^{-1} N.$

2.3.4. MVT controllers Design

According to the state feedback control law, the control vector is given by:

$$u(t) = -K_0 e(t) \tag{2-58}$$

Where K_0 is the controller's gain matrix and $e_c(t)$ is the state error vector given by:

$$e_c(t) = x(t) - x_c(t) \tag{2-59}$$

In (2-59), x_c is the desired states

From (2-29) and (2-59), we can write the error dynamic equation as:

$$\dot{e}_c(t) = \dot{x}(t) - \dot{x}_c(t) \tag{2-60}$$

Because $x_c(t)$ is a stepwise signal, so, $\dot{x}_c(t) = 0$ then from (2-29) and (2-60) we can write:

$$\dot{e}_c(t) = (A_0 - B_0K_0)e(t) + \Big(\Phi\big(x(t)\big) - \Phi\big(x_c(t)\big)\Big) \tag{2-61}$$

The objective is to determine the gain matrix K_0 such that the non-linear lipchitz system (2-61) becomes asymptotically stable.

The MVT and the sector nonlinearity transformation are then applied to the nonlinear part of the Lipchitz system (-36) (the approaches are presented in the last subsection 3.1.), so, when applied the MVT, the system (-36) becomes:

$$\dot{e}_c(t) = \left(A_0 - B_0K_0 + \sum_{i=1}^{n}\sum_{j=1}^{n} e_n(i)e_n^T(j)\frac{\partial \emptyset_i}{\partial x_j}(z_{1i}) \right) e(t) \tag{2-62}$$

When applied sector nonlinearity transformation, the system (2-62) becomes

$$\dot{e}_c(t) = \sum_{r=1}^{2} {\delta_{ij}}^r \left(A_0 - B_0K_0 + \mathcal{A}_j\right)e(t) \tag{2-63}$$

2.3.4.1. Stability analysis

The stability analysis of the dynamic of the state error represented in (2-63) will study by the quadratic Lyapunov function with common matrix as follows[20]:

$$W\big(e(t)\big) = e^T(t)Pe(t)\,, \qquad S = S^T > 0 \tag{2-64}$$

The stability is checked when the derivative of the Lyapunov function (2-65) is lower than zero

$$\dot{W}\big(e_c(t)\big) \leq 0 \tag{2-65}$$

The stability is related to the derivative of (2-64), so:

$$\dot{W}\big(e(t)\big) = {e_c}^T(t)\left((A_0^TS + SA_0 - K_0^TB_0^TS - SB_0K_0) + \mathcal{A}_j^TP + P\mathcal{A}_j\right)e_c(t) \tag{2-66}$$

The stability of the estimation error dynamic is ensured if the time derivative of the Lyapunov equation (2-66) is negative definite, such that the following LMIs is with time-independent

$$(A_0^T S + S A_0 - K_0^T B_0^T S - S B_0 K_0) + \mathcal{A}_j^T P + P \mathcal{A}_j < 0 \qquad (2\text{-}67)$$

To express the inequality (2-67) in term of LMI, the change of variables $M = K_0 P$ is used and the LMIs conditions are obtained as follows, with the addition of β representing the rate of convergence.

***Theorem 6*:** The dynamics of system (2-67) is asymptotically stable, if there exist $S = S^T > 0$, such that:

$$A_0^T S + S A_0 + \mathcal{A}_j^T S + S \mathcal{A}_j - M^T B_0^T - B_0 M + \beta B < 0 \qquad (2\text{-}68)$$

For $j = 1, \dots, r$.
The observer gain is $K_0 = M S^{-1}$.

References of Chapter II

[1] K. Tanaka, "Stability analysis of fuzzy control systems using Lyapunov's direct method," *Proc. of NAFIPS'90*, 1990.

[2] K. Tanaka and M. Sugeno, "Stability analysis and design of fuzzy control systems," *Fuzzy sets and systems*, vol. 45, pp. 135-156, 1992.

[3] K. Tanaka and H. O. Wang, *Fuzzy control systems design and analysis: a linear matrix inequality approach*: John Wiley & Sons, 2004.

[4] T. Takagi and M. Sugeno, "Fuzzy identification of systems and its applications to modeling and control," in *Readings in Fuzzy Sets for Intelligent Systems*, ed: Elsevier, 1993, pp. 387-403.

[5] M. Sugeno and G. Kang, "Structure identification of fuzzy model," *Fuzzy sets and systems*, vol. 28, pp. 15-33, 1988.

[6] M. Sugeno, "Fuzzy control," *Nikkan Kougyou Shinbunsha Publisher, Tokyo*, 1988.

[7] S. Kawamoto, K. Tada, A. Ishigame, and T. Taniguchi, "An approach to stability analysis of second order fuzzy systems," in *[1992 Proceedings] IEEE International Conference on Fuzzy Systems*, 1992, pp. 1427-1434.

[8] M. Sugeno and G. Kang, "Fuzzy modelling and control of multilayer incinerator," *Fuzzy sets and systems*, vol. 18, pp. 329-345, 1986.

[9] H. O. Wang, K. Tanaka, and M. Griffin, "Parallel distributed compensation of nonlinear systems by Takagi-Sugeno fuzzy model," in *Proceedings of 1995 IEEE International Conference on Fuzzy Systems.*, 1995, pp. 531-538.

[10] H. O. Wang, K. Tanaka, and M. Griffin, "An analytical framework of fuzzy modeling and control of nonlinear systems: stability and design issues," in *Proceedings of 1995 American Control Conference-ACC'95*, 1995, pp. 2272-2276.

[11] R. E. Kalman, "On the general theory of control systems," in *Proceedings First International Conference on Automatic Control, Moscow, USSR*, 1960.

[12] K. Tanaka and H. O. Wang, "Fuzzy regulators and fuzzy observers: a linear matrix inequality approach," in *Proceedings of the 36th IEEE Conference on Decision and Control*, 1997, pp. 1315-1320.

[13] K. Tanaka, T. Ikeda, and H. O. Wang, "Fuzzy regulators and fuzzy observers: relaxed stability conditions and LMI-based designs," *IEEE Transactions on fuzzy systems*, vol. 6, pp. 250-265, 1998.

[14] K. Tanaka and M. Sano, "On the concept of fuzzy regulators and fuzzy observers," in *Proceedings of Third IEEE International Conference on Fuzzy Systems*, 1994, pp. 767-772.

[15] D. P. Atherton and D. P. Atherton, *Nonlinear control engineering*: Van Nostrand Reinhold New York, 1982.

[16] D. Ichalal, B. Marx, S. Mammar, D. Maquin, and J. Ragot, "Observer for Lipschitz nonlinear systems: mean value theorem and sector nonlinearity transformation," in *Intelligent Control (ISIC), 2012 IEEE International Symposium on*, 2012, pp. 264-269.

[17] P. Sahoo and T. Riedel, *Mean value theorems and functional equations*: World Scientific, 1998.

[18] G. Phanomchoeng, "State, parameter, and unknown input estimation problems in active automotive safety applications," 2011.

[19] A. Zemouche, M. Boutayeb, and G. I. Bara, "Observer Design for Nonlinear Systems: An Approach Based on the Differential Mean Value Theorem," in *Decision and Control, 2005 and 2005 European Control Conference. CDC-ECC'05. 44th IEEE Conference on*, 2005, pp. 6353-6358.

[20] A. Allag, A. Benakcha, M. Allag, I. Zein, and M. Y. Ayad, "Classical state feedback controller for nonlinear systems using mean value theorem: closed loop-FOC of PMSM motor application," *Frontiers in Energy*, vol. 9, p. 413, 2015.

CHAPTER III

Modeling of Permanent Magnet Synchronous Machines

3.1. Introduction

The permanent magnet synchronous machine has permanent magnets instead of field windings. The permanent magnet synchronous machines can be classified into two main groups according to the installation of the permanent magnet materials on the rotor, Surface Mounted Permanent Magnet (SMPM) machines and Interior Permanent Magnet (IPM) machines. The magnets can be mounted on the rotor surface or they can be internal to the rotor. The permanent magnets are located on the outer surface of the rotor core in surface mounted permanent magnet machines, as shown in Figure 3.1 [1].

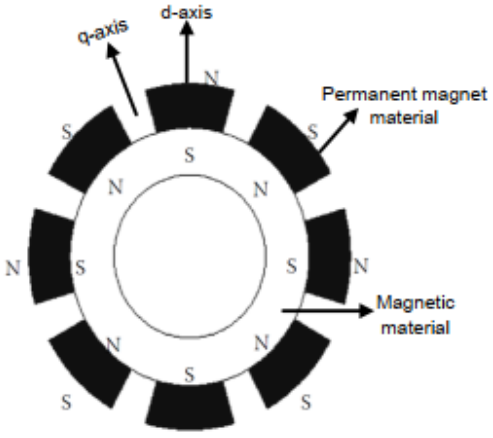

Figure 3.1 Permanent magnet rotor construction using surface mounted magnets[1]

In interior permanent magnet machines, the permanent magnets are embedded inside the rotor core. The structure of the interior permanent magnet machine is given in Figure 3.2.

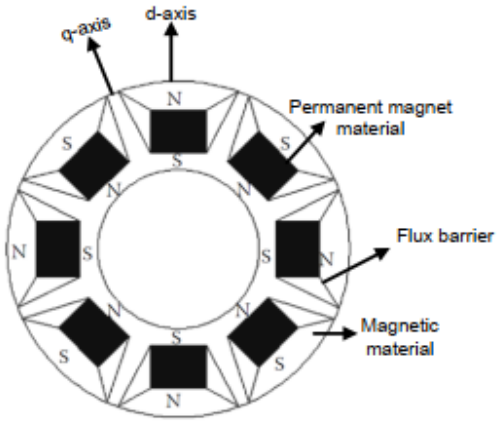

Figure 3.2 Permanent magnet rotor construction using embedded magnets[1]

The rotor magnetic axis is called direct axis (d-axis) or field flux axis and the principal path of the flux is through the magnets. The torque axis (quadrature axis or q-axis) of rotor is electrically orthogonal to the direct axis. Regardless of the manner of mounting the permanent magnets on the rotor, the basic principle of operation of machines are same. An important difference exists between the direct and quadrature axes inductances for different types of permanent magnet synchronous machines. The SMPM machines have many small permanent magnet materials that are placed whole surface of the rotor. Therefore, they have symmetrical reluctance in both axes and they are non-salient pole synchronous machines. In other words, the d and q axes reactances of SMPM machines are equal ($L_q = L_d$). The arrangement of the permanent magnets to the rotor surface provides the highest air gap flux density as is directly faces the air gap without the interruption of any other medium such as part of rotor laminations. Drawbacks of such an arrangement are; lower structural integrity and lower mechanical robustness. Besides that, the interior construction relieves the problem of retaining the magnets against centrifugal force. Therefore the interior construction is suitable for high-speed applications [1].

3.2. Steady-state machine modeling of PMSM

This section presents steady-state analysis of the surface mounted synchronous machines considering the per-phase steady-state equivalent circuit shown as in Figure 3.3 [2].

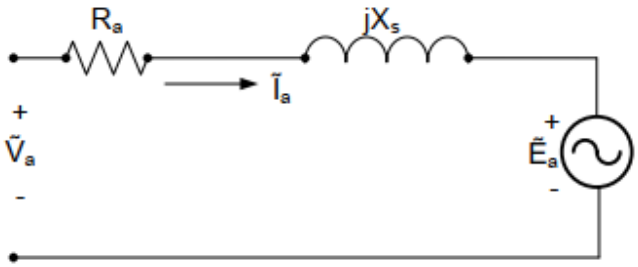

Figure 3.3 Per-phase equivalent circuit of non-salient surface mounted permanent magnet synchronous machine[2]

In Figure 3.3, $\tilde{V}_a$ is the motor terminal voltage, $\tilde{E}_a$ is the back-emf voltage induced due to the permanent magnet flux and $\tilde{I}_a$ is the motor phase current. And R_a and X_s are the per-phase winding resistance and synchronous reactance. From the equivalent circuit, we can write

$$\tilde{V}_a = \tilde{E}_a + \tilde{I}_a R_a + j\tilde{I}_a X_s \tag{3-1}$$

The average power input to the machine;

$$P_{in} = 3V_a I_a \cos\theta \tag{3-2}$$

Where θ is the power-factor angle between the applied voltage and the phase current. V_a and I_a are the RMS values of phase voltage and current.

The total copper (electrical) loss in a surface mounted permanent magnet synchronous machine is;

$$P_{cu} = 3{I_a}^2 R_a \tag{3-3}$$

By subtracting the total copper loss from the power input, we obtain the power developed by a surface mounted permanent magnet synchronous machine as;

$$P_{out} = 3V_a I_a \cos\theta + P_{cu} \tag{3-4}$$

Eddy current and hysteresis losses are also assumed as negligible.

Steady-state phasor diagram for the SMPM machine by neglecting the winding resistor is given in Figure 3.4.

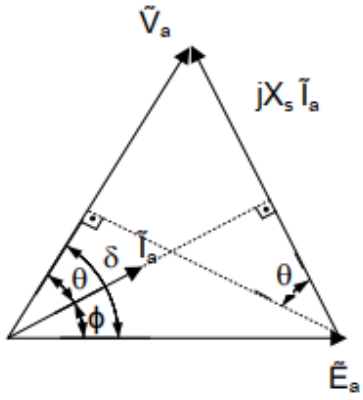

Figure 3.4 Phasor diagram of the non-salient PMSM machine[2].

From the per-phase equivalent circuit in Fig.3. 3, the total output power can be written as [2];

$$P_{out} = 3E_a I_a \ cos\,\Phi \tag{3-5}$$

For the flux linkage λ_f due the permanent magnets and the electrical speed w_e, the back-emf is given by;

$$E_a = w_e \lambda_f \tag{3-6}$$

If Ω is the angular velocity (rad/s) of the motor, the electromagnetic torque developed by the motor is then given as;

$$T_e = \frac{P_{out}}{\Omega} = \frac{3E_a I_a \ cos\,\Phi}{\Omega} \tag{3-7}$$

Ω and w_e are related by;

$$w_e = \Omega p \tag{3-8}$$

Where, p is the pole pair number.

Then, from (3-6) – (3-8) the electromagnetic torque equation can be obtained as;

$$T_e = 3p\lambda_f I_a \ cos\,\Phi \tag{3-9}$$

It is obvious that the maximum torque can be achieved by controlling the magnitude and phase of the phase current $\tilde{I}_a$.

3.3. Dynamic modeling of the PMSM machine

In the previous section, steady-state analysis of the surface mounted permanent magnet synchronous machines was introduced. This section presents the dynamic model of permanent magnet synchronous machine. The mathematical model of permanent magnet synchronous machine is developed with the help of Park and Clarke transformations which are derived in Appendix A. Actually; the model of permanent magnet synchronous machine is nonlinear. For simplicity, the following assumptions are made in the derivation:

- Saturation in machine is neglected,
- The back-emf is purely sinusoidal,
- Eddy currents and hysteresis losses are negligible,
- Balanced three-phase voltage source is considered.

There is no external voltage supply connected to the rotor side and the permanent magnet flux variation is negligible. Therefore, rotor voltage equations need not to be taken into account in the SMPM synchronous machine modeling [3].

The circuit equations of the three stator windings in terms of phase variables can be written as:

$$\begin{bmatrix} V_a \\ V_b \\ V_c \end{bmatrix} = \begin{bmatrix} R_a & 0 & 0 \\ 0 & R_b & 0 \\ 0 & 0 & R_c \end{bmatrix} \begin{bmatrix} i_a \\ i_b \\ i_c \end{bmatrix} + \frac{d}{dt} \begin{bmatrix} L_a & L_{ab} & L_{ac} \\ L_{ba} & L_b & L_{bc} \\ L_{ca} & L_{cb} & L_c \end{bmatrix} \begin{bmatrix} i_a \\ i_b \\ i_c \end{bmatrix} + \begin{bmatrix} e_a \\ e_b \\ e_c \end{bmatrix} \tag{3-10}$$

Where R_a, R_b and R_c are the stator resistances, L_a, L_b and L_c the self-inductances, and L_{ab}, L_{ba}, L_{ac}, L_{ca}, L_{bc}, L_{cb} the mutual inductances. Assume that the stator windings are balanced and there is no change in the rotor reluctance with rotor position change for surface mounted permanent magnet synchronous machines, then

$$\begin{aligned} R_a = R_b = R_c = R_s \\ L_a = L_b = L_c = L_s \\ L_{ab} = L_{ba} = L_{ac} = L_{ca} = L_{bc} = L_{cb} = M \end{aligned} \tag{3-11}$$

$$\begin{bmatrix} V_a \\ V_b \\ V_c \end{bmatrix} = \begin{bmatrix} R_s & 0 & 0 \\ 0 & R_s & 0 \\ 0 & 0 & R_s \end{bmatrix} \begin{bmatrix} i_a \\ i_b \\ i_c \end{bmatrix} + \frac{d}{dt} \begin{bmatrix} L_s & M & M \\ M & L_s & M \\ M & M & L_s \end{bmatrix} \begin{bmatrix} i_a \\ i_b \\ i_c \end{bmatrix} + \begin{bmatrix} e_a \\ e_b \\ e_c \end{bmatrix} \quad (3\text{-}12)$$

Where $i_a = -i_b - i_c$ and we have that;

$$\begin{bmatrix} V_a \\ V_b \\ V_c \end{bmatrix} = \begin{bmatrix} R_s & 0 & 0 \\ 0 & R_s & 0 \\ 0 & 0 & R_s \end{bmatrix} \begin{bmatrix} i_a \\ i_b \\ i_c \end{bmatrix} + \frac{d}{dt} \begin{bmatrix} L_s - M & 0 & 0 \\ 0 & L_s - M & 0 \\ 0 & 0 & L_s - M \end{bmatrix} \begin{bmatrix} i_a \\ i_b \\ i_c \end{bmatrix} + \begin{bmatrix} e_a \\ e_b \\ e_c \end{bmatrix} \quad (3\text{-}13)$$

In Figure 3.5, a dynamic phase equivalent circuit of PMSM is presented.

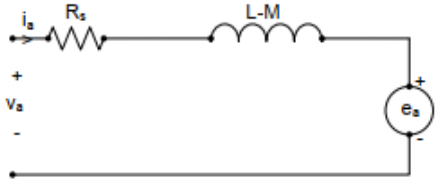

Figure 3.5 Phase equivalent circuit of a PMSM

A two-phase equivalent equations and d-q model of a permanent magnet synchronous machine rotating at the synchronous speed is obtained by using Park and Clarke transformations which are given in Appendix A.

$$\begin{bmatrix} v_d \\ v_q \end{bmatrix} = \frac{3}{2} \begin{bmatrix} cos(\Phi) & cos(\Phi - \frac{2\pi}{3}) & cos(\Phi - \frac{2\pi}{3}) \\ -\sin(\Phi) & -\sin(\Phi - \frac{2\pi}{3}) & -\sin(\Phi - \frac{2\pi}{3}) \end{bmatrix} \begin{bmatrix} v_a \\ v_b \\ v_c \end{bmatrix} \quad (3\text{-}14)$$

$$v_d = R_s i_d + L_d \frac{di_d}{dt} - w_e L_q i_q \quad (3\text{-}15)$$

$$v_q = R_s i_q + L_q \frac{di_q}{dt} + w_e L_d i_d + w_e \Phi_f \quad (3\text{-}16)$$

Figures 3.6-(a) and 3.6-(b) show the dynamic two-phase equivalent circuit.

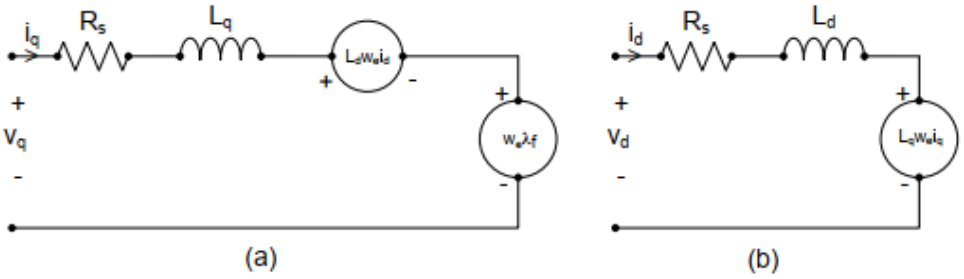

Figure 3.6 Two-phase (d, q) equivalent model of PMSM machine[2]

For three-phase permanent magnet synchronous machines, the input power (P_{in}) can be represented as:

$$P_{in} = v_a i_a + v_b i_b + v_c i_c \tag{3-17}$$

Which in terms of d, q variables is;

$$P_{in} = \frac{3}{2}(v_d i_d + v_q i_q) \tag{3-18}$$

The output power, P_{out} can be obtained from the (3-18) by ignoring the copper losses.

$$P_{out} = \frac{3}{2}(-w_e \lambda_q i_d + w_e \lambda_d i_q) \tag{3-19}$$

Where,

$$\lambda_q = L_q i_q \tag{3-20}$$

$$\lambda_d = L_d i_d + \Phi_f \tag{3-21}$$

The instantaneous torque T_e is obtained by dividing the output power, P_{out} by mechanical speed Ω

$$T_e = \frac{3}{2} p(\Phi_f i_q + (L_d - L_q) i_q i_d) \tag{3-22}$$

The torque equation includes two terms. First term is called as “the mutual reaction torque” that is produced from the interaction between the permanent magnet flux, Φ_f and i_q current component.

The second term corresponds to the "reluctance torque" due to the differences between d-axis and q-axis reluctances. In order to produce additive reluctance torque, i_d must be negative and L_q must be greater than L_d. Besides that, the reluctance variation between the direct (d-axis) and quadrature (q-axis) axes is fairly small in non-salient surface mounted permanent magnet synchronous machine. Therefore, the second term, "reluctance torque", can be neglected for this machine type [3]. The output torque (T_e) is linearly dependent with the magnet flux and q-axis current;

$$T_e = \frac{3}{2} p \Phi_f i_q \tag{3-23}$$

3.3.1. Mechanical equation

The mechanical equation of the machine is given by:

$$J \frac{d\Omega}{dt} = T_e - T_L - T_f \tag{3-24}$$

The (3-23) is replaced in (3-24), so the dynamic rotor speed becomes:

$$\frac{d\Omega}{dt} = \frac{3p}{2J} \Phi_f i_q - \frac{1}{J} T_L - \frac{f}{J} \Omega \tag{3-25}$$

One can deduce the final form of the dynamic model of the PMSM in the d-q referential as follows:

$$\begin{aligned} \frac{di_d}{dt} &= -\frac{R_s}{L_d} i_d + \frac{L_q}{L_d} p i_q \Omega + \frac{1}{L_d} v_d \\ \frac{di_q}{dt} &= -\frac{R_s}{L_q} i_q - \frac{L_d}{L_q} p i_d \Omega - \frac{p}{L_q} \Phi_f \Omega + \frac{1}{L_q} v_q \\ \frac{d\Omega}{dt} &= \frac{3p}{2J} \Phi_f i_q - \frac{1}{J} T_L - \frac{f}{J} \Omega \end{aligned} \tag{3-26}$$

Equation (3-26) can be written in a state space form with the stator current (i_d and i_q) and rotor speed as the state variables, as follows:

$$\begin{cases} \dot{x}(t) = f(x(t)) + Bu(t) \\ y(t) = Cx(t) \end{cases} \tag{3-27}$$

Where

$$f(x(t)) = \begin{bmatrix} -\frac{R_s}{L_d}x_1 - \frac{L_q}{L_d}px_2x_3 \\ -\frac{R_s}{L_q}x_2 - \frac{L_d}{L_q}px_1x_3 + -\frac{p}{L_q}\Phi_f x_3 \\ \frac{3p}{2J}\Phi_f x_2 - \frac{f}{J}x_3 - \frac{1}{J}T_L \end{bmatrix}; B = \begin{bmatrix} \frac{1}{L_d} & 0 \\ 0 & \frac{1}{L_q} \\ 0 & 0 \end{bmatrix}; C = \begin{bmatrix} 1 & 0 & 0 \\ 0 & 1 & 0 \end{bmatrix} \quad (3\text{-}28)$$

And

$$x(t) = \begin{bmatrix} x_1 \\ x_2 \\ x_3 \end{bmatrix} = \begin{bmatrix} i_d \\ i_q \\ \Omega \end{bmatrix}; u(t) = \begin{bmatrix} v_d \\ v_q \end{bmatrix}$$

References of Chapter III

[1] R. Krishnan, *Permanent magnet synchronous and brushless DC motor drives*: CRC press, 2009.

[2] B. S. Guru and H. R. Hiziroglu, *Electric machinery and transformers* vol. 3: Oxford University Press New York, 2001.

[3] R. Krishnan, *Electric motor drives: modeling, analysis, and control* vol. 626: Prentice Hall New Jersey, 2001.

CHAPTER IV

Advanced Control and Observation Techniques Based on the MVT Applied to the PMSM Drives

4.1. Introduction

The focus of this chapter is on the notion of an extended observer based on a state feedback controller. The mean value theorem and sector non-linearity approaches were implemented for a class of the Lipchitz model of PMSM. Based on these mathematical approaches, the proposed design allows the expression of non-linear error dynamics for the state control and the extended observer becomes a convex combination of known matrices that have time varying coefficients. This is similar to a LPV systems after the non-linear system of the PMSM is represented in the Lipchitz form. Through the Lyapunov theory, one can obtain and express the stability conditions in a term of LMI's. The extended observer and the controller gains are separately determined based on the separation principles and have gotten by the exploitation of YALMIP software computer. Furthermore, these gains have completely independent from the PMSM states. As a proof of the efficacy of the proposed approach, one applies an illustrative simulation to the sensorless FOC of the PMSM drive by utilizing the MATLAB/SIMULINK environment.

4.2. Extended observer based controller design: a PMSM drive application

4.2.1. Extended dynamics model of PMSM

By setting the assumption that the load torque and the rotor position can be taken as state variables, one can write the mathematical model of the PMSM, which is utilised for observations, as follows:

$$\begin{cases} \dfrac{dI_d}{dt} = -\dfrac{R_s}{L_d} I_d + \dfrac{L_q}{L_d} I_q p\Omega + \dfrac{1}{L_d} u_d \\ \dfrac{dI_q}{dt} = -\dfrac{R_s}{L_q} I_q - \dfrac{L_d}{L_q} p\Omega I_d + \dfrac{\Phi_f}{L_q} p\Omega + \dfrac{1}{L_q} u_q \\ \dfrac{d\Omega}{dt} = \dfrac{1}{J}(T_e - T_L - f\Omega) \\ \dfrac{d\theta}{dt} = \Omega \\ \dfrac{dT_L}{dt} = 0 \end{cases} \tag{4-1}$$

The electromagnetic torque is written by:

$$T_e = \frac{3}{2} p[\Phi_f I_q] \tag{4-2}$$

From (4-1) and (4-2), the extended state model is rewritten as

$$\begin{cases} \dot{x}_e(t) = f_e(x_e(t)) + B_e u(t) \\ y_e(t) = C_e x_e(t) \end{cases} \tag{4-3}$$

Such that

$$f_e(x_e(t)) = \begin{bmatrix} a_1 x_{e1} + a_2 x_{e2} x_{e3} \\ b_1 x_{e2} + b_2 x_{e1} x_{e3} + b_3 x_{e3} \\ c_1 x_{e2} + c_2 x_{e3} + c_3 x_{e5} \\ x_{e3} \\ 0 \end{bmatrix} \tag{4-4}$$

And

$$B_e = \begin{bmatrix} \lambda_d & 0 \\ 0 & \lambda_q \\ 0 & 0 \\ 0 & 0 \\ 0 & 0 \end{bmatrix}; \; C_e = \begin{bmatrix} 1 & 0 & 0 & 0 & 0 \\ 0 & 1 & 0 & 0 & 0 \end{bmatrix}$$

Where

$x_e = [x_{e1} \;\; x_{e2} \;\; x_{e3} \;\; x_{e4} \;\; x_{e5}]^T = [i_d \;\; i_q \;\; \Omega \;\; \theta \;\; T_L]^T$ And $u = [u_d \;\; u_q]^T$

$a_1 = -\dfrac{R_s}{L_d}$, $a_2 = \dfrac{L_q}{L_d} p$, $b_1 = -\dfrac{R_s}{L_q}$, $b_2 = -\dfrac{L_d}{L_q} p$, $b_3 = \dfrac{\Phi_f}{L_q} p$, $c_1 = \dfrac{3p}{2J} \Phi_f$, $c_2 = -\dfrac{f}{J}$

$c_3 = -\dfrac{1}{J}$, $\lambda_d = \dfrac{1}{L_d}$, $\lambda_q = \dfrac{1}{L_q}$,

4.2.2. Problem statement

First, one can transfer the model (4-3) of the PMSM into the Lipchitz form as:

$$\begin{cases} \dot{x}_e(t) = AA_0 x_e(t) + BB_0 u(t) + \emptyset_e(x_e(t)) \\ y_e(t) = C_e x_e(t) \end{cases} \quad (4\text{-}5)$$

Where

$$AA_0 = \begin{bmatrix} a_1 & 0 & 0 & 0 & 0 \\ 0 & b_1 & b_3 & 0 & 0 \\ 0 & c_1 & c_2 & 0 & 0 \\ 0 & 0 & 1 & 0 & 0 \\ 0 & 0 & 0 & 0 & 0 \end{bmatrix}$$

And $\emptyset_e(x_e(t))$ is defined by

$$\emptyset_e(x_e(t)) = f_e(x_e(t)) - AA_0 x_e(t) \quad (4\text{-}6)$$

One can also present the state equation of the extended observer in the Lipchitz form:

$$\begin{cases} \dot{\hat{x}}_e(t) = AA_0 \hat{x}_e(t) + BB_0 u(t) + \emptyset_e(\hat{x}_e(t)) + L_0(y_e(t) - \hat{y}_e(t)) \\ \hat{y}_e(t) = C_e \hat{x}_e(t) \end{cases} \quad (4\text{-}7)$$

Where $\emptyset_e(\hat{x}_e(t))$ is defined by

$$\emptyset_e(\hat{x}_e) = f_e(\hat{x}_e(t)) - AA_0 \hat{x}_e(t) \quad (4\text{-}8)$$

Thus, the state estimation error $e_o(t)$ is defined in such a way that $e_o(t) = x_e(t) - \hat{x}_e(t)$. Using (4-5) and (4-7), one can obtain the dynamic of the state estimation error:

$$\dot{e}_o(t) = (AA_0 - L_0 C_e) e_o(t) + (\emptyset_e(x_e) - \emptyset_e(\hat{x}_e)) \quad (4\text{-}9)$$

4.2.3. Observer based controller case

The structure of the dynamic equation that is utilised for the controller case can be given in the Lipchitz form:

$$\begin{cases} \dot{x}(t) = A_0 x(t) + B_0 u(t) + \emptyset(x(t)) + D\, T_L \\ y(t) = Cx(t) \end{cases} \quad (4\text{-}10)$$

Where $D = [0\ 0\ -1/J]$

The classical feedback P control law is stated as:

$$u(t) = -K_0(\underline{\hat{x}}_e(t) - x_r(t)) = -K_0 e_c(t) \quad (4\text{-}11)$$

Where K_0 represents the controller's matrix gain. The desired states, $x_r = [i_{dr} \;\; i_{qr} \;\; \Omega_r]$, are meant to serve as stepwise signals or zeros, while $\underline{\hat{x}_e}(t)$ refers to the estimated states where $\underline{\hat{x}_e} = [\hat{x}_{e1} \;\; \hat{x}_{e2} \;\; \hat{x}_{e3}] = [\hat{\imath}_d \;\; \hat{\imath}_q \;\; \hat{\Omega}]$.

When (4-5) and (4-11) are used in the regulation case, the augmented dynamic systems can be obtained with $x_r(t) = 0$ (or a stepwise signal) as follows:

$$\begin{cases} \dot{x}(t) = (A_0 - B_0K_0)x(t) + \widetilde{B_0K_0}e_0(t) + \emptyset\big(x(t)\big) + B_0K_0x_r(t) + D\,T_L \\ \dot{e}_o(t) = (AA_0 - L_0C_e)e_o(t) + \Big(\emptyset_e\big(x_e(t)\big) - \emptyset_e\big(\hat{x}_e(t)\big)\Big) \end{cases} \tag{4-12}$$

Where $\widetilde{B_0K_0} = [B_0K_0 \;\; \mathbf{0}]$

When we apply The MVT on the nonlinear parts in (4-12), so, the augmented dynamic systems becomes[1, 2]:

$$\begin{bmatrix} \dot{x} \\ \dot{e}_o \end{bmatrix} = \begin{bmatrix} A_0 - B_0K_0 + \sum_{i=1}^{n}\sum_{j=1}^{n} e_n(i)e_n^T(j)\frac{\partial \emptyset_i}{\partial z_j}(z_{1i}) & \widetilde{B_0K_0} \\ \mathbf{0} & AA_0 - L_0C_e + \sum_{i=1}^{n}\sum_{j=1}^{n} e_n(i)e_n^T(j)\frac{\partial \emptyset_{ei}}{\partial z_{ej}}(z_{2i}) \end{bmatrix}\begin{bmatrix} x \\ e_o \end{bmatrix} + B_0K_0\begin{bmatrix} x_r \\ \mathbf{0} \end{bmatrix} + D\begin{bmatrix} T_L \\ \mathbf{0} \end{bmatrix} \tag{4-13}$$

Then, when we apply the sector nonlinearity transformations[3] on (4-13) the system can be obtain as LPV system as follows:

$$\begin{bmatrix} \dot{x} \\ \dot{e}_o \end{bmatrix} = \sum_{i=1}^{r}\sum_{j=1}^{r}\mu_i(\varepsilon)\mu_j(\zeta)\begin{bmatrix} A_0 - B_0K_0 + \mathcal{A}_i & \widetilde{B_0K_0} \\ \mathbf{0} & AA_0 - L_0C_e + \mathcal{A}\mathcal{A}_j \end{bmatrix}\begin{bmatrix} x \\ e_o \end{bmatrix} + A_0\begin{bmatrix} x_r \\ \mathbf{0} \end{bmatrix} + D\begin{bmatrix} T_L \\ \mathbf{0} \end{bmatrix} \tag{4-14}$$

If we chose $A_0 + \mathcal{A}_i = A_i$, we can obtain:

$$\begin{bmatrix} \dot{x} \\ \dot{e}_o \end{bmatrix} = \sum_{i=1}^{r}\sum_{j=1}^{r}\mu_i(\varepsilon)\mu_j(\zeta)\begin{bmatrix} A_i - B_0K_0 & \widetilde{B_0K_0} \\ \mathbf{0} & AA_0 - L_0C_e + \mathcal{A}\mathcal{A}_j \end{bmatrix}\begin{bmatrix} x \\ e_o \end{bmatrix} + B_0K_0\begin{bmatrix} x_r \\ \mathbf{0} \end{bmatrix} + D\begin{bmatrix} T_L \\ \mathbf{0} \end{bmatrix} \tag{4-15}$$

4.2.4. Augmented state feedback controller

Then, the PI control law is presented below as known as:

$$u(t) = -[K_0 \quad K_I]\begin{bmatrix} e_c(t) \\ e_I(t) \end{bmatrix} = -\overline{K}\begin{bmatrix} e_c(t) \\ e_I(t) \end{bmatrix} \tag{4-16}$$

Such that:

$$\dot{e}_I(t) = \underline{\hat{x}}_e(t) - x_r(t) \tag{4-17}$$

One can express the dynamics of the augmented closed-loop control state equation as:

$$\dot{\bar{x}}(t) = \sum_{j=1}^{r} \mu_i(\varepsilon)\,(\bar{A}_i - \bar{B}\bar{K})\bar{x}(t) + \overline{\widetilde{B_0K_0}}e_o(t) + \bar{D}\bar{w}(t) \tag{4-18}$$

Where $\zeta \in [x, \hat{x}]$, $\varepsilon \in [x, x_r]$ and

$$\bar{A}_i = \begin{bmatrix} A_0 + \mathcal{A}_i & \mathbf{0} \\ \boldsymbol{I} & \mathbf{0} \end{bmatrix};\ \bar{B} = \begin{bmatrix} B_0 \\ \mathbf{0} \end{bmatrix};\ \bar{D} = \begin{bmatrix} B_0K_0 & D \\ \mathbf{0} & \mathbf{0} \end{bmatrix};\ \bar{w} = \begin{bmatrix} x_r \\ T_L \end{bmatrix};\ \overline{\widetilde{B_0K_0}} = \begin{bmatrix} \widetilde{B_0K_0} \\ \mathbf{0} \end{bmatrix}$$

Therefore, the global state equation (observer/controller) under the control is:

$$\begin{bmatrix} \dot{\bar{x}} \\ \dot{e}_o \end{bmatrix} = \sum_{i=1}^{r}\sum_{j=1}^{r} \mu_i(\varepsilon)\mu_j(\zeta) \begin{bmatrix} \bar{A}_i - \bar{B}\bar{K} & \overline{\widetilde{B_0K_0}} \\ \mathbf{0} & AA_0 - L_0C_e + \mathcal{A}\mathcal{A}_j \end{bmatrix} \begin{bmatrix} \bar{x} \\ e_o \end{bmatrix} + \bar{D}\begin{bmatrix} \bar{w} \\ \mathbf{0} \end{bmatrix} \tag{4-19}$$

One can obtain the design of the controller gain and the Extended observer of the equation (4-19) by using the separation principle [4]. Consequently, one can separately analyse the stability of the augmented equations by utilising a quadratic Lyapunov function having a common matrix for every state equation below [5]:

$$\dot{\bar{x}}(t) = \sum_{j=1}^{r} \mu_i(\varepsilon)\,(\bar{A}_i - \bar{B}\bar{K})\bar{x}(t) + \overline{\widetilde{B_0K_0}}e_o(t) + \bar{D}\bar{w}(t) \tag{4-20}$$

And

$$\dot{e}_o(t) = \sum_{j=1}^{r} \mu_j(\zeta)\left(AA_0 - L_0C_e + \mathcal{A}\mathcal{A}_j\right)e_o(t) \tag{4-21}$$

4.2.5. Stability analysis

$$V\big(\bar{x}(t)\big) = \bar{x}^T(t)P\bar{x}(t)\,, \qquad P = P^T > 0 \tag{4-22}$$

And

$$W\big(e_o(t)\big) = {e_o}^T(t)Se_o(t)\,, \qquad S = S^T > 0 \tag{4-23}$$

Respectively

When one obtains the derivative of the Lyapunov functions (4-22) and (4-23) as follows:

$$\dot{V}\big(\bar{x}(t)\big) = \bar{x}^T(t)\left({\bar{A}_i}^T P + P\bar{A}_i - \bar{K}^T\bar{B}^T P - P\bar{B}\bar{K}\right)\bar{x}(t) \tag{4-24}$$

And

$$\dot{W}\left(e_o(t)\right) = {e_o}^T(t)\left((A_0^T S + SA_0 - C^T L_0^T S - SL_0 C) + \mathcal{A}_j^T S + \mathcal{A}_j\right) e_o(t) \quad (4\text{-}25)$$

Theorem 3: *One can classify the augmented dynamics systems (4-26) and (4-27) as asymptotically stable, if there exist* $S = S^T > 0$, $P = P^T > 0$, *in such a way that*

$$P{\bar{A}_i}^T + \bar{A}_i P - M^T \bar{B}^T - \bar{B}M + \alpha P < 0 \quad (4\text{-}26)$$

And

$$AA_0^T S + SAA_0 + \mathcal{A}\mathcal{A}_j^T S + S\mathcal{A}\mathcal{A}_j - {C_e}^T N^T - NC_e + \beta S < 0 \quad (4\text{-}27)$$

One can determine the gains of the controller and the observer as follows:

$\bar{\boldsymbol{K}} = MP^{-1}$, $\boldsymbol{L_0} = S^{-1}N$ *respectively.*

4.2.6. Simulation results

The proposed extended observer-based control is applied based on the MVT theory. The results of the simulation are obtained through the MATLAB/SIMULINK environment. As proof of the efficacy of this approach, it's applied to a PMSM drive, which has the parameters in Appendix 2:

Figure 1 presents the general scheme of the extended observer-based PI-MVT controller. This is used to estimate the two-line stator currents, the rotor speed, the rotor position, and the load torque.

The determination of the observer and controller gains was done using theorems (4-26) and (4-27) by the exploiting of the YALMIP software computer and their values are given below:

$$\boldsymbol{L_0} = \mathbf{10^2} * \begin{bmatrix} \mathbf{12} & \mathbf{-45} \\ \mathbf{-20} & \mathbf{180} \\ \mathbf{260} & \mathbf{-467} \\ \mathbf{-30} & \mathbf{-310} \\ \mathbf{-1730} & \mathbf{1220} \end{bmatrix}$$

$$\overline{\boldsymbol{K}} = \begin{bmatrix} \mathbf{-43} & \mathbf{106} & \mathbf{56} & \mathbf{-12162} & \mathbf{7610} & \mathbf{-0.391} \\ \mathbf{23} & \mathbf{-27} & \mathbf{319} & \mathbf{-5134} & \mathbf{-65} & \mathbf{2413} \end{bmatrix}$$

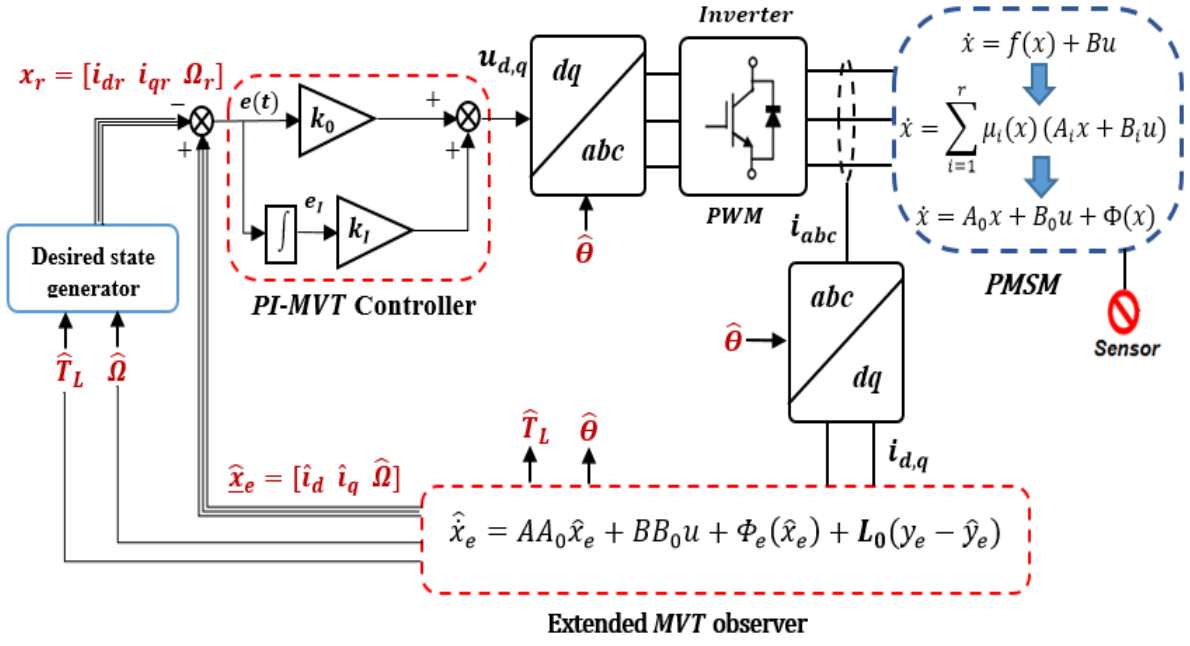

Figure 4.1 Overall scheme of the suggested extended *MVT* observer based *PI-MVT* controller.

It has been proposed that the simulation results can be used to demonstrate the efficacy of the approach with a PWM inverter, as presented in figure 4.2 The desired states were selected through the orange line, where the estimated and the real states were presented by the dashed red and black lines, respectively. The desired rotor speed's trajectory begins by a step of 150 rad/sec and goes down to 50 rad/sec at t = 0.5 sec. To conduct the negative tests, a desired speed of -150 rad/sec is selected at t = 1 sec. alternatively, the zero speed is implemented at t = 1.5 sec until the test is finished. First, the PMSM is unloaded until t = 0.2 sec, then, it applies a load torque of 6 Nm to the motor for all the remaining time. This is illustrated in figure 4.2-g. Both figure 4.2-b and figure 4.2-c demonstrate the desired, the real, and the estimated d, q axis stator currents, respectively. In figure 4.2-d, the three-phase line stator currents are demonstrated. The real and estimated values for the rotor position and the load torque are given in figure 4.2-e and figure 4.2-g, respectively, on the other hand, their estimation errors are given in figure 4.2-f and figure 4.2-h.

In order to illustrate the stability and the efficiency of the MVT extended observer, the initial estimated states ($\hat{x}_{e0}$) are selected to be $[0\ 0\ -20\ 0\ 0]^T$.

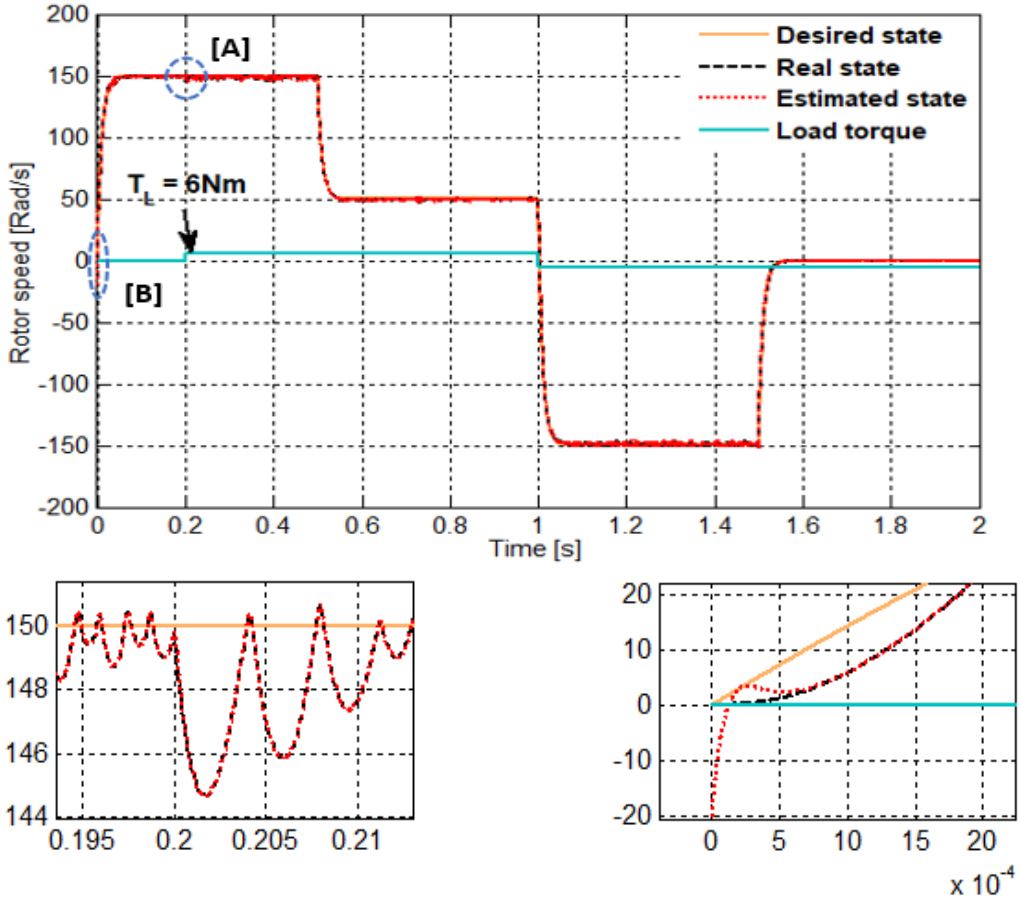

Zoom of [A] ***Zoom of [B]***

(a)

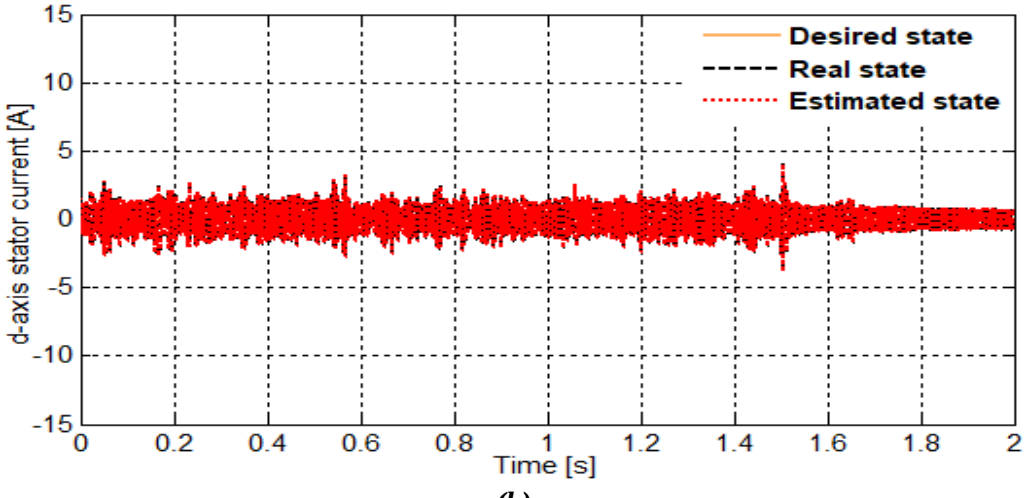

(b)

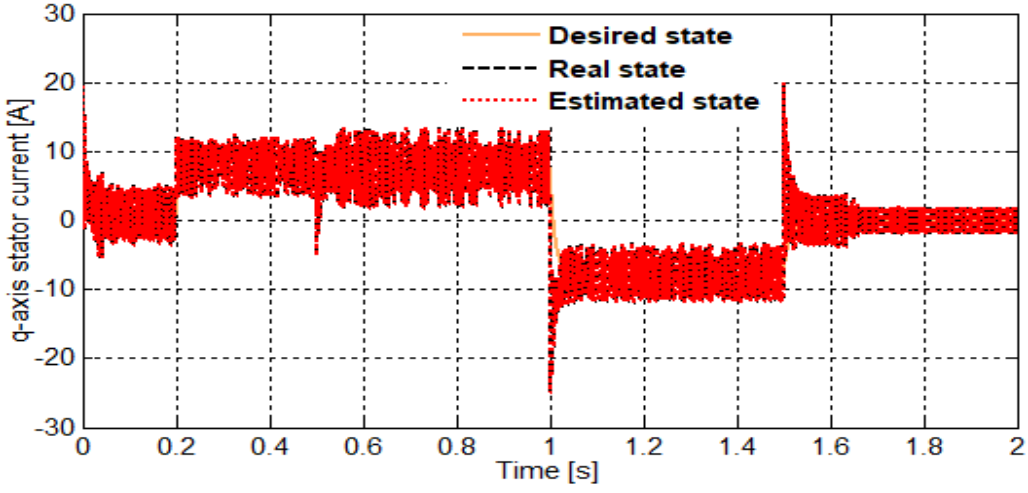
Desired state
Real state
Estimated state
q-axis stator current [A]
Time [s]

(c)

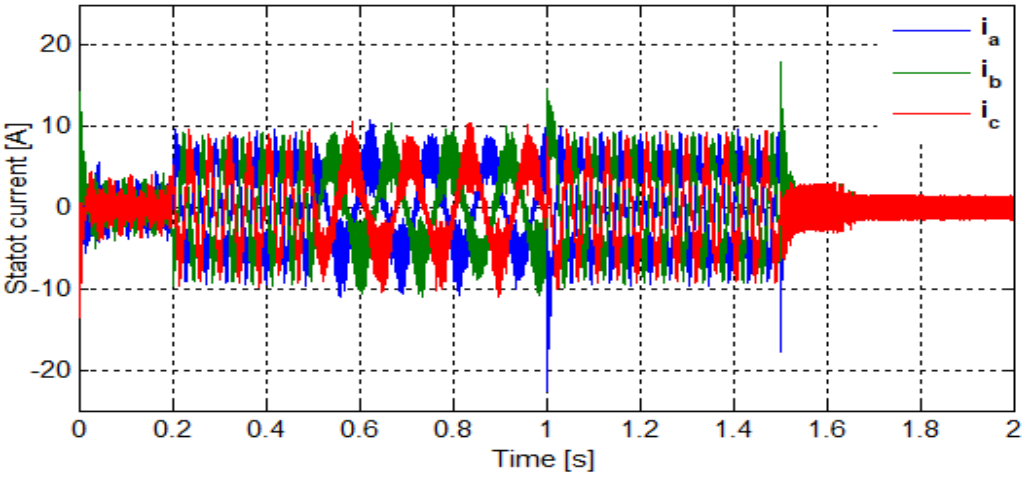
i_a
i_b
i_c
Statot current [A]
Time [s]

(d)

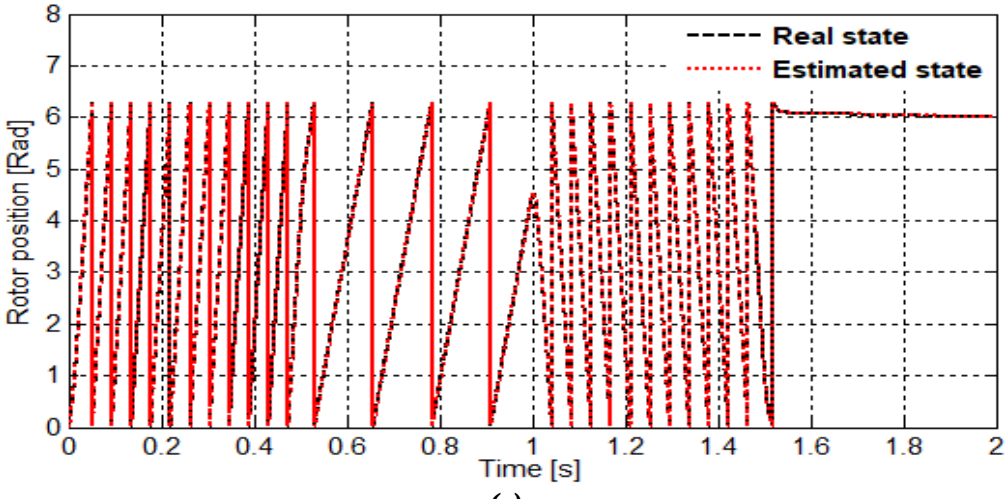
Real state
Estimated state
Rotor position [Rad]
Time [s]

(e)

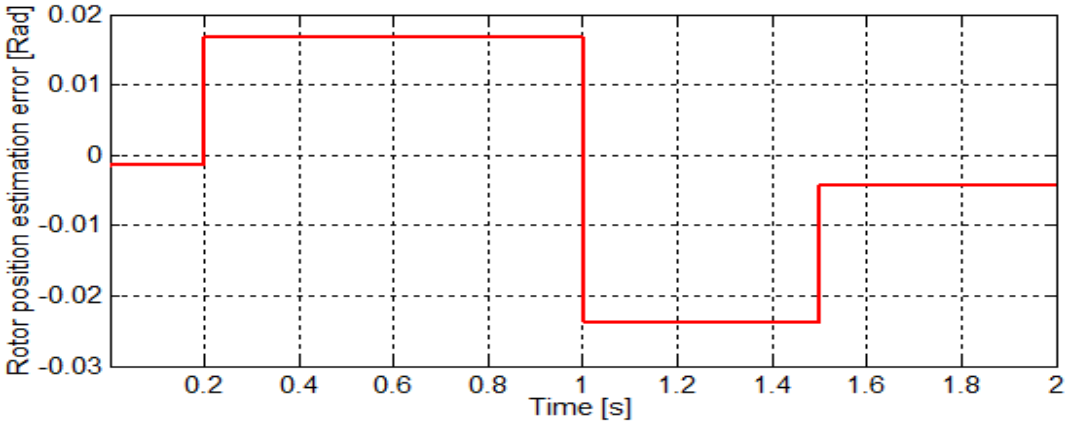

(f)

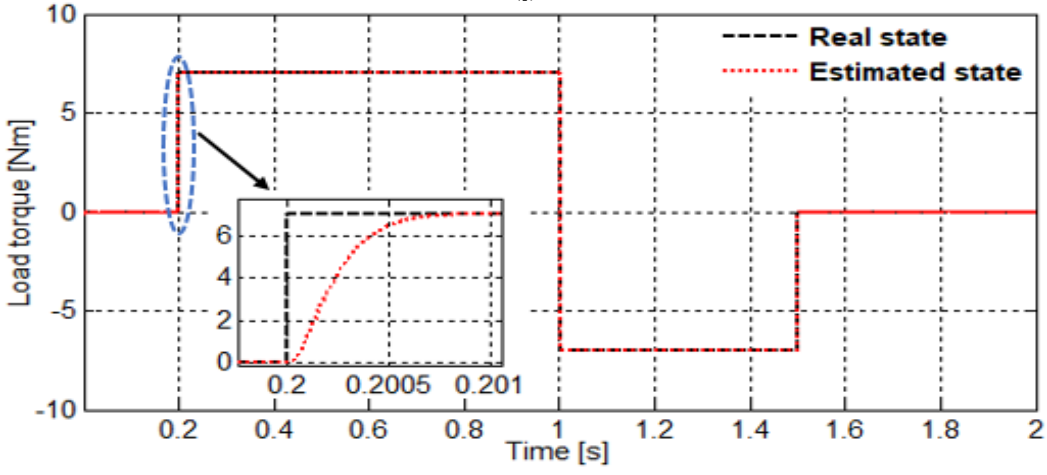

(g)

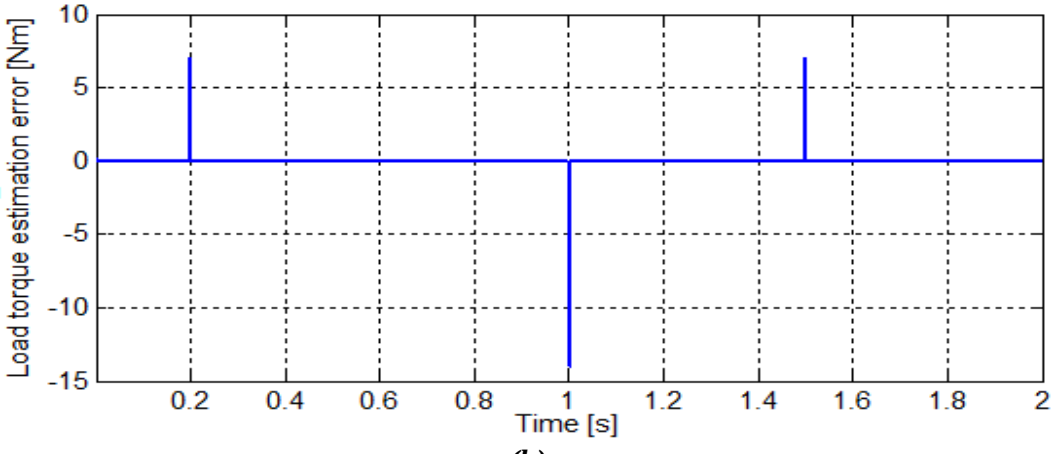

(h)

Figure 4.2 Simulation results of extended observer based *PI-MVT* controller with a PWM inverter: *(a)* Rotor speed; *(b)* d-axis stator current; *(c)* q-axis stator current ; *(d)* i_{abc} stator currents; *(e)* Real and estimate rotor position; *(f)* Rotor position estimation error; *(g)* Real and estimate load torque; *(h)* load torque estimation error.

It was emphasized that the PWM inverter exhibited chattering on the stator currents and the rotor speed as a result of the switching of the inverter. Based on figure 4.2-a, it has been observed that the estimated and the real states of the rotor speed are in closer proximity to its desired value. In despite of the application of the nominal load torque at t = 0.2 sec, the rotor speed still subject to the control and the estimation conditions with a minimum effect on these conditions.

It was also observed that the real and the estimated states of d-axis stator current stayed near zero ($I_d = 0$), whereas its q-axis is a reproduction to the torque which shows that the FOC is assured at the moment where the estimation errors is approximately zero as shown in figures 4.2-b and 4.2-c.

However, the load torque and the rotor position are not originally considered as states of the PMSM drive, the estimation error of the rotor position doesn't exceed 0.02 and for the load torque is near zero as shown in figure 4.2-f and figure 4.2-h, respectively. The estimated states are considered to be close to their real values despite the fact that the starting conditions of the estimated states are not zero. In all the simulation results given above, there is guaranteed success for the proposed extended observer-based PI-MVT controller and it can replace the other technics in the industrial applications due its effectiveness, simplicity and low cost.

4.2.7. Conclusion

In this part of the chapter, an extended observer based-controller was applied to the PMSM drive. This concept is based on the combination of the MVT approach and the sector non-linearity theory. The non-linear model of the PMSM was transformed to the Lipchitz form and based on that form, it was possible to express the PMSM drive's non-linear augmented system dynamics as an LPV system. This study mainly aims to stabilize the MVT control-based observer by separately finding each gain that does not rely on the PMSM drive states. The stability analyses of observer based controller were assured through a proven methodology based on the Lyapunov theory. The obtained results mentioned above prove the effectiveness of this approach, the stability of all the system is proven, the simplicity of the implementation, the low cost of the hardware. This concept can substitute the non-linear and the complex approaches in the industrial applications.

4.3. PI-MVT controller for PMSM application

In this part, a nonlinear controller for a field-oriented control (FOC) of a PMSM based on MVT is presented. Using MVT and sector nonlinearity transformation, the nonlinear error dynamics of the state feedback system is represented by an LPV system. By using Lyapunov theorem, stability conditions are expressed in terms of LMIs, whereby the gains of the controller can be calculated. To study the effectiveness of the proposed controller, an experiment of a controller for a field-oriented control on a 415 W PMSM is conducted. Results indicated that in spite of the varying load torque disturbances, good speed tracking and field orientation are achieved.

4.3.1. Controller design

4.3.1.1. Problem statement

The state space form with the stator current (i_d and i_q) and rotor speed as the state variables, can be written as follows:

$$\begin{aligned} \dot{x}(t) &= f\big(x(t)\big) + Bu(t) \\ y(t) &= Cx(t) \end{aligned} \tag{4-28}$$

Where

$$f\big(x(t)\big) = \begin{bmatrix} -\frac{R_s}{L_d}x_1 + \frac{L_q}{L_d}p\,x_2x_3 \\ -\frac{R_s}{L_q}x_2 - \frac{L_d}{L_q}p\,x_1x_3 + \frac{\Phi_f}{L_q}p\,x_3 \\ \frac{3P}{2J}\Phi_f\,x_2 - \frac{f_c}{J}x_3 - \frac{1}{J}\,T_L \end{bmatrix};\ B = \begin{bmatrix} \frac{1}{L_d} & 0 \\ 0 & \frac{1}{L_q} \\ 0 & 0 \end{bmatrix};\ x = \begin{bmatrix} x_1 \\ x_2 \\ x_3 \end{bmatrix} = \begin{bmatrix} i_d \\ i_q \\ \Omega \end{bmatrix};\ u = \begin{bmatrix} u_d \\ u_q \end{bmatrix}$$

These equations can be transformed into Lipchitz form as follows:

$$\begin{aligned} \dot{x}(t) &= A_0x(t) + B_0u(t) + \emptyset\big(x(t)\big) \\ y(t) &= Cx(t) \end{aligned} \tag{4-29}$$

Where

$$A_0 = \begin{bmatrix} -\frac{R_s}{L_d} & 0 & 0 \\ 0 & -\frac{R_s}{L_q} & \frac{\Phi_f}{L_q}p \\ 0 & \frac{3p}{2J}\Phi_f & -\frac{f_c}{J} \end{bmatrix}$$

And $\emptyset(x(t))$ is given by:

$$\emptyset(x(t)) = f(x(t)) - A_0 x(t)$$

4.3.1.2. State feedback regulator design with MVT

According to the state feedback control law, the control vector is given by:

$$u(t) = -K_0 e(t) \tag{4-30}$$

$$e(t) = x(t) - x_r(t) \tag{4-31}$$

In (4-31), x_c is the desired states, given by $x_c = [i_{dc} \quad i_{qc} \quad \Omega_c]^T$.

The objective is to determine the gain matrix K_0 such that the non-linear system (4-29) becomes asymptotically stable.

$$\dot{e}(t) = \dot{x}(t) - \dot{x}_c(t) \tag{4-32}$$

With $\dot{x}_c(t) = 0$ (a stepwise signal), then from (4-29) and (4-32) we can write:

$$\dot{e}(t) = \dot{x}(t) = (A_0 - B_0 K_0)e(t) + \{\emptyset(x) - \emptyset(x_c)\} + A_0 x_c \tag{4-33}$$

The MVT and the sector nonlinearity transformation are then applied to the nonlinear part of the Lipchitz system in (4-33), such that

$$\dot{x}(t) = \sum_{i=1}^{r} \mu_i(\varepsilon)\,(A_i - B_0 K_0)e(t) + A_0 x_c \tag{4-34}$$

Where $A_i = A_0 + \mathcal{A}_i$

4.3.1.3. Augmented feedback regulator (PI)

In order to obtain zero steady-state error states, an integral action is added to forward path; thus, the structure of the controller becomes similar to the PI controller. With the integration in the state error, new state variables are added, i.e.

$$(t) = -[K_0 \quad K_I]\begin{bmatrix} e(t) \\ e_I(t) \end{bmatrix} = \bar{K}\bar{e}(t), \tag{4-35}$$

Where the derivative of the state error for the new states is given by:

$$\dot{e}_I(t) = x(t) - x_c(t) \tag{4-36}$$

By replacing (4-35) and (4-36) into (4-29) and applying the same steps as before, the dynamics of the augmented closed-loop control state equation is obtained as:

$$\dot{\bar{x}}(t) = \sum_{i=1}^{r} \mu_i(\varepsilon)\left((\bar{A}_i - \bar{B}\bar{K})\bar{e}(t)\right) \tag{4-37}$$

Where $\bar{A}_i = \begin{bmatrix} A_0 + \mathcal{A}_i & 0 \\ I & 0 \end{bmatrix}$ and $\bar{B} = \begin{bmatrix} B_0 \\ 0 \end{bmatrix}$

The stability can be studied using the quadratic Lyapunov function, given by

$$V\left(\bar{e}(t)\right) = \bar{e}^T(t)P\bar{e}(t)\,, \qquad P = P^T > 0 \tag{4-38}$$

For more details about the stability analysis see chapter III. So the closed-loop control of dynamics systems is said to be asymptotically stable if there exist $P = P^T > 0$, such that

$$P\bar{A_i}^T + \bar{A_i}P - M^T B_0^T - B_0 M + \alpha P < 0 \tag{4-39}$$

For $i = 1, \ldots, r$, where α is the rate of convergence.

Finally, the gains of the controller can be determined from $\bar{K} = MP^{-1}$. From the parameters of the PMSM (Appendix C), the matrix gain $\bar{\boldsymbol{K}}$ is obtained as:

$$\bar{\boldsymbol{K}} = \begin{bmatrix} -4.548 & 0.231 & 42.65 & -12162 & 7610 & -0.391 \\ 0.231 & -4.548 & 319 & -5134 & -65 & 2413 \end{bmatrix}$$

4.3.2. Experimental results

As proof of the efficacy of the control strategies developed in this paper applied to the PMSM drive under FOC, an experimental test bench, shown in figure 4.4, is built in the electrical engineering laboratory of Biskra University (LGEB), where the parameters data of the PMSM are given in Appendix C. It consists mainly of: 415 Watt permanent magnet synchronous motor, a DC generator supplies a resistive three-phase load using as a load torque, an incremental position sensor, a controlled voltage source, a pulse width modulation (PWM) SEMIKRON inverter, built around three IGBT modules and three-phase AC/DC converter with a common capacitive DC link. The control algorithms are implemented with a DSPACE 1104 single card from Texas instruments with a TMS32F240 DSP, using Matlab-Simulink package. The connection between the DSPACE card and the power converters are carried out by an interface card, which adapts the control signal levels. The different currents and voltages are ensured, respectively by LA25NP and LV25P hall sensors, as indicated in figure 4.4. The figure 4.3 demonstrate the synoptic of the PI-MVT control strategy under FOC which used in this work.

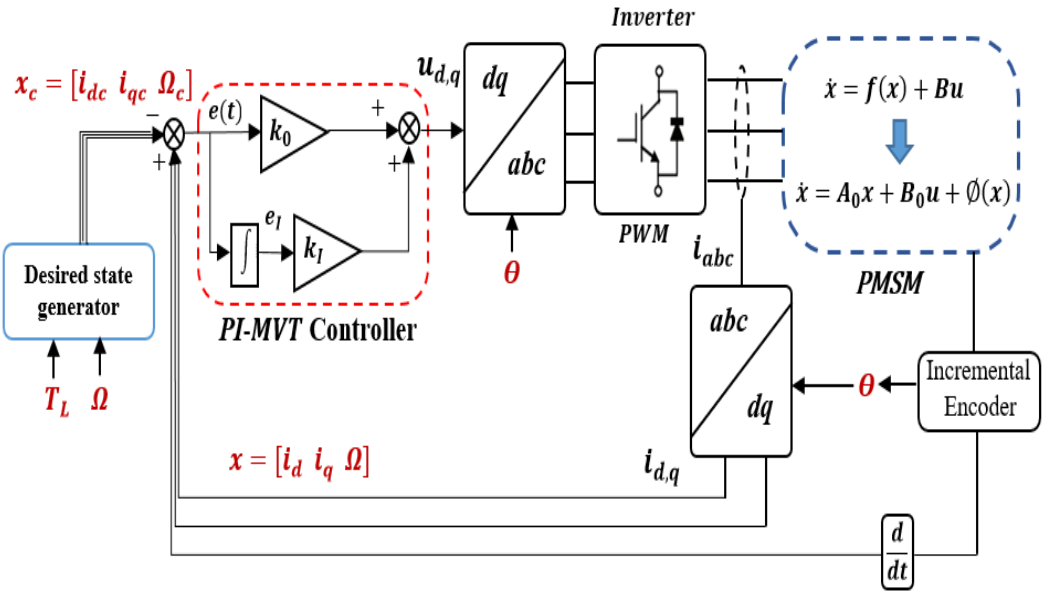

Figure 4.3 Synoptic of the PI-MVT control strategy.

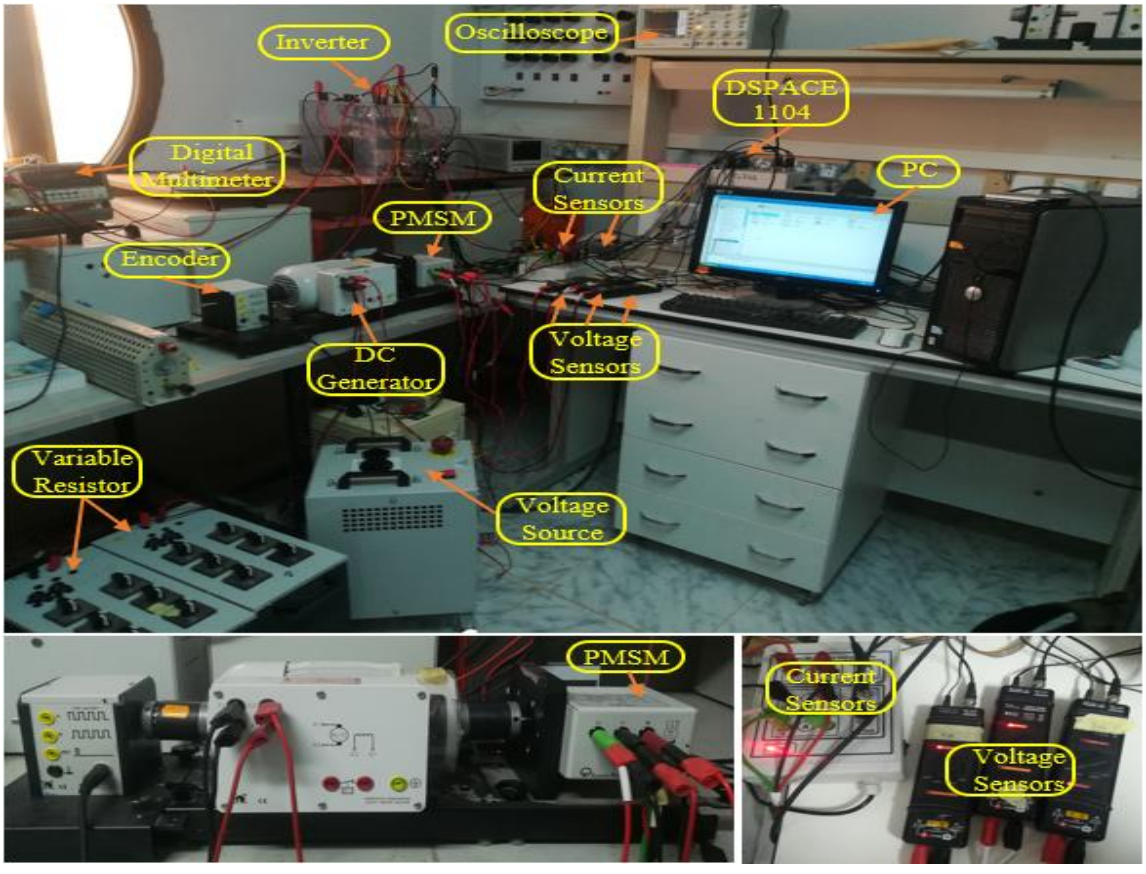

Figure 4.4 Global system experimental test.

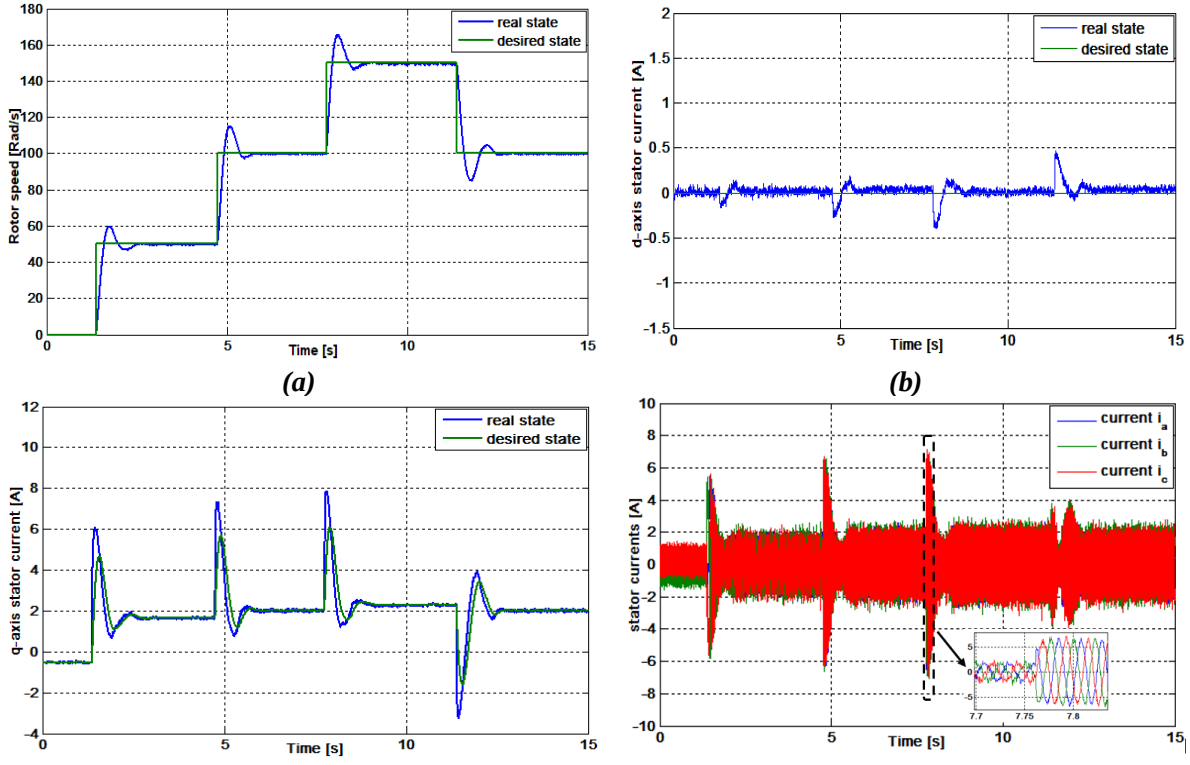

Figure 4.5 Experimental results of *PI-MVT* controller without load torque: ***(a)*** Rotor speed, ***(b)*** d-axis stator current; ***(c)*** q-axis stator current, ***(d)*** Three phase stator currents.

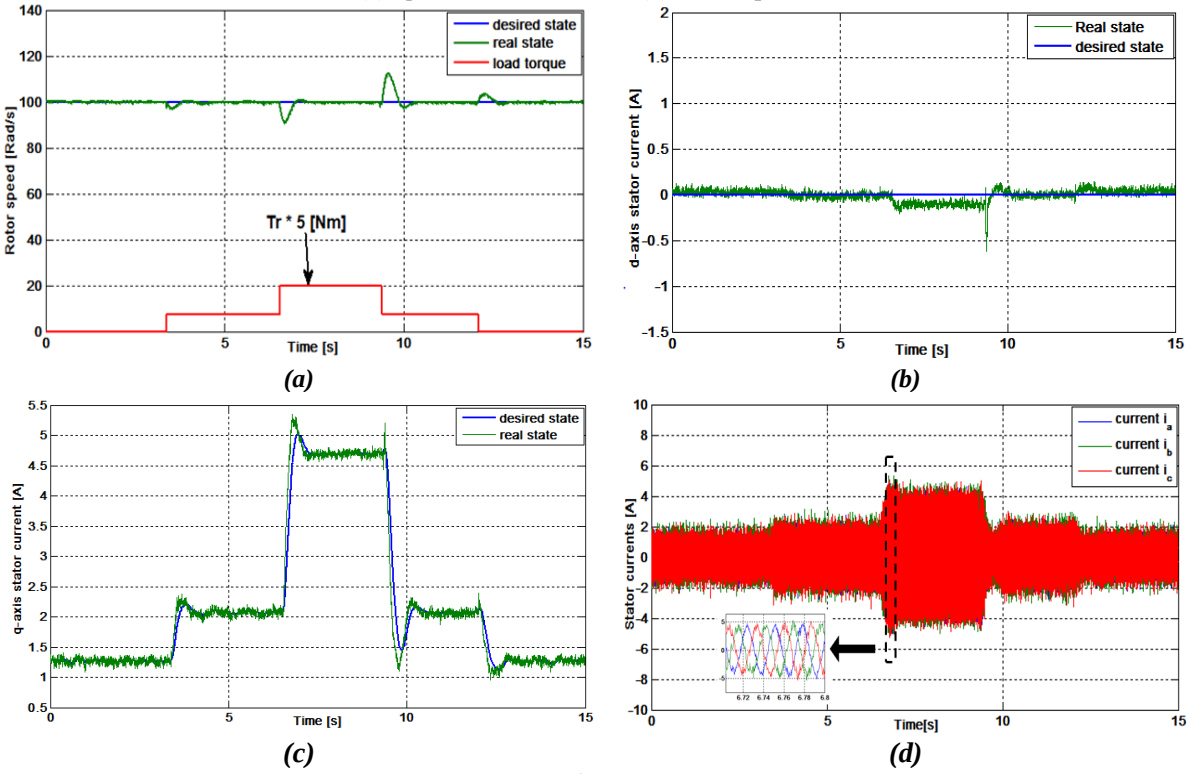

Figure 4.6 Experimental results of *PI-MVT* controller with load torque:

(a) Rotor speed, ***(b)*** d-axis stator current; ***(c)*** q-axis stator current, ***(d)*** Three phase stator currents.

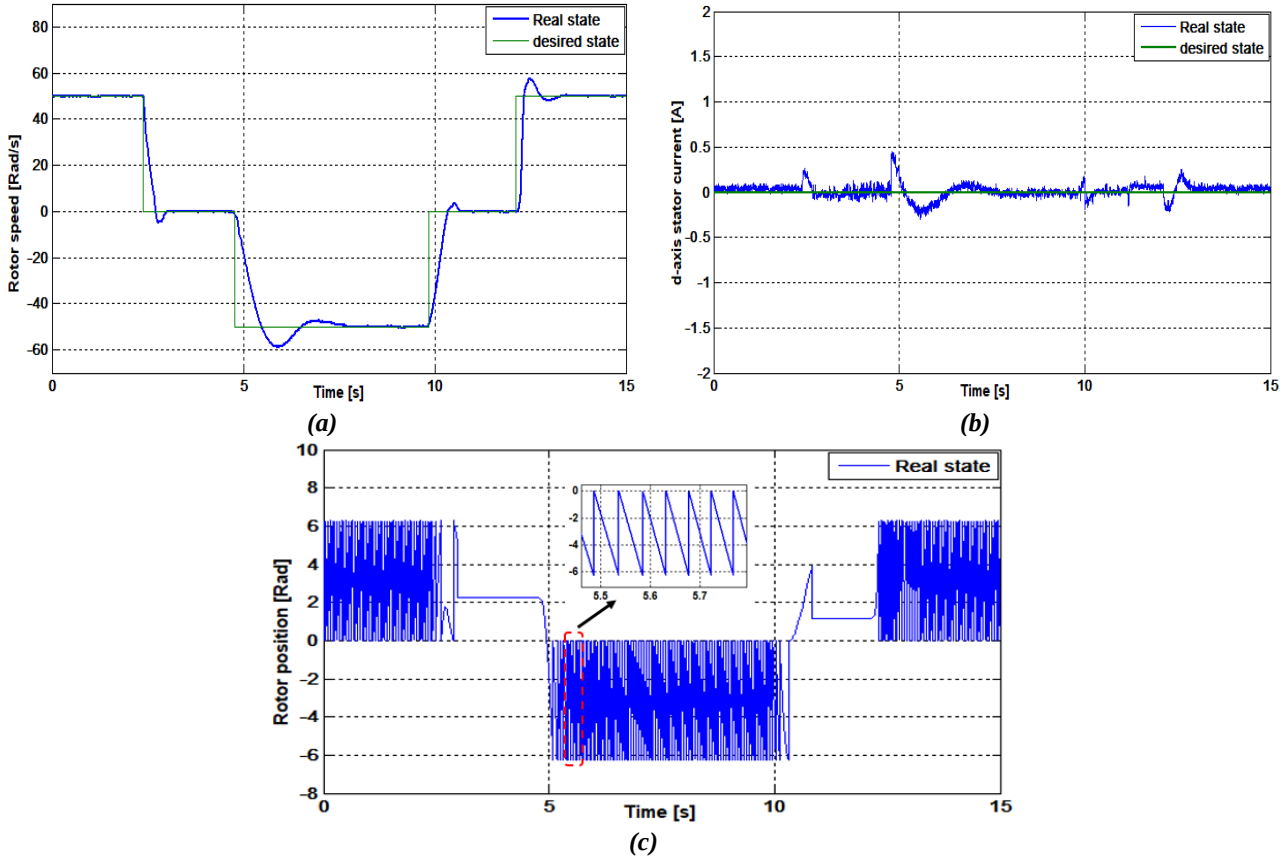

Figure 4.7 Experimental results of *PI-MVT* controller with reversal of speed: ***(a)*** Rotor speed, ***(b)*** d-axis stator current, ***(c)*** Rotor position.

As can be seen that the structure of the controller is similar to having 3 PI controllers, one for each state. The desired states $(i_{dc}\ \ i_{qc}\ \ \Omega_c)^T$ are generated from the load torque and FOC torque equations $(i_{dc} = 0)$. Three sets of experiments were conducted: (1) Step changes in rotor speed reference (of 50 rad/s per step) with $T_L = 0$. Experiment (2) step changes in load torque T_L with constant rotor speed at 100 rad/s, and experiment (3) step changes in rotor speed in reverse direction with constant load torque T_L. Figure 3 shows the results for experiment (1) which clearly indicates the quick and precise speed tracking. The d-axis stator current remains zero and the q-axis component of the stator current indicates fast torque response with zero steady-state tracking error. In experiment (2), the load variation causes slight deviation in speed response; however, the speed managed to recover due to the quick torque (i_q) response. Finally, experiment (3)

demonstrates the capability of the controller to perform in the reverse speed. The rotor position clearly shows the stationary and reversal speed operations with

4.4. Conclusion

In this part of chapter, the design of the controller for FOC of PMSM based on state feedback using MVT is presented. The structure of the proposed controller is similar to the PI controller, with the gains calculated by solving the LMIs formulated using the Lyapunov stability conditions. The experimental results indicated that the proposed controller managed to perform effectively under load torque disturbances and reference speed variation, despite its simple implementation.

References of chapter IV

[1] M. Y. Hammoudi, A. Allag, M. Becherif, M. Benbouzid, and H. Alloui, "Observer design for induction motor: an approach based on the mean value theorem," *Frontiers in Energy*, vol. 8, pp. 426-433, 2014.

[2] D. Ichalal, B. Marx, S. Mammar, D. Maquin, and J. Ragot, "Observer for Lipschitz nonlinear systems: mean value theorem and sector nonlinearity transformation," in *Intelligent Control (ISIC), 2012 IEEE International Symposium on*, 2012, pp. 264-269.

[3] G. Phanomchoeng, R. Rajamani, and D. Piyabongkarn, "Nonlinear observer for bounded Jacobian systems, with applications to automotive slip angle estimation," *IEEE Transactions on Automatic Control*, vol. 56, pp. 1163-1170, 2011.

[4] J. Yoneyama, "Nonlinear control design based on generalized Takagi–Sugeno fuzzy systems," *Journal of the Franklin Institute*, vol. 351, pp. 3524-3535, 2014.

[5] K. Tanaka and H. O. Wang, *Fuzzy control systems design and analysis: a linear matrix inequality approach*: John Wiley & Sons, 2004.

CHAPTER V

Robust Extended H_∞ Observer and Controller Based on the MVT Approach Applied to the PMSM Drive

5.1. Introduction

In this chapter, we will focus on the synthesis of an extended H_∞ observer and H_∞ controller. The observer and controller are based on the MVT approach applied to the PMSM drive, the extended observer is under the Open Loop Field Oriented Control (OL-FOC).

The extended observer and controller design are based on the MVT combined with the sector nonlinearity approach to stabilizing the observer and controller dynamic errors of PMSM drive and ensured a minimum disturbance attenuation level to the error. The dynamics of the error are exhibited as a convex theory association of known matrices with time-varying parameters after representing the nonlinear system of the PMSM as a Lipschitz form. Using the Lyapunov theory, the stability terms are obtained and expressed in form of LMIs, the extended observer gain and the controller gain are calculated offline by solving the LMIs. With two line currents are measured, the extended observer estimates all PMSM drive states and moreover the rotor position. At the end, the suggested approach is applied to PMSM machine under OL-FOC through an illustrative simulation to affirm the effectiveness of the concept.

5.2. Robust extended MVT_H_∞ observer design

5.2.1. Problem declaration

By setting the assumption that the rotor position can be taken as state variable, one can write the mathematical model of the PMSM, which is utilised for observation, as follows[1]:

$$\begin{cases} \dot{x}_e(t) = f_e\big(x_e(t)\big) + B_e u(t) + D_w w(t) \\ y_e(t) = C_e x_e(t) \end{cases} \tag{5-1}$$

Where

$$f_e\left(x_e(t)\right) = \begin{bmatrix} -\frac{R_s}{L_d}x_{e1} + \frac{L_q}{L_d}px_{e2}x_{e3} \\ -\frac{R_s}{L_q}x_{e2} + -\frac{L_d}{L_q}px_{e1}x_{e3} + \frac{\Phi_f}{L_q}px_{e3} \\ \frac{3p}{2J}\Phi_f x_{e2} + -\frac{f}{J}x_{e3} \\ x_{e3} \end{bmatrix} \quad (5\text{-}2)$$

$$B_e = \begin{bmatrix} \frac{1}{L_d} & 0 \\ 0 & \frac{1}{L_q} \\ 0 & 0 \\ 0 & 0 \end{bmatrix};\ D_w = \begin{bmatrix} 0 & 0 & -\frac{1}{J} & 0 \end{bmatrix}^T$$

$x_e = [x_{e1}\ x_{e2}\ x_{e3}\ x_{e4}]^T = [i_d\ \ i_q\ \ \Omega\ \ \theta]^T$, $u = [u_d\ \ u_q]^T$ and $w(t) = T_L$

The extended state model of the PMSM (5-1) can be transferred into the Lipchitz form as [2]:

$$\begin{cases} \dot{x}_e(t) = A_{e0}x_e(t) + B_e u(t) + \emptyset_e\left(x_e(t)\right) + D_w w(t) \\ y_e(t) = C_e x_e(t) \end{cases} \quad (5\text{-}3)$$

Where

$$A_{e0} = \begin{bmatrix} a_1 & 0 & 0 & 0 \\ 0 & b_1 & b_3 & 0 \\ 0 & c_1 & c_2 & 0 \\ 0 & 0 & 1 & 0 \end{bmatrix}$$

And $\emptyset_e(x_e(t))$ is defined by

$$\emptyset_e(x_e(t)) = f_e(x_e(t)) - A_{e0}x_e(t) \quad (5\text{-}4)$$

The state equation of the observer can also be presented in the following Lipchitz form

$$\begin{cases} \dot{\hat{x}}_e(t) = A_{e0}\hat{x}_e(t) + B_e u(t) + \emptyset_e\left(\hat{x}_e(t)\right) + L_0\left(y_e(t) - \hat{y}_e(t)\right) \\ \hat{y}_e(t) = C_e\hat{x}_e(t) \end{cases} \quad (5\text{-}5)$$

Where $\emptyset_e(\hat{x}_e(t))$ is defined by

$$\emptyset_e\left(\hat{x}_e(t)\right) = f_e(\hat{x}_e(t)) - A_{e0}\hat{x}_e(t) \quad (5\text{-}6)$$

For that purpose, let us define the estimation error $e_o(t)$ such that $e_o(t) = x_e(t) - \hat{x}_e(t)$. Using (5-5) and (5-1), the dynamic of the state estimation error is obtained as follows

$$\dot{e}_o(t) = (A_{e0} - L_0 C_e) e_o(t) + \left(\emptyset_e\left(x_e(t)\right) - \emptyset_e\left(\hat{x}_e(t)\right)\right) + D_w w(t) \tag{5-7}$$

The MVT and the sector nonlinearity transformation are then applied to the nonlinear part of the Lipchitz system in (5-7), such that [3-8]:

$$\dot{e}_o(t) = \sum_{i=1}^{q} \mu_i(\xi)\,(F_i e(t)) + D_w w(t) \tag{5-8}$$

With $F_i = A_{e0} - L_0 C_e + \mathcal{A}_i$ and $\xi \in [x, \hat{x}]$

5.2.2. Extension for H_∞ performance

In this section, we illustrate the formulation for H_∞ performance for the extended MVT observer. The existence of the disturbances $w(t)$ will affect to the control performances. So as to minimize the effect of the disturbance $w(t)$, the H_∞ performances related the state feedback control error has been taken into account [9, 10].

Definition .1:

We call Nome H_∞ of the transfer T_∞ between $w(t)$ and $e(t)$:

$$\|T_{ew}\|_\infty = sup_{\|w(t)\|_2 \neq 0} \frac{\|e(t)\|_2}{\|w(t)\|_2} \tag{5-9}$$

Where

$$\|w(t)\|_2 = \int_0^\infty \sigma^T(t)\,\sigma(t)\,dt \tag{5-10}$$

The objective is to determine a control law which attenuates the effect of the external disturbances $w(t)$ on the quantity to be stabilized $e(t)$, that is to say, which minimizes the transfer between $w(t)$ and $e(t)$ such that$\|T_{ew}\|_\infty < \gamma$, with γ is the attenuation rate. In this case, we can rewrite the criterion H_∞ in the form:

$$\int_0^\infty {e_o}^T(t)\, e_o(t)\, dt \leq \gamma^2 \int_0^\infty w^T(t)\, w(t)\, dt \tag{5-11}$$

5.2.3. Stability analysis

Consider the quadratic Lyapunov function as[11, 12]:

$$V\left(e_o(t)\right) = {e_o}^T(t) P e_o(t) \tag{5-12}$$

Where $P = P^T > 0$

So, as to develop the asymptotic stability of (5-11) and to attain the H_∞ performance of the state error, the time derivative of $V(e(t))$ becomes as the following condition:

$$\dot{V}(e_o(t)) + {e_o}^T(t)e_o(t) - \gamma^2 w^T(t)w(t) < 0 \tag{5-13}$$

Replacing (5-12) in (5-13), the pervious equation becomes as a LMI form as follows:

$${\dot{e}_o}^T(t)Pe_o(t) + {e_o}^T(t)P\dot{e}_o(t) + {e_o}^T(t)e_o(t) - \gamma^2 w^T(t)w(t) < 0 \tag{5-14}$$

This is equivalent to:

$$\sum_{i=1}^{r} \mu_i(\xi(t))\, {e_o}^T(t)\left[{F_i}^T P + PF_i + I\right]e_o(t) + w^T(t)\left[{D_w}^T P\right]e_o(t) + {e_o}^T(t)[PD_w]w(t) - \gamma^2 w^T(t)w(t) < 0 \tag{5-15}$$

So,

$$\sum_{i=1}^{r} \mu_i(\xi(t))\, [{e_o}^T(t) \quad w^T(t)] \begin{bmatrix} {F_i}^T P + PF_i + I & PD_w \\ {D_w}^T P & -\gamma^2 I \end{bmatrix} \begin{bmatrix} e_o(t) \\ w(t) \end{bmatrix} < 0 \tag{5-16}$$

The stability of the state equation is verified if the time derivative of Lyapunov (5-13) is negative definite, which leads to the following time dependent LMIs:

$$\begin{bmatrix} \left[{F_i}^T P + PF_i\right] + I & PD_w \\ {D_w}^T P & -\gamma^2 I \end{bmatrix} < 0 \tag{5-17}$$

It is possible to write (5-17) as:

$$\begin{bmatrix} \left[{F_i}^T P + PF_i\right] & PD_w \\ {D_w}^T P & -\gamma^2 I \end{bmatrix} \begin{bmatrix} I & 0 \\ 0 & 0 \end{bmatrix} < 0 \tag{5-18}$$

This mean:

$$\begin{bmatrix} \left[{F_i}^T P + PF_i\right] + I & PD_w \\ {D_w}^T P & -\gamma^2 I \end{bmatrix} \begin{bmatrix} I \\ 0 \end{bmatrix} [I \quad 0] < 0 \tag{5-19}$$

Using the Schur complement, (5-19) becomes as follow

$$\begin{bmatrix} \left[{F_i}^T P + PF_i\right] & PD_w & I \\ {D_w}^T P & -\gamma^2 I & 0 \\ I & 0 & -I \end{bmatrix} < 0 \tag{5-20}$$

By applying the congruence transformation, multiplying to the right and to the left by the $diag\ [P^T, \quad I, \quad I]$ we get:

$$\begin{bmatrix} P^{-1} & 0 & 0 \\ 0 & I & 0 \\ 0 & 0 & I \end{bmatrix} \begin{bmatrix} {F_i}^T P + P F_i & P D_w & I \\ {D_w}^T P & -\gamma^2 I & 0 \\ I & 0 & -I \end{bmatrix} \begin{bmatrix} P^{-1} & 0 & 0 \\ 0 & I & 0 \\ 0 & 0 & I \end{bmatrix} < 0 \tag{5-21}$$

The previous equation can be developed to:

$$\begin{bmatrix} P^{-1}\left[{F_i}^T P + P F_i\right] P^{-1} & P^{-1} P D_w & P^{-1} \\ {D_w}^T P P^{-1} & -\gamma^2 I & 0 \\ P^{-1} & 0 & -I \end{bmatrix} < 0 \tag{5-22}$$

If we consider that $S^{-1} = P$ and $M = P L_\infty = X^{-1} L_\infty$, we can obtain the final LMIs to solving:

$$\begin{bmatrix} {A_{e0}}^T S + S A_{e0} + {\mathcal{A}_i}^T S + S \mathcal{A}_i - M C_e - {C_e}^T M^T + \alpha S & D_w & S \\ {D_w}^T & -\gamma^2 I & 0 \\ S & 0 & -I \end{bmatrix} < 0 \tag{5-23}$$

Such as the observer gain has been obtained as follows:

$$L_\infty = S^{-1} M \tag{5-24}$$

5.3. Open loop field oriented control of the PMSM

In this part, a design of the open loop control strategy of the PMSM is suggested by replacing the states of the PMSM $x_e = [i_d \;\; i_q \;\; \Omega \;\; \theta\,]^T$ by the references signals $x_{er} = [i_{dr} = 0 \;\; i_{qr} \;\; \Omega_r \;\; \theta_r]^T$ in (5-1), we can find:

$$\dot{x}_r = \begin{bmatrix} 0 \\ \dot{i}_{qr} \\ \dot{\Omega}_r \\ \dot{\theta}_r \end{bmatrix} = \begin{bmatrix} \dfrac{L_q}{L_d} p \Omega_r + \dfrac{1}{L_d} u_{dr} \\ -\dfrac{R_s}{L_q} i_{qr} + \dfrac{\Phi_f}{L_q} p \Omega_r + \dfrac{1}{L_q} u_{qr} \\ \dfrac{3 p \Phi_f}{2J} i_{qr} - \dfrac{1}{J} T_L - \dfrac{f}{J} \Omega_r \\ \Omega_r \end{bmatrix} \tag{5-25}$$

From the first and the second equations in (5-25), the formula of the open loop control of the PMSM is gotten as:

$$\begin{cases} U_{dr} = -\,L_q\, p\, \Omega_r i_{qr} \\ U_{qr} = L_q \left(\dot{i}_{qr} + \dfrac{R_s}{L_q} i_{qr} - \dfrac{\Phi_f}{L_q} p \Omega_r \right) \end{cases} \tag{5-26}$$

5.4. Simulation results and discussion

The proposed H_∞ extended observer based on the MVT theory is applied. The simulation results are obtained through the MATLAB/SIMULINK environment. As proof of the efficacy of this approach, it's applied to a PMSM drive, which has the parameters in Appendix B. The robust extended observer gain is calculated as (5-24) by solving the LMIs (5-23) given as:

$$L_\infty = \begin{bmatrix} 7793.4 & 58.0899 \\ -40.8568 & 7798.1 \\ -327.7158 & -505.1727 \\ 513.6569 & -309.3417 \end{bmatrix}$$

Figure 5.1 presents the general scheme of the extended MVT_H_∞ observer. For estimate the two-line d-q stator currents, the rotor speed, and the rotor position.

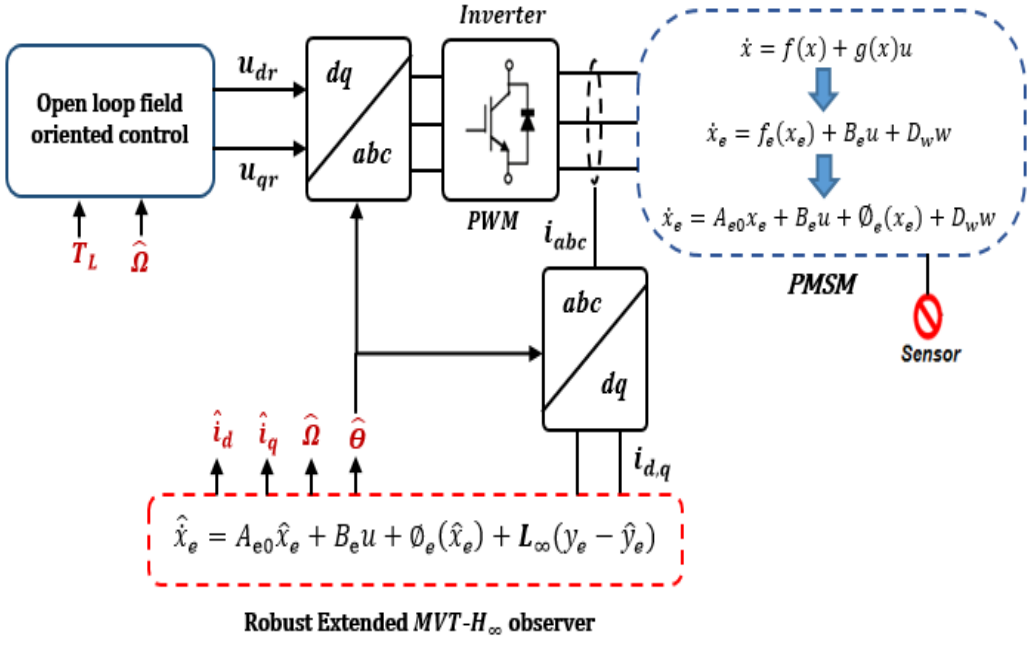

Figure 5.1 Global scheme of the robust extended MVT_H_∞ observer for the PMSM

It has been proposed that the simulation results can be used to demonstrate the efficacy of the approach, as presented in Figure 5.2. The estimated and the real states were presented by the dashed red and black lines, respectively. The rotor speed's trajectory begins by a step of 150 rad/sec and goes down to 30 rad/sec at t = 1sec until the test is finished. First, the PMSM is unloaded until t = 0.4sec, then, it applies a load torque of 9 Nm to the motor until t = 0.8sec, then, the motor is unloaded until t = 1.4 sec, one more time, the motor is loaded also by 9 Nm until the

test is finished, This is illustrated in Figure 5.2-(a) Both Figure 5.2-(b) and Figure 5.2-(c) demonstrate the real and the estimated d, q axis stator currents, respectively. The real and estimated rotor position are given in Figure 5.2-(d). The estimation errors of the rotor speed, d-axis stator current, q-axis stator current and rotor position are given in Figure 5.2-(e) respectively.

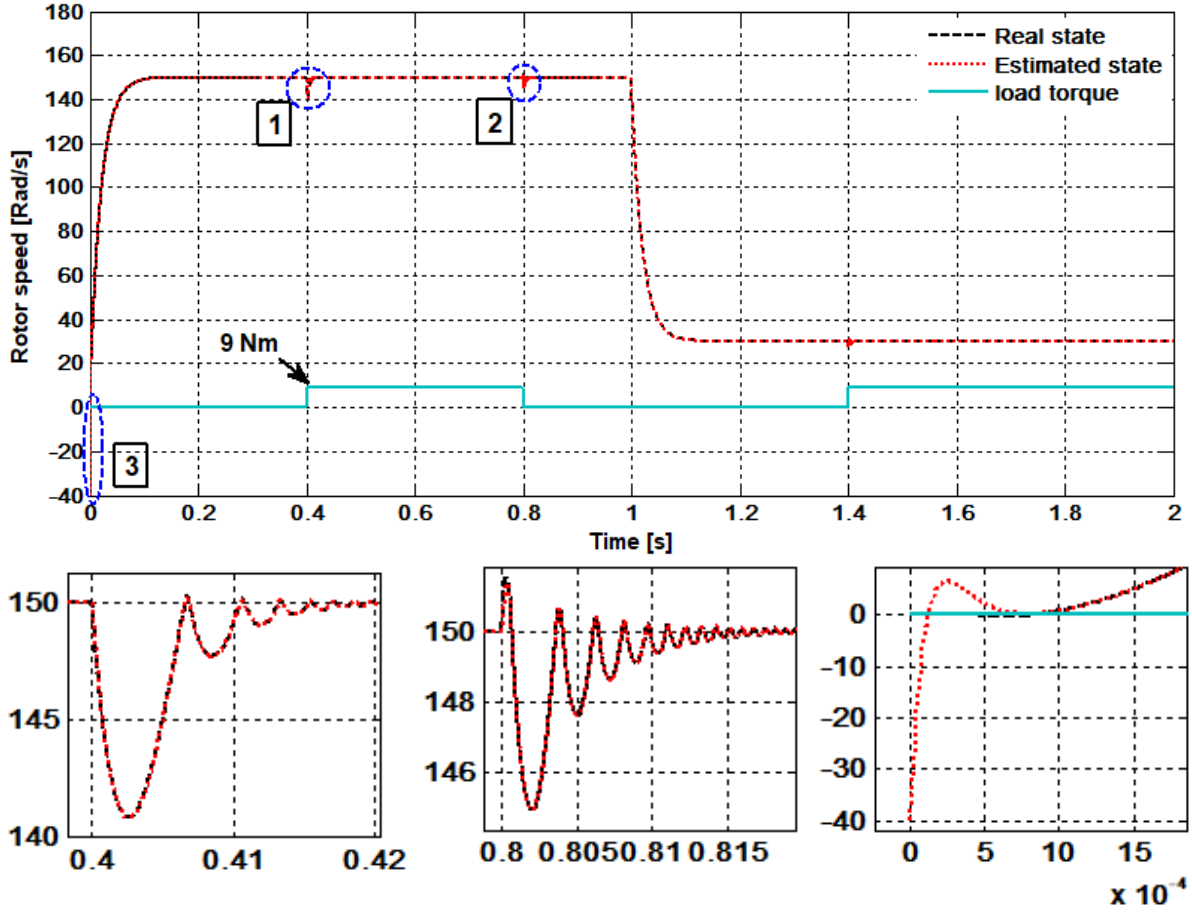

a) Real and estimaation rotor speed

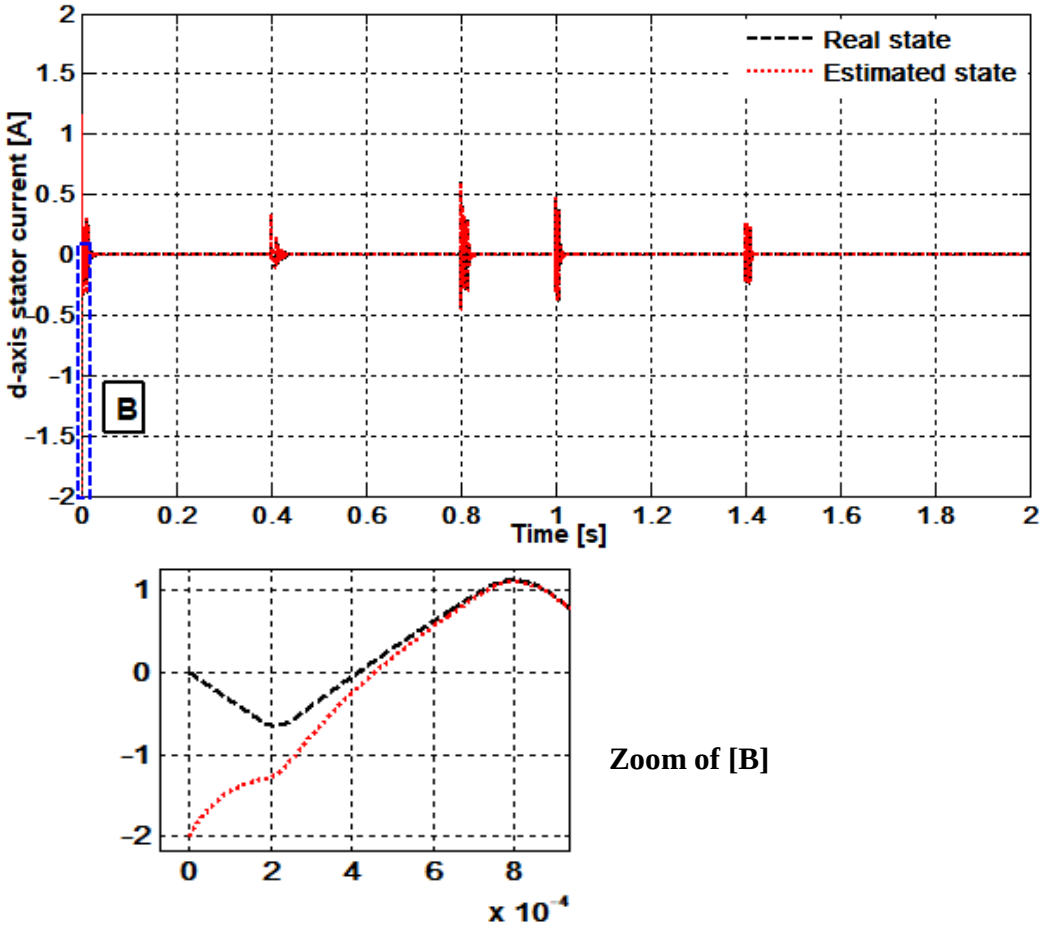

b) Real and estimaation d-axis stator current

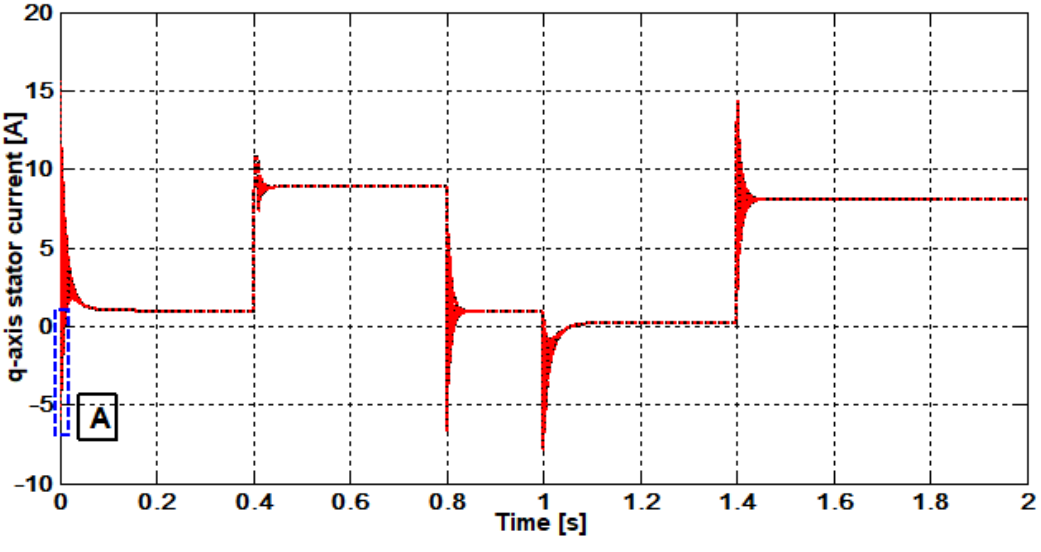

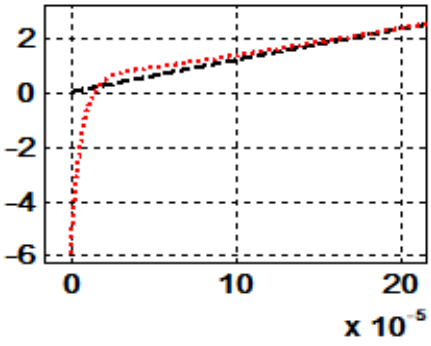

Zoom of [A]

c) Real and estimaation q-axis stator current

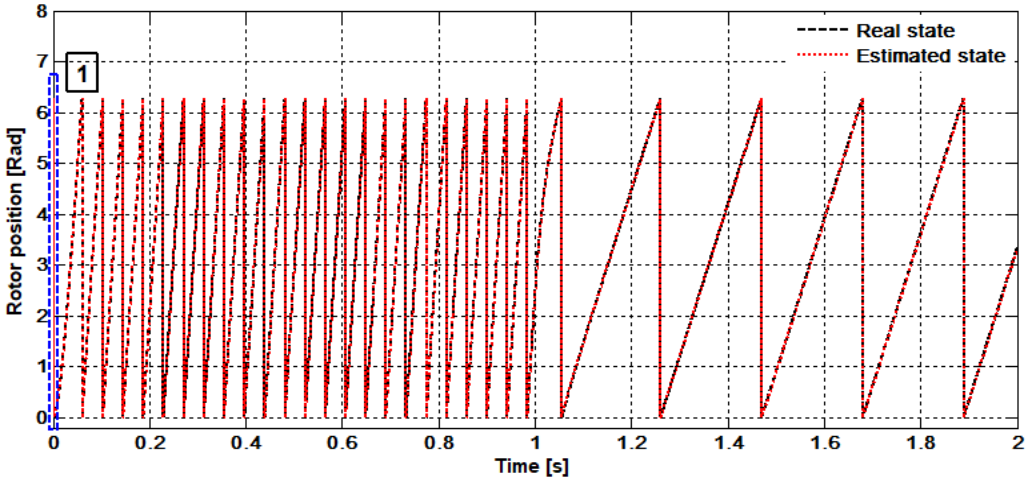

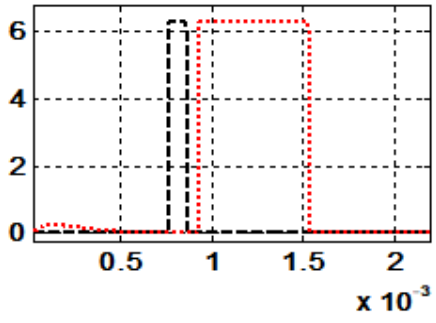

Zoom of [1]

d) Real and estimaation rotor position

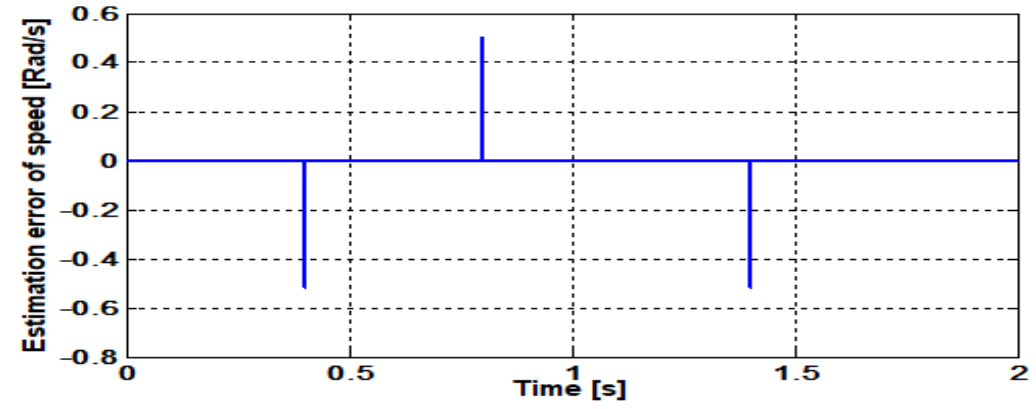
Estimation error of speed [Rad/s]
0.6
0.4
0.2
0
-0.2
-0.4
-0.6
-0.8
0
0.5
1
1.5
2
Time [s]

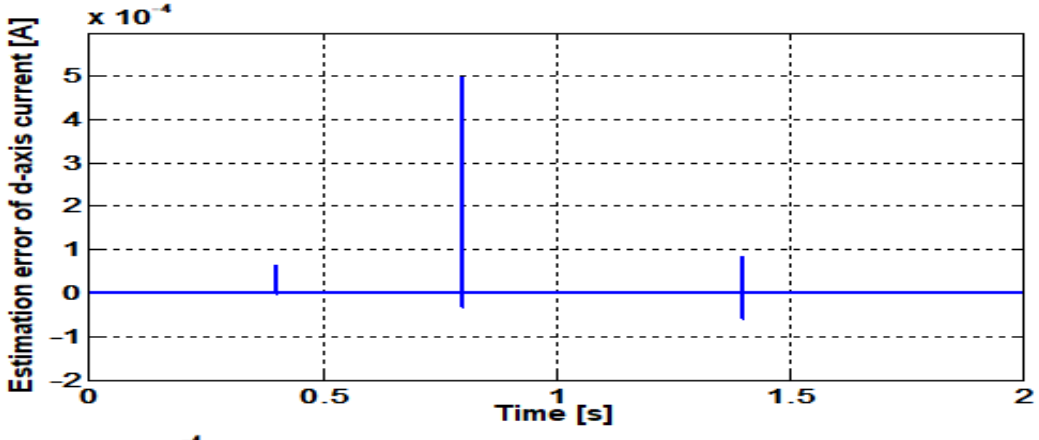
Estimation error of d-axis current [A]
x 10⁻⁴
5
4
3
2
1
0
-1
-2
0
0.5
1
1.5
2
Time [s]

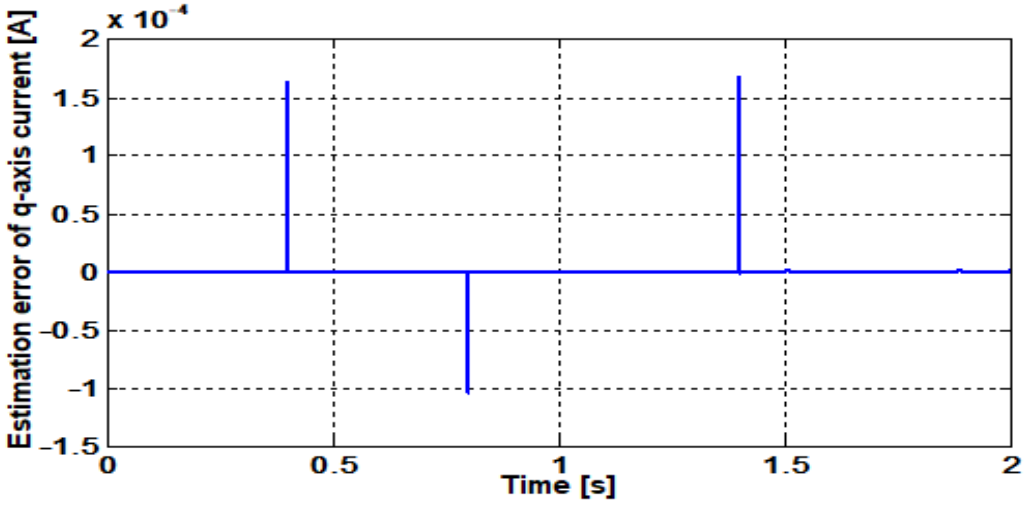
Estimation error of q-axis current [A]
x 10⁻⁴
2
1.5
1
0.5
0
-0.5
-1
-1.5
0
0.5
1
1.5
2
Time [s]

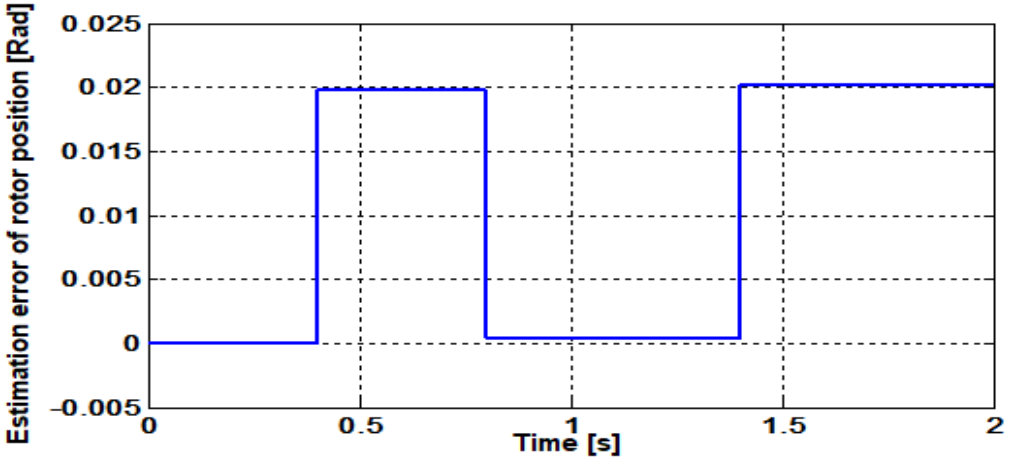

e) Estimation errors of rotor speed, d-axis stator current, q-axis stator current and rotor position.

Figure 5.2 Simulation results of extended MVT_H_∞ observer under OL-FOC of PMSM.

❖ **Effectiveness test of parameter variation**

To demonstrate the robustness of the proposed Observer a parameters variation is applied and presented in Figure 5.3, where, the rotor speed begin by a step of 150 rad/sec, this remains until the test is finished. The PMSM is unloaded until 0.4sec, then, we apply a load torque of 9 Nm to the motor until the test is finished. Figure 5.3-(a) show the real and estimation rotor speed when the stator resistor R_s is changed by 20% at time 0.8sec, at time t = 1.4sec we return the nominal R_s And then, Figure 5.2-b) show the real and estimation rotor speed when the stator inductance L_s is changed by 20% at time 0.8sec, at time t = 1.4sec we return the nominal L_s.

Moreover and in order to illustrate the stability and the efficiency of the MVT_H_∞ extended observer, the initial conditions of estimated states $(\hat{x}_0)$ are selected to be [-2 -6 -40 0]^T.

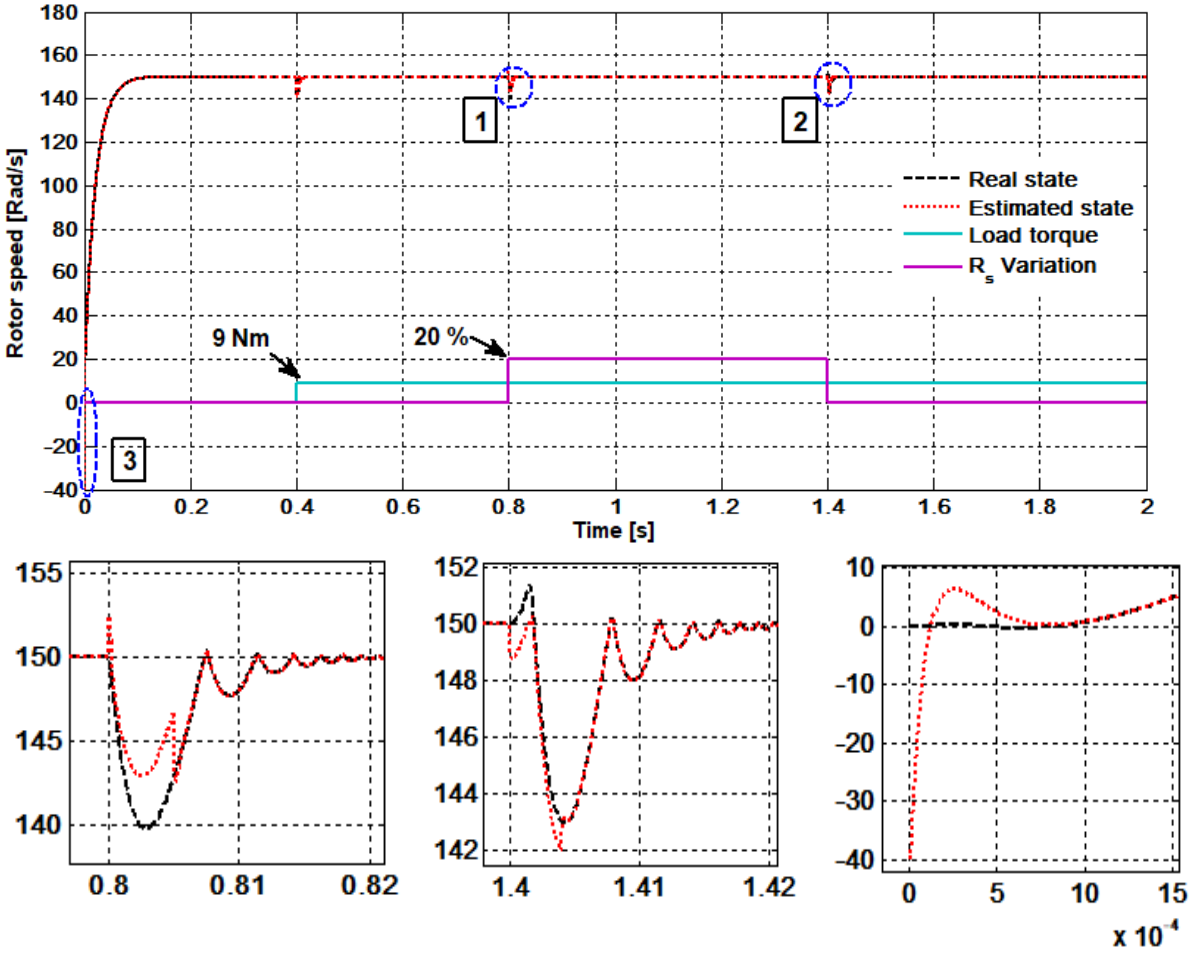

Zoom of [1] **Zoom of [2]** **Zoom of [3]**

(a)

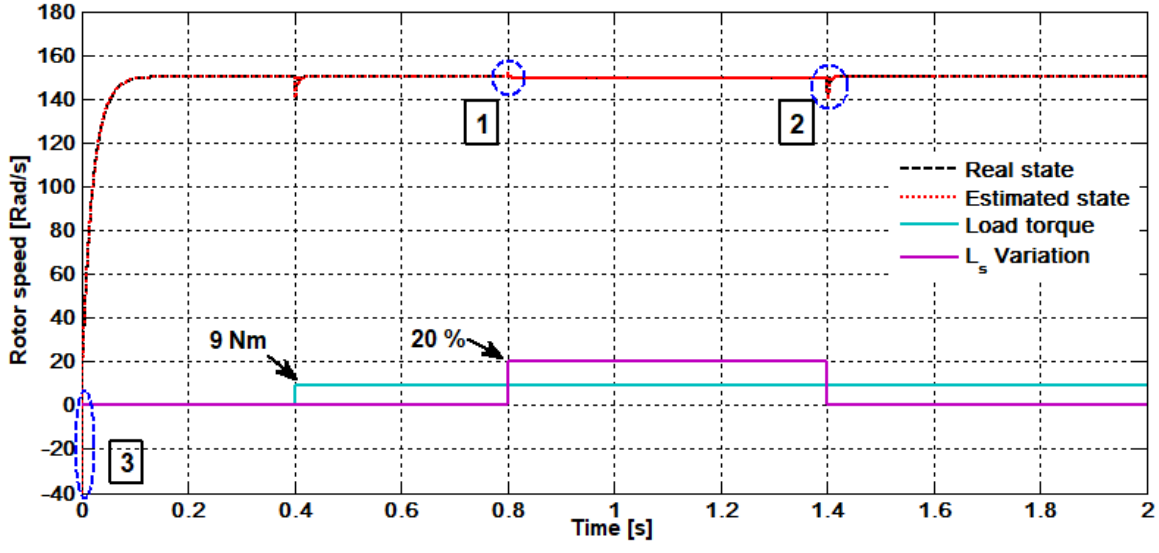

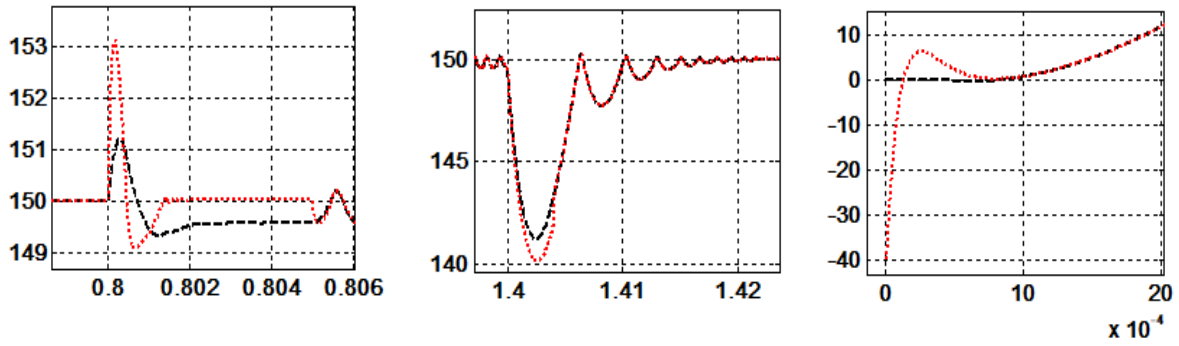

Zoom of [1] **Zoom of [2]** **Zoom of [3]**

(b)

Figure 5.3 Test of extended MVT_H_∞ observer with parameter variation
a) R_s variation
b) $L_s$variation

Based on Figure 5.2, it has been observed that the estimated states of the rotor speed is in closer proximity to its real value. In despite of the application of the load torque by 9 Nm at t= 0.4 sec which is more than the nominal value (6 Nm), the estimated states of the rotor speed still match to the real states with a minimum effect on the estimation error.

It was also remark that the real and the estimated states of d-axis stator current stayed near zero ($I_d = 0$), whereas its q-axis is a reproduction to the torque which shows that the OL-FOC is assured at the moment where the estimation errors is approximately zero as shown in Figure 5.2-(b) and figure 5.2-(c).

However, the rotor position are not originally considered as states of the PMSM drive, the estimation error of the rotor position doesn't exceed 0.02 Rad as shown in Figure 5.2-(d). The estimated states are considered to be close to their real values despite the fact that the initial conditions of the estimated states are not zero. Based on Figure 5.3, it has been observed that the effect of the parameters variation (20% of R_s, 20% of L_s) on the proposed MVT_H_∞ observer is very small.

So the simulation results given above, there is guaranteed success of the proposed extended observer under OL-FOC and it can replace the other technics in the industrial applications due its effectiveness, simplicity and low cost.

5.5. Robust $PI\_MVT\_H_\infty$ controller design

We can use directly the dynamic state equation of controller error, after applying the MVT and the sector nonlinearity transformation approaches as follows (for avoid repetition):

$$\dot{e}_c(t) = \sum_{i=1}^{r} \mu_i(\sigma)\, G_i e_c(t) + D_w \overline{w}(t) \tag{5-27}$$

Such that

$$G_i = A_i - B_0 K_0$$

And

$A_i = A_0 + \mathcal{A}_i$, $D_w = [A_0 \quad D]$, $\overline{w}(t) = \begin{bmatrix} x_r(t) \\ w(t) \end{bmatrix}$ and $\sigma \in [x, x_r]$

To eliminate the perturbation effects and parametric steady-state uncertainties it is preferable to add an integral action, then the modified control law is given by:

$$u(t) = -[K_0 \quad K_I] \begin{bmatrix} e(t) \\ e_I(t) \end{bmatrix} = \overline{K} \bar{e}_c(t) \tag{5-28}$$

Such as the state related to integral action:

$$\dot{e}_I(t) = x(t) - x_r(t) \tag{5-29}$$

Using (5-28) and (5-29), and after some steps the dynamics of the augmented closed-loop control error state equation is expressed as follows:

$$\dot{\bar{e}}_c(t) = \sum_{i=1}^{r} \mu_i(\sigma) \left(\bar{G}_i \bar{e}_c(t) + \overline{D}_w \overline{w}(t) \right) \tag{5-30}$$

Where

$$\bar{G}_i = \bar{A}_i - \bar{B}\overline{K}$$

And

$$\bar{A}_i = \begin{bmatrix} A_0 + \mathcal{A}_i & 0 \\ I & 0 \end{bmatrix};\ \bar{B} = \begin{bmatrix} B_0 \\ 0 \end{bmatrix};\ \overline{D}_w = \begin{bmatrix} A_0 & D \\ 0 & 0 \end{bmatrix};\ \overline{w}(t) = \begin{bmatrix} x_c(t) \\ w(t) \end{bmatrix}$$

5.5.1. Stability analysis

Consider the quadratic Lyapunov function given by:

$$V\left(\bar{e}(t)\right) = \bar{e}^T(t) P \bar{e}(t) \tag{5-31}$$

In the case of the quadratic Lyapunov candidate function (5-34), the closed loop system (5-29) is stable and also the trajectory tracking via the control law (5-27) under the H_∞ performance, if:

$$\dot{V}\left(\bar{e}(t)\right) + \bar{e}^T(t)\bar{e}(t) - \gamma^2\bar{w}^T(t)\bar{w}(t) < 0 \tag{5-32}$$

Replacing the derivative of $V\left(\bar{e}(t)\right)$ in (5-35):

$$\dot{\bar{e}}^T(t)P\bar{e}(t) + \bar{e}^T(t)P\dot{\bar{e}}(t) + \bar{e}^T(t)\bar{e}(t) - \gamma^2\bar{w}^T(t)\bar{w}(t) < 0 \tag{5-33}$$

For avoid the repetitions, can be use the steps of the analysis stability represented in previous subsection (3.3). So the final LMI will be presented as follows:

Lemma 1. The quadratic stability of the closed-loop system is guaranteed for an attenuation of the external disturbances $w(t)$ according to the rate $\delta = \gamma^2$ if there is a matrices, such as: $X = X^T > 0$ and

$$\begin{bmatrix} \bar{A}_i X + X\bar{A}_i{}^T - \bar{B}Y - Y^T\bar{B}^T & \bar{D}_w & X \\ \bar{D}_w{}^T & -\gamma^2 I & 0 \\ X & 0 & I \end{bmatrix} < 0 \tag{5-34}$$

Such as the gain $\bar{K}_\infty$ is calculated by:

$$\bar{K}_\infty = YX^{-1}$$

5.5.2. Simulation results

The proposed $PI\_MVT\_H_\infty$ controller was applied. The simulation results are obtained through the MATLAB/SIMULINK environment. As proof of the efficacy of this approach, which applied to the PMSM drive, which has the parameters in Appendix B. The robust controller gain is calculated as (5-34) by solving the LMIs (5-34) given as:

$$\bar{\boldsymbol{K}} = 10^2 * \begin{bmatrix} 2.336 & -0.041 & 12.752 & -10.592 & 19.332 & -0.388 \\ 0.041 & -33.453 & 8.951 & -68.321 & -54.326 & 66.233 \end{bmatrix}$$

Figure 5.4 presents the general scheme of the $PI\_MVT\_H_\infty$ controller applied to the PMSM drive

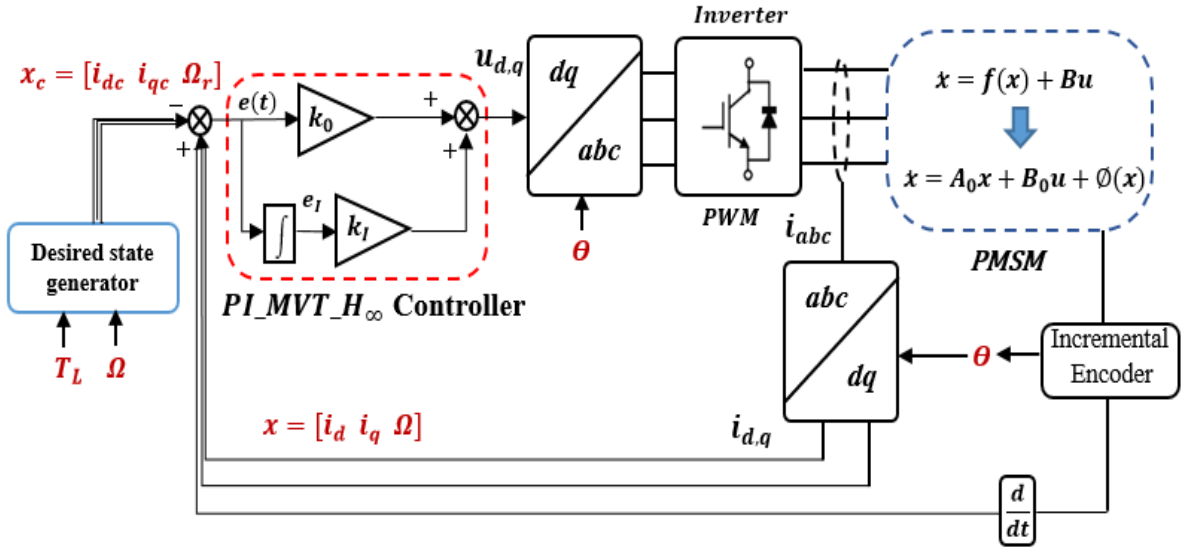

Figure 5.4 Control scheme using an integral action based on MVT theorem and H_∞ performance

The simulation results are introduced for the trajectory of the rotor speed, so, the desired and real rotor speed are illustrated in Fig 5.5-(a), The desired rotor speed's trajectory begins by a step of 150 rad/sec and goes down to 30 rad/sec at t = 0.5sec. To conduct the negative tests, a desired speed of -150 rad/sec is selected at t = 1sec. alternatively, the zero speed is implemented at t = 1.5sec until the test is finished. First, the PMSM is unloaded until t = 0.2sec, then, it applies a load torque of 9 Nm to the motor for all the remaining time, this is illustrated in Figure 5.5-(a). Both Figure 5.5-(b) and Figure 5.5-(c) demonstrate the desired and the real d, q axis stator currents, respectively. In Figure 5.5-(d), the three-phase line stator currents are demonstrated. The real values of the rotor position is given in Figure 5.5-(e).

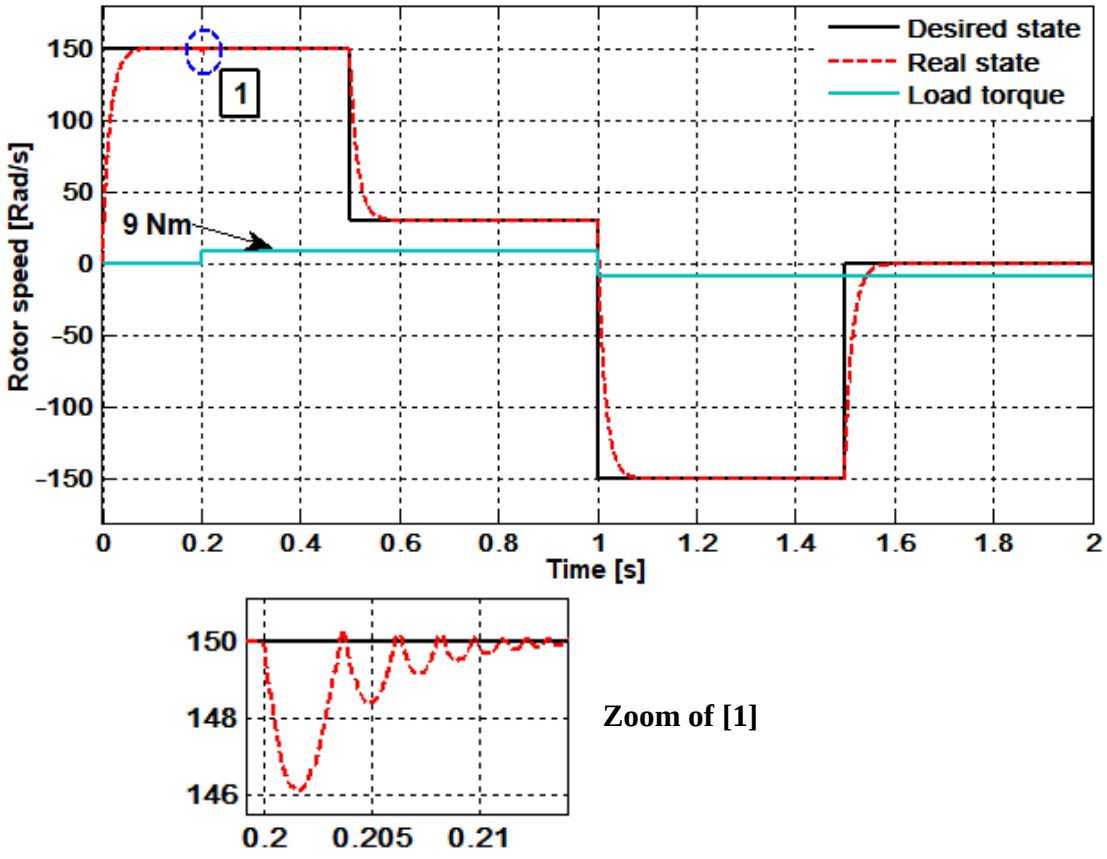

a) Real and desired rotor speed.

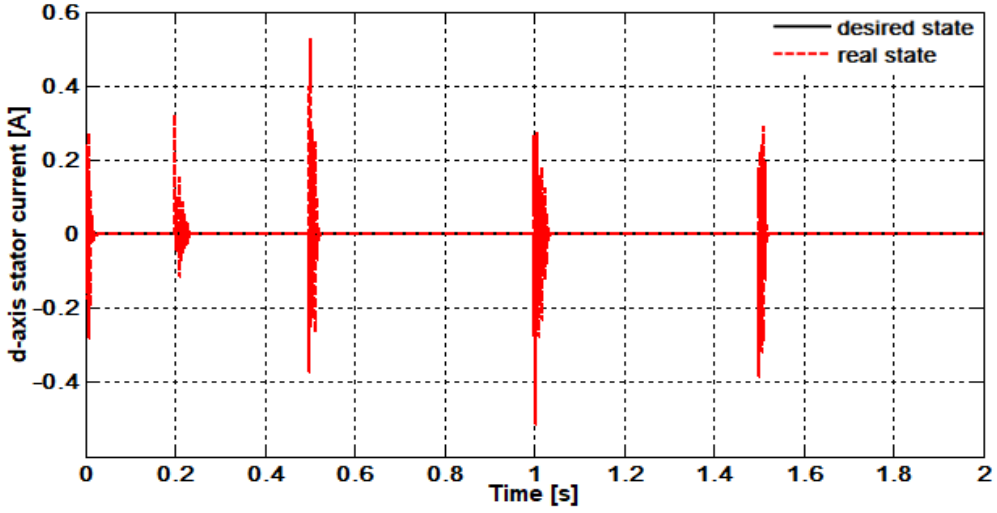

b) Real and desired d-axis stator current.

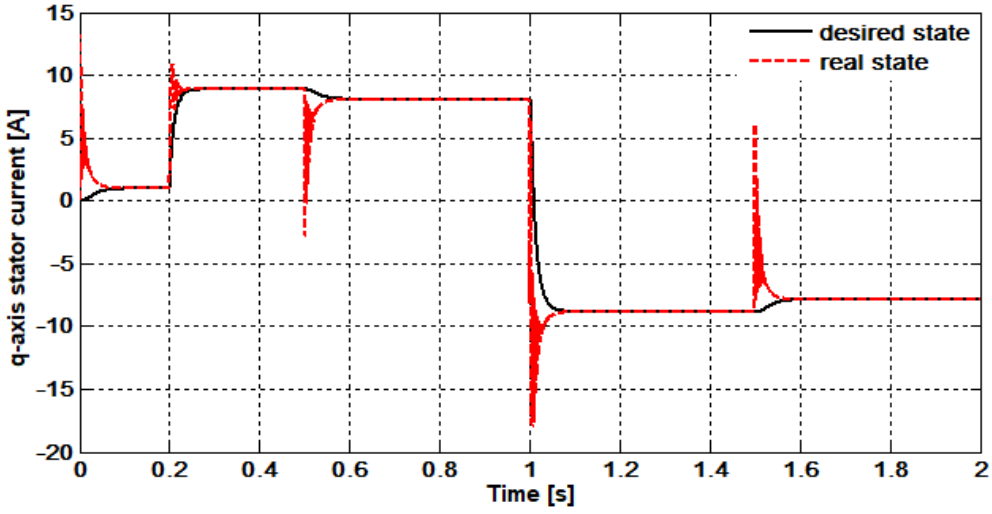

c) Real and desired d-axis stator current.

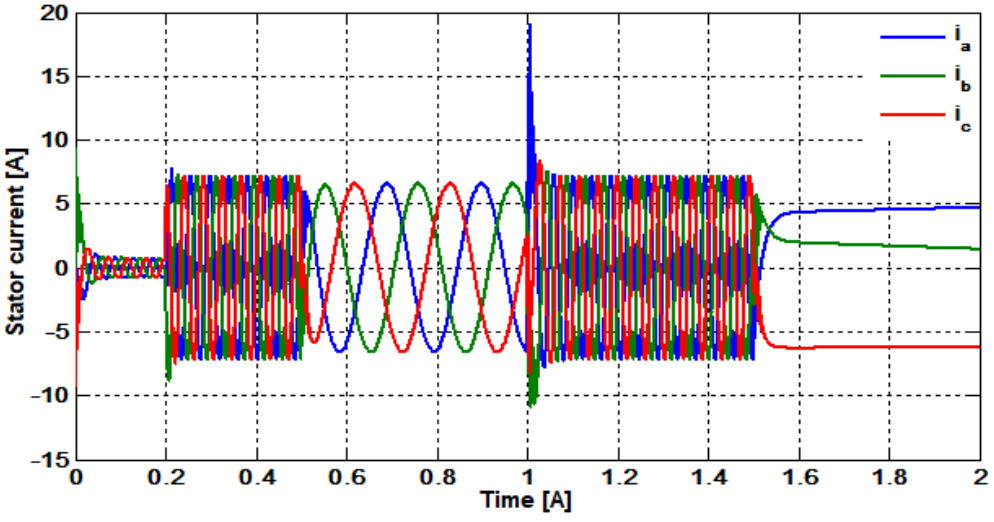

d) Three phase stator current.

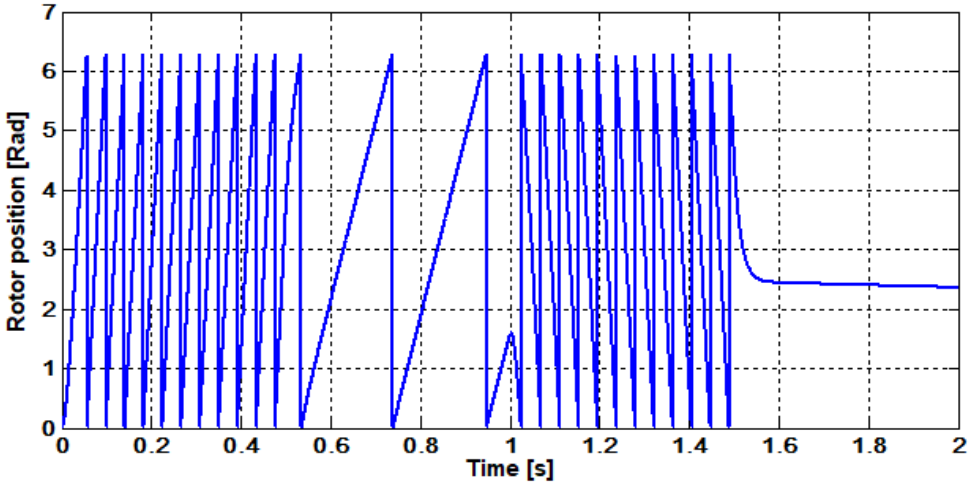

e) Rotor position.

Figure 5.5 Simulation results of $PI\_MVT\_H_\infty$ controller applied to PMSM.

Figure 5.6 shown a comparison between a deferent control technics. Control-1: $PI\_MVT\_H_\infty$ controller. Control-2: PI_MVT controller. Control-3: OL_FOC control. So, the desired rotor speed stile 150 rad/sec from the beginning until the test is finished. First, the motor drive is unloaded until t = 0.3sec, then, it applies a load torque of 6 Nm to the motor for all the remaining time.

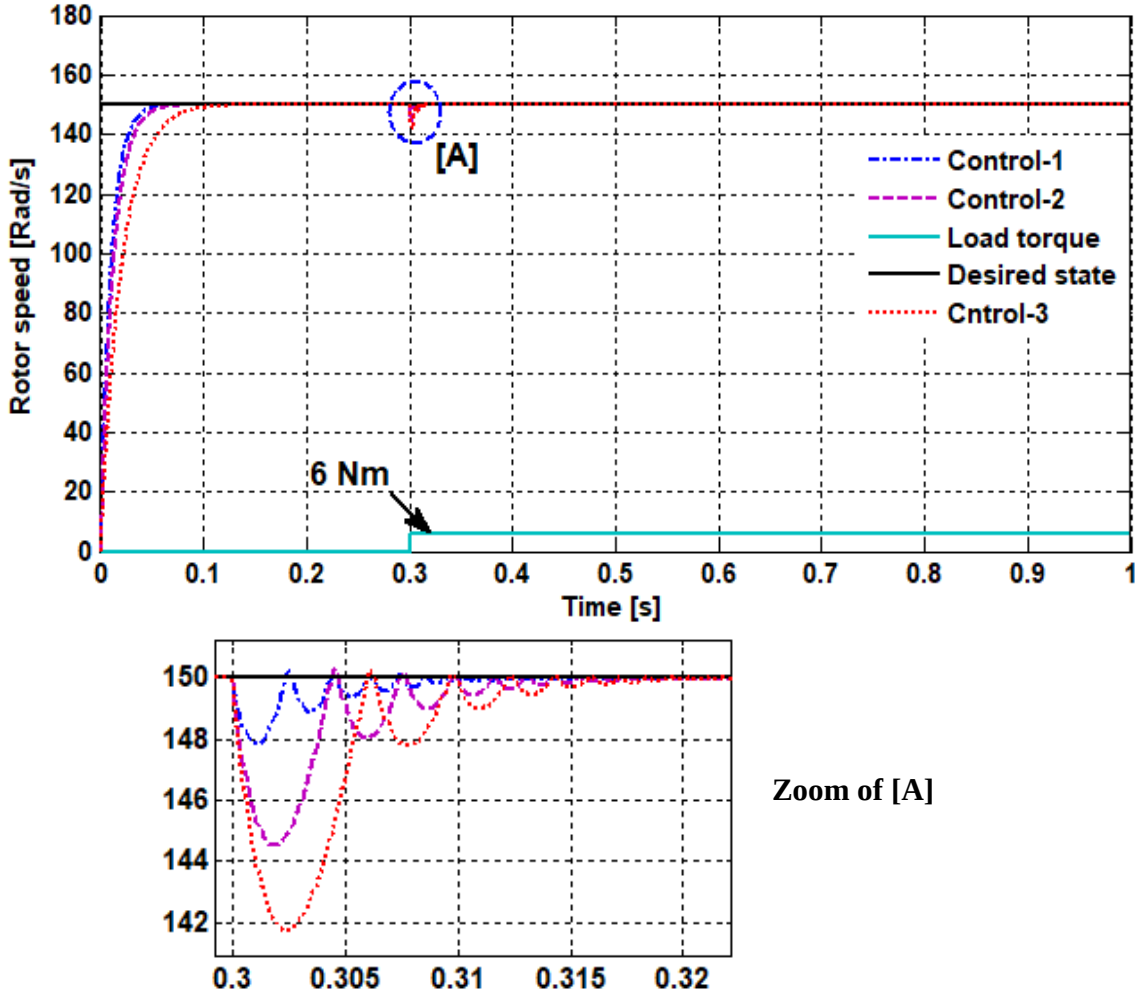

Figure 5.6 Real and desired rotor speed for a deferent control.
Control-1: $PI\_MVT\_H_\infty$ controller.
Control-2: PI_MVT controller.
Control-3: OL_FOC control.

Based on Figure 5.5-(a), it has been remarked that the real state of the rotor speed is in closer proximity to its desired value. In despite of the application of the load torque by 9 Nm at t= 0.2 sec which is more than the nominal value (6 Nm), the real states of the rotor speed still match to

the desired states with a minimum effect on the estimation error. The same remark in the d-q axis stator currents.

It was also remark that the real state of d-axis stator current stayed near zero ($I_d = 0$), whereas its q-axis is a reproduction to the torque which shows that the FOC is assured at the moment where the regulation errors is approximately zero as shown in Figure 5.5-(b) and figure 5.5-(c).

After the comparison between a deferent control technics represented in Figure 5.6 one can note well the efficacy of the $PI\_MVT\_H_\infty$ controller compared to the other controllers, this shown in the time of response and when we applied the load torque.

5.6. Conclusion

This Chapter was concentrated on the idea of the robust extended H_∞ observer and robust H_∞ controller based on the MVT essentially, applied to the PMSM drive, the extended observer is under the Open Loop Field Oriented Control (OL-FOC). The robust extended observer and controller design are based on the MVT and the sector nonlinearity approaches to stabilizing the observer and controller dynamic errors of PMSM. Through an illustrative simulation implemented in MATLAB/SIMULINK, the simulation results were confirmed and demonstrated the effectiveness of the proposed algorithms and ensured a minimum disturbance attenuation level to the estimation error or the control error.

References of Chapter V

[1] D. P. Atherton and D. P. Atherton, *Nonlinear control engineering*: Van Nostrand Reinhold New York, 1982.

[2] G. Phanomchoeng, R. Rajamani, and D. Piyabongkarn, "Nonlinear observer for bounded Jacobian systems, with applications to automotive slip angle estimation," *IEEE Transactions on Automatic Control*, vol. 56, pp. 1163-1170, 2011.

[3] B. Hamidani, A. Allag, O. Zeghib, and A. Allag, "An extended H∞ observer based on the mean value theorem approach applied to open loop FOC of PMSM drive," in *2018 International Conference on Communications and Electrical Engineering (ICCEE)*, 2018, pp. 1-8.

[4] M. Y. Hammoudi, M. H. Benbouzid, N. Rizoug, and A. Allag, "New state observer based on Takagi-Sugeno fuzzy controller of induction motor," in *Systems and Control (ICSC), 2015 4th International Conference on*, 2015, pp. 145-150.

[5] D. Ichalal, B. Marx, S. Mammar, D. Maquin, and J. Ragot, "Observer for Lipschitz nonlinear systems: mean value theorem and sector nonlinearity transformation," in *Intelligent Control (ISIC), 2012 IEEE International Symposium on*, 2012, pp. 264-269.

[6] A. Zemouche, M. Boutayeb, and G. I. Bara, "Observer Design for Nonlinear Systems: An Approach Based on the Differential Mean Value Theorem," in *Decision and Control, 2005 and 2005 European Control Conference. CDC-ECC'05. 44th IEEE Conference on*, 2005, pp. 6353-6358.

[7] A. Allag, A. Benakcha, M. Allag, I. Zein, and M. Y. Ayad, "Classical state feedback controller for nonlinear systems using mean value theorem: closed loop-FOC of PMSM motor application," *Frontiers in Energy*, vol. 9, p. 413, 2015.

[8] M. Y. Hammoudi, A. Allag, M. Becherif, M. Benbouzid, and H. Alloui, "Observer design for induction motor: an approach based on the mean value theorem," *Frontiers in Energy*, vol. 8, pp. 426-433, 2014.

[9] A. Moez, S. Mansour, C. Mohamed, and M. Driss, "Takagi-Sugeno Fuzzy Control of Induction Motor," *Proc. Int. Journal of Electrical and Electronics Engg*, vol. 2, 2009.

[10] A. Zemouche, M. Boutayeb, and G. I. Bara, "Observers for a class of Lipschitz systems with extension to H∞ performance analysis," *Systems & Control Letters*, vol. 57, pp. 18-27, 2008.

[11] K. Tanaka and H. O. Wang, *Fuzzy control systems design and analysis: a linear matrix inequality approach*: John Wiley & Sons, 2004.

[12] K. Tanaka, T. Ikeda, and H. O. Wang, "Fuzzy regulators and fuzzy observers: relaxed stability conditions and LMI-based designs," *IEEE Transactions on fuzzy systems*, vol. 6, pp. 250-265, 1998.

CHAPTER VI

Fault Detection and Diagnosis Based on Extended MVT Observer Applied to the PMSM

6.1. Introduction and general diagnosis

With the increased demand for sophisticated controls for electric motors in industry, reliability and predictability of motor operations is now a major requirement in many applications. Reliability of a motor operation is especially important where an unexpected shut-down might result in the interruption of critical services such as medical, transportation or military operations where failure potentially could lead to costly maintenance or loss of life.

Those electrical motor faults that potentially lead to the shut-down of a system can be classified in two parts (electrical and mechanical) as follows [1-3]:

A. Electrical faults

a) Open or shorts in motor windings (mainly due to insulation failure)
b) Wrong connection of windings
c) High resistance contact to conductor

B. Mechanical faults

a) Broken rotor bars
b) Cracked end-rings
c) Bent shaft
d) Bearing failure
e) Gearbox failure
f) Air gap irregularity

These fault conditions create specific symptoms during a motor operation which can be described as follows:

a) Motor vibration
b) Temperature increase
c) Irregular air gap torque

d) Instantaneous power variation
e) Audible noise
f) Stator voltage changes
g) Stator current changes
h) Speed variations

Based on monitoring and analyzing these symptoms, a motor fault diagnosis technique might be performed through the following strategies:

A. Single symptom analysis

a) Motor vibration analysis
b) Temperature measurement
c) Acoustic noise analysis
d) Electromagnetic field monitoring through inserted coil
e) Chemical analysis
f) Infrared analysis
g) RF emission monitoring
h) Partial discharge measurement
i) Motor current signature analysis (MCSA)
   - ❖ FFT analysis
   - ❖ Wavelet analysis
   - ❖ Complex Park vector analysis

B. Multi-symptom analysis

a) Neural network
b) Fuzzy logic analysis
c) Statistical analysis of relevant information

C. Simulations

a) Finite element analysis (FEA)
b) Time step coupled finite element-state space (TSCFE-SS)

D. Model Based Fault Detection and Diagnosis

a) Fault detection with parity relations
b) Fault detection with diagnostic observers

c) Fault detection with parameter estimation

6.2. Fault specification of PMSM drives

6.2.1. Stator winding faults:

The stator winding fault due to short-circuited turns is known as the most common electrical fault in electrical machine. The majority of winding fault are caused by the breakdown of turn-to-turn insulation as a result of the voltage, current, or thermal stress acted on the stator winding. The process of insulation breakdown is a complex one. Beginning with partial discharge and very localized heating and progressing to a low resistance short circuit capable of carrying considerable current.

Some of the most frequent causes of stator winding failures [4] are:

- High stator core or winding temperatures,
- Slack core lamination, slot wedges, and joints,
- Loose bracing for end winding,
- Contamination caused by oil, moisture, and dirt,
- Short circuits,
- Starting stresses,
- Electrical discharges,
- Leakages in the cooling systems.

It is believed that phase-to-ground or phase-to-phase and coil to coil faults start as undetected turn-to-turn faults that finally grow and culminate into major ones [5-7]. Although short-circuit current is limited to a rated value by designing the machine with a high phase inductance, short circuit between turns is the most critical fault in the machine and is quite difficult to detect and almost impossible to remove.

In the case of a short circuit in a PMSM, there is a risk of irreversibly demagnetization of the permanent magnets of the motor due to the strong opposing magnetic field from the short-circuit current. The high torque at a short circuit can also lead to mechanical failures of the machine, the shaft coupling, or the load [8].

6.2.2. Open phase, phase to ground, line to line, line to line to ground faults

An important fault class for a PMSM machine is considered in which one of the phases becomes open-circuited. This type of fault can be caused by mechanical failure of a machine terminal connector, an internal winding rupture, or by an electrical failure in one of the inverter phase legs [9].

The open-phase fault produces electromagnetic torque oscillations which cause abnormal rotor vibrations and give abnormalities in the drive's operation [7]. The amplitude of current increases by approximately 60 %, and the two phases currents are shifted 2π, thus the risk of destruction of stator winding.

6.2.3. Unbalanced voltage fault

Unbalanced voltage is one of the most frequent interferences in electrical systems. Large single phase loads, unbalance loads, system faults, etc. are some of the causes of unbalanced voltage. Most of the standards only specify the percentage of unbalanced voltage without indicating the unbalanced condition. In fact, there are many unbalanced voltage cases which have the same unbalanced voltage factor but have different effects on loads. Unbalanced Voltage causes the performance of motor to deviate from desirable condition as shown in [10-12].

It must be consider that operation of motor under high percentages unbalanced voltage tests, it doesn't take a long time because, the temperature rises more than that of the motor operating under the same condition with balanced voltages.

For a 3-phase system, there are two different definitions of the unbalanced voltage: IEC standard definition and NEMA standard definition. The IEC standard definition defines the unbalanced voltage as the ratio between the amplitude of the negative sequence component, V_2, to that of the positive sequence component, V_1, as in (6-1):

$$Percent\ Voltage\ Unbalance = \frac{V_2}{V_1} \times 100 \tag{6-1}$$

While the NEMA standard defines the voltage unbalance as the ratio between the maximum deviation from the mean value of 3 line voltage magnitudes, V_{ab}, V_{bc} and V_{ca}, to the mean value of these 3 line voltages, The voltage unbalance percentage may be defined as in (6-2):

$$Percent\ Voltage\ Unbalance = \frac{V_{max} - V_{avrage}}{V_{avrage}} \times 100 \quad (6\text{-}2)$$

6.2.4. Demagnetization fault

Magnet faults include microscopic fissures, chips, disintegration due to corrosion, complete or even partial demagnetization. Among these, demagnetization fault play a more important role in magnet failure as claimed in [13-15].

Demagnetization can be complete, that is, all over the pole, or partial, on a certain region of the pole. Depending on the severity of fault, demagnetization can be reversible or irreversible. However it has been verified that irreversible demagnetization does not arise in the PMs under the steady states. Instead, it arises under transient states [16-18].

The demagnetization phenomenon can be due to the armature reaction, especially under conditions of operation requiring strong torque for example at high loads or during sharp transients or even high temperature [18-20].

During the normal operation of the PMSM, the electrical current of the stator winding produces an inverse magnetic field that opposes the remnant induction of the permanent magnets. This repeated phenomenon can cause demagnetization in the permanent magnets too. In addition, a major fault condition of permanent-magnet machines is the stator fault in the opening or shorting of one or more of stator phase windings [21-23].

The approximate maximum operation temperature of some commercial magnets is illustrated [24] in figure 6.1

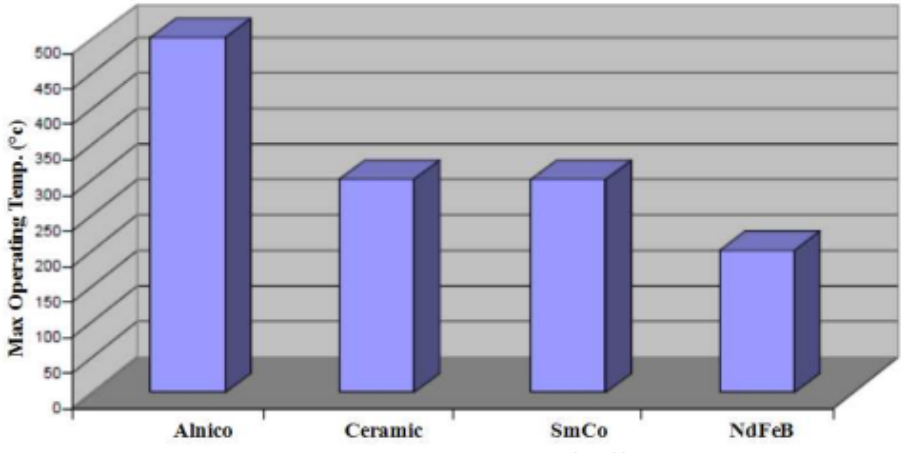

Figure 6.1 : Maximum operating temperature of different magnet materials

6.2.5. Eccentricity fault

Almost 50 % of all motor failures are related to mechanical faults, and they lead to a noise and vibrations, and even to the total damage of the machine and the mechanics coupled to it if the failure is not detected and isolated [21, 25].

Due to tolerance in manufacture and assembly, where the inherent level of eccentricity is expected to be within 5%–10% of the air gap, every machine possesses a certain degree of eccentricity entailing a non-uniform air gap thickness and magnetic field [16, 26, 27].

When eccentricity becomes large, the resulting unbalanced radial forces (also known as unbalanced magnetic pull or UMP) can cause stator to rotor rub, which result in a serious damage to stator core and windings [13].

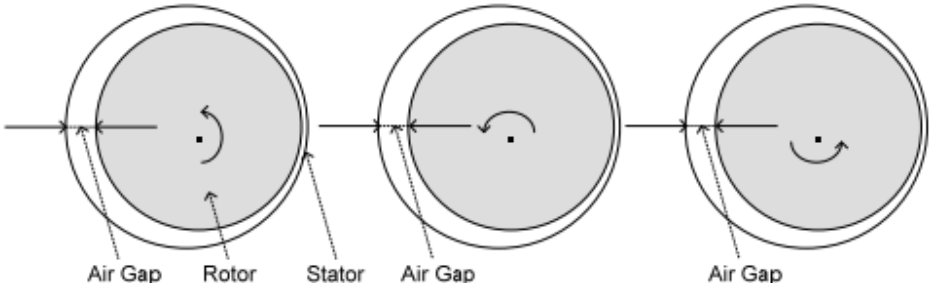

Figure 6.2 Static eccentricity.

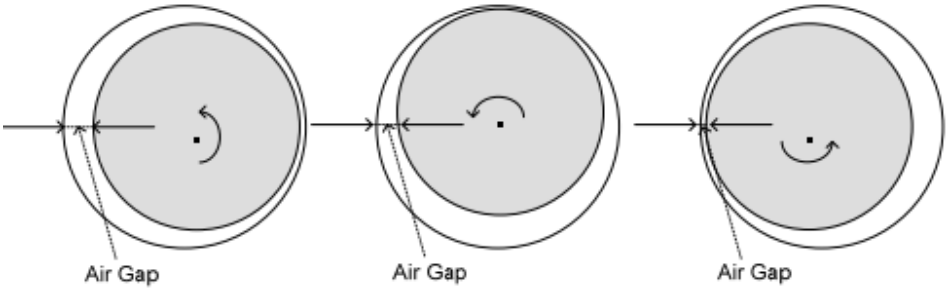

Figure 6.3 Dynamic eccentricity[28].

Static eccentricity may be caused by the ovality of the stator core or by the incorrect positioning of the rotor or stator at the commissioning stage. Assuming that the rotor-shaft assembly is sufficiently stiff, the level of static eccentricity does not change. The dynamic eccentricity may be caused by several factors, such as manufacturing tolerances, wear of bearings, or misalignment, mechanical resonance at critical speed, and incorrect manufacture of the machine components.

Rotor “whirl” near a critical speed is another source of dynamic eccentricity and is an important consideration in larger, flexible-shaft machines

6.3. Model Based Fault Detection and Diagnosis

Study of model based FDD began in 1970’s. FDD is generally considered to have entered its modern era with the publications of Mehra and Peschon (1971), as well as Lainiotis and Park (1973) [29, 30]. In these papers, the proposed FDD algorithms were applied to chemical plants and airplanes. In 1976, Willsky wrote the first major survey paper on model based FDD [31], especially on linear time invariant (LTI) systems. After that, Isermann reviewed FDD design based on modeling and estimation method in 1984 [32]. In 1988, Gertler summarized the main features of model based FDD and presented the robustness and sensitivity considerations in [33]. Meanwhile, Basseville presented both online and offline FDD algorithms in his survey paper with a particular emphasis on statistical methods for detection [34]. With the development of Artificial Intelligence (AI), a lot of AI based FDD designs were proposed. This topic was surveyed by Frank in 1990 [35]. In 1997, Frank and Köppen-Seliger did a followup survey on AI based FDD in [36]. This 1997 paper focused on fuzzy logic and introduced the concept of knowledge observer. In the mid-1990s, some nonlinear model based FDD methods were proposed, a survey on which was made by García and Frank [37].

In general, a model based FDD system consists of two modules: residual generator and residual evaluator, as shown in Figure 6.4 In this diagram, the residual generator uses system measurements as input to generate residuals as fault symptoms. Then, these residuals are sent to the residual evaluator to make diagnosis decisions

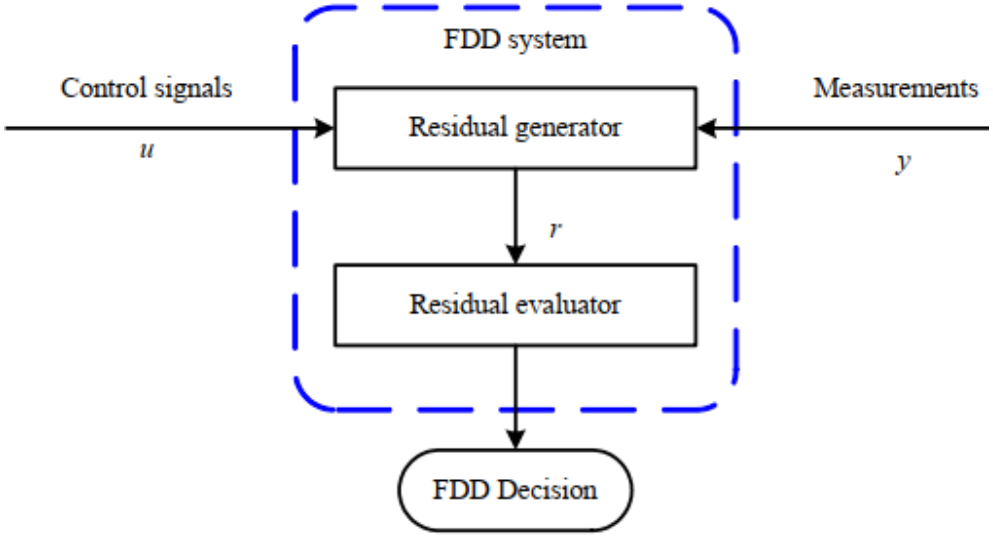

Figure 6.4 A two stage model based FDD system[28]

6.3.1. Fault detection with parity relations

Parity relation sometimes is also called consistency relation, or analytical redundancy relation. This approach was first introduced by Frank [35]. Parity relations directly check the consistency between the model and measured system outputs, thus is the most intuitive fault detection method. The main idea of this method is shown in Figure 6.5 G_P represents the monitored system, and G_M is the analytical model of that system. Residual r based on parity relations can then be mathematically expressed in (6-3) with u denoting the control signal input.

$$r = (G_P - G_M)u \tag{6-3}$$

While being the most computationally efficient and simplest in implementation, the parity relation based approach assumes that the model parameters are known and constant. Thus, residuals based on this method are susceptible to model inaccuracies due to system uncertainties. To overcome the problem of imprecise models, robust parity relations were introduced in the mid-1980s, by Chow and Willsky [38], Lou, Willsky and Verghese [39].

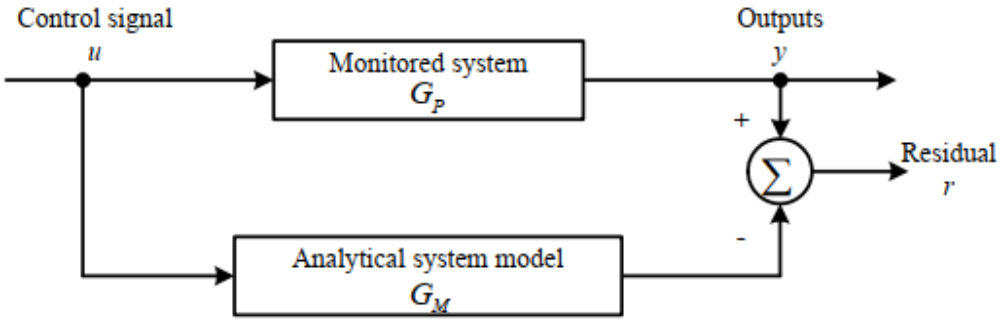

Figure 6.5 Parity relation based residual generation[28]

6.3.2. Fault detection with diagnostic observers

If a system is observable, observers can be used to estimate states of a system using measured data. The estimated states can then be used to observe the system outputs. Diagnostic observers utilize the errors between estimated and measured outputs as residuals. The schematic diagram of this approach is shown in Figure 6.6 In this figure, y_e denotes the estimated system output, y denotes the measured system output, and r denotes the residual, which can be calculated according to (6-4)[28].

$$r = y - y_e \tag{6-4}$$

Diagnostic observer design takes advantages of widely used observer designs. This method is especially useful when dealing with the cases where states or outputs are not measurable. Similar to parity relation method, diagnostic observers also require accurate knowledge of system model

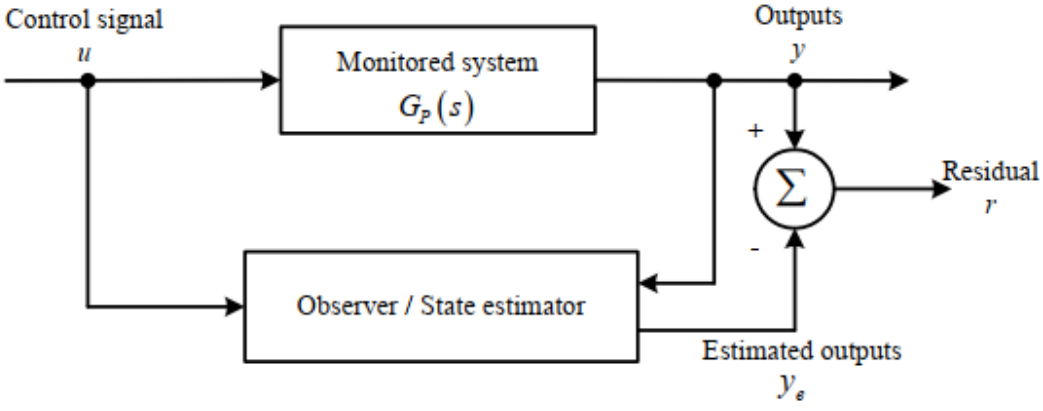

Figure 6.6 Diagnostic observer[28].

parameters. The relationship between diagnostic observers and parity relation based designs was discussed by Mgni and Mouyon for linear systems [40]. Since accurate system models are often

unavailable for practical systems, robust designs are important for diagnostic observers. Some related work can be found in [41, 42][30][31][32].

6.3.3. Fault detection with parameter estimation

Both the parity relations and the diagnostic observers require an accurate model of the system. For some problems, the parameters of a system model may normally vary continuously in certain ranges. Since the above two methods cannot handle this problem, parameter estimation based fault detection is used for FDD. Parameter estimation is proved to be advantageous in this regard according to Gertler, Hofling, and Isermann [43, 44]. Parameter estimation methods only require the structure of the system model to be known. The parameters of the model are estimated and compared to their values during normal operating conditions. This parameter estimation based fault detection method is illustrated in Figure 6.7. In this figure, p_e represents the estimated parameter, p represents p_e's nominal value, and r represents the residual as calculated in (6-5):

$$r = p - p_e \tag{6-5}$$

In [35], Isermann (1991) states that parameter estimation provides deeper insights into system dynamics and thus makes fault diagnosis easier. In many cases, changes in model parameters are directly related to system internal faults. Thus, the parameter estimation approach is especially suitable for the detection of the multiplicative faults according to Gertler (1998) and Isermann (1984, 2005) [32, 45]. Also, parameter estimation allows the detection of very small changes of the system conditions, including slowly developing faults. In [43, 44], Gertler (1995), Hofling and Isermann (1995) proved the mathematical equivalence between the parameter estimation and the parity relation with an accurate model. A disadvantage of this method is that a Persistent Excitation (PE) condition is usually required.

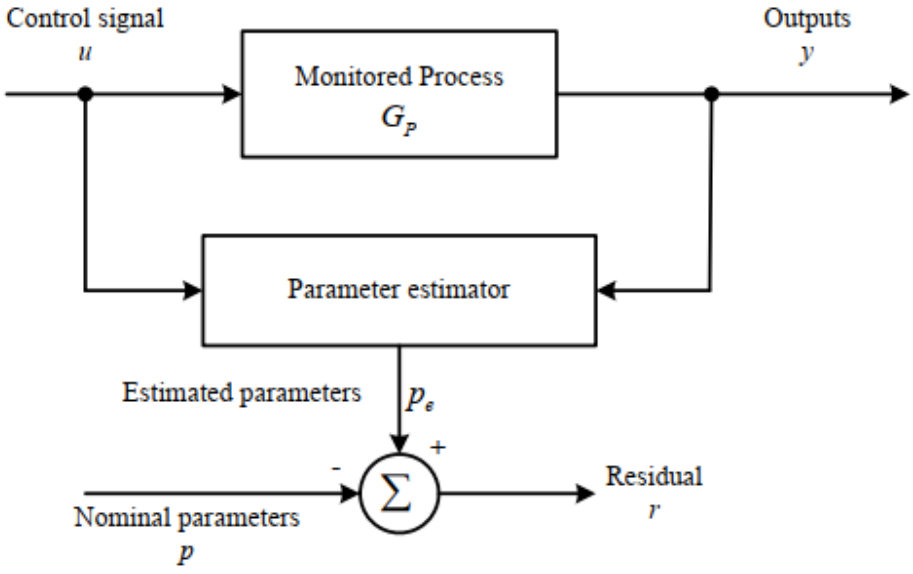

Figure 6.7 Parameter estimation[28]

6.4. Modeling of the PMSM machine in the presence of stator faults:

6.4.1. Model based on a "healthy" PMSM structure

This modeling is based on the simplifying assumptions commonly used, as we used in Chapter III for simplicity.

According to the equations present in the three-phase reference (Chapter III), the electrical equations of the stator in the reference d, q are written:

$$[V_s]_{dq} = R_s[I_s]_{dq} + L_s[\dot{I}_s]_{dq} + wL_s\begin{bmatrix}0 & 1\\ -1 & 0\end{bmatrix}[I_s]_{dq} + [E]_{dq} \tag{6-6}$$

Where $L_s = L_p - M$, and $w = {d\theta}/{dt}$

The angle θ traditionally chosen corresponds to the electrical position of the rotor relative to the stator, denoted θ_e. In the case where the fem are purely sinusoidal and balanced, this makes it possible to cancel the component of $[E]_{dq}$ on the axis d:

$$[E]_{dq} = P(\theta_e)T_{23}[X]_{\alpha\beta} = \begin{bmatrix}0\\ K_e w\end{bmatrix} \tag{6-7}$$

Where

K_e : Constant of fem.

$$P(\theta_e) = \begin{bmatrix} \cos\theta_e & \sin\theta_e \\ -\sin\theta_e & \cos\theta_e \end{bmatrix}$$

$$[X]_{\alpha\beta} = T_{23}[X]_{abc}$$

$$T_{23} = \sqrt{\frac{2}{3}}\begin{bmatrix} 1 & -\frac{1}{2} & -\frac{1}{2} \\ 0 & \frac{\sqrt{3}}{2} & -\frac{\sqrt{3}}{2} \end{bmatrix}$$

Finally, applying the standard Park transformation, this PMSM modeling allowed as the following state equations:

$$\begin{cases} \dot{I}_d = -\frac{R_s}{L_s} I_d + I_q w + \frac{1}{L_s} v_d \\ \dot{I}_q = -\frac{R_s}{L_s} I_q - I_d w_r - \frac{K_e}{L_s} w + \frac{1}{L_s} v_q \end{cases} \quad (6\text{-}8)$$

This formulation, represented graphically in Figure 6.8, shows the different parameters that can be estimated via the extended MVT observer, namely the electric pulsation w, the stator resistance R_s, the inverse of the cyclic inductance $1/L_s$ and the constant of fem K_e.

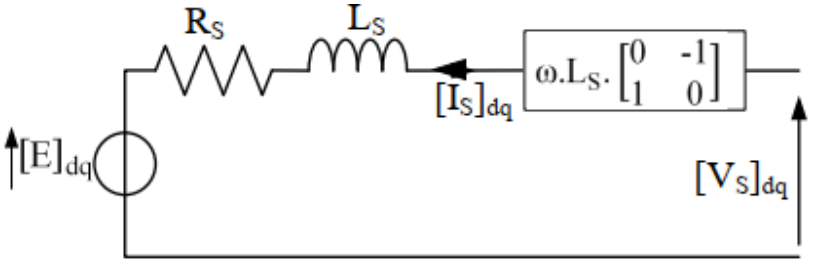

Figure 6.8 "Healthy" PMSM Model in Park reference.

The use of extended MVT observer for estimating the various parameters of this model (w, R_s, $K_e, 1/L_s$).

6.4.2. Model based on a "faulty" PMSM structure

The faulty PMSG model used for inter-turn short-circuit detection is based on a former study [12-Aubert 2013] with less modeling assumptions (voltage drops due to short-circuit reduction is taken into account) to make the PMSG model more sensitive to windings faults. The model enables the fault localization with the use of angle $\theta_{s/c}$ (equal to 0, 2π/3 or 4π/3 for a short circuit respectively

on phase A, phase B or phase C) and the determination of the number of short-circuited turns $n_{s/c}$ (ratio between the number of short-circuited turns and the entire turns number on a stator winding).

Figure 6.9 shows the basic model for fault diagnosis with inter-turn short-circuit on phase A ($\theta_{s/c}$ = 0).

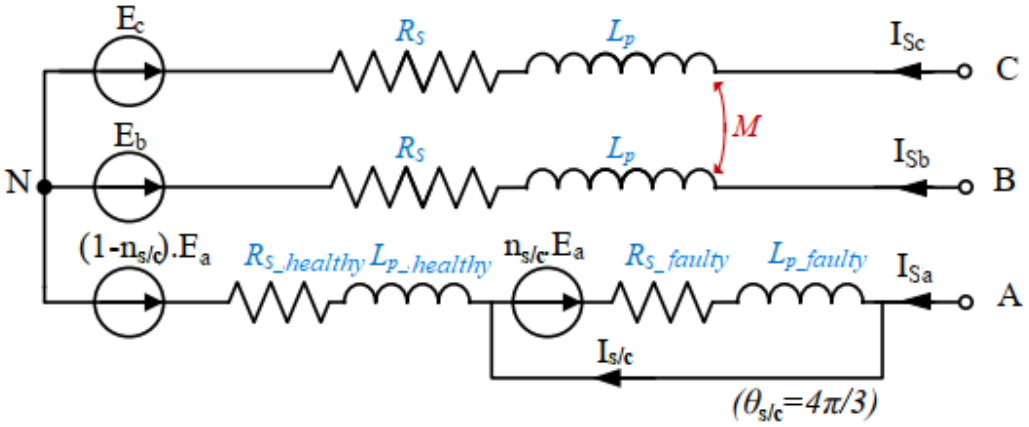

Figure 6.9 scheme of the faulty model of PMSM in the three-phase reference (fault on phase A)[28]

Compared to the model of the healthy PMSM (Figure 6.8), it inserts a short-circuit loop characterized by two new parameters:

- **The angle of localization of the fault $\boldsymbol{\theta_{s/c}}$** which makes it possible to detect the faulty phase. Its value is equal to 0, 2π/3 or 4π/3 such that the inter-turn short-circuit is located respectively on phase A, B or C.
- **Percentage of turns in short circuit $\boldsymbol{n_{s/c}}$** which corresponds to the ratio between the numbers of turns in fault on the total number of turns constituting a stator phase.

In order to write the model's electrical equations, the resistors and inductors of the faulty phase must be defined. Concerning the resistances, they are considered to be proportional to the number of turns. So:

$$\begin{cases} R_{S\_healthy} = (1 - n_{s/c})R_s \\ R_{S\_faulty} = n_{s/c}\, R_s \end{cases} \tag{6-9}$$

The inductances of the faulty phase (the leakage inductances are neglected in this formulation which implies $M = -{}^{L_p}/_{2}$) are:

$$\begin{cases} L_{p\_healthy} = (1 - n_{s/c})^2 L_p \\ L_{p\_faulty} = {n_{s/c}}^2 \, L_p \\ M_{healthy\_faulty} = n_{s/c}(1 - n_{s/c}) L_p \\ M_{s\_healthy} = (1 - n_{s/c}) M = -(1 - n_{s/c}) \dfrac{L_p}{2} \\ M_{s\_faulty} = n_{s/c} \, M = -n_{s/c} \dfrac{L_p}{2} \end{cases} \quad (6\text{-}10)$$

From the expressions of the resistances (6-9) and the inductances (6-10) related to the phase in default, the electrical equations to the stator can be expressed in the three-phase reference:

$$\begin{cases} [V_S] = [R_S].[I_S] + [L_S].[\dot{I}_S] + [E] - n_{s/c}.R_S.T_{s/c}I_{s/c} - \sqrt{\dfrac{3}{2}}.n_{s/c}.L_P.T_{32}.\begin{bmatrix} cos\theta_{s/c} \\ sin\theta_{s/c} \end{bmatrix}.\dot{I}_{s/c} \\ 0 = n_{s/c}.R_S.T_{s/c}^T.[I_S] + \sqrt{\dfrac{3}{2}}.n_{s/c}.L_P.\left(T_{32}.\begin{bmatrix} cos\theta_{s/c} \\ sin\theta_{s/c} \end{bmatrix}\right)^T.[\dot{I}_S] - n_{s/c}.T_{s/c}^T.[E] + n_{s/c}.R_S.I_{s/c} + n_{s/c}^2.L_p.\dot{I}_{cc} \end{cases} \quad (6\text{-}11)$$

Where

$$T_{32} = \frac{1}{\sqrt{3}}.\begin{bmatrix} \sqrt{2} & 0 \\ \frac{-1}{\sqrt{2}} & \sqrt{\frac{3}{2}} \\ \frac{-1}{\sqrt{2}} & -\sqrt{\frac{3}{2}} \end{bmatrix} \quad and \quad X_{abc} = T_{32}.X_{\alpha\beta}$$

$$T_{s/c} = \frac{1}{3}\begin{bmatrix} 1 + 2\cos(\theta_{s/c}) \\ 1 + 2\cos\left(\theta_{s/c} - \frac{2\pi}{3}\right) \\ 1 + 2\cos\left(\theta_{s/c} - \frac{4\pi}{3}\right) \end{bmatrix} : \text{Short-circuit matrix}$$

$$T_{s/c} = \begin{bmatrix} 1 \\ 0 \\ 0 \end{bmatrix} \text{ si } \theta_{s/c} = 0 \; ; \; T_{s/c} = \begin{bmatrix} 0 \\ 1 \\ 0 \end{bmatrix} \text{ si } \theta_{s/c} = \frac{2\pi}{3} \; ; \; T_{s/c} = \begin{bmatrix} 0 \\ 0 \\ 1 \end{bmatrix} \text{ si } \theta_{s/c} = \frac{4\pi}{3}$$

Applying the Concordia transformation to (6-11), the electrical equations becomes:

$$\begin{cases} [V_S]_{\alpha\beta} = R_S[I_S]_{\alpha\beta} + L_S\left[\dot{I}_S\right]_{\alpha\beta} + [E]_{\alpha\beta} - n_{s/c}R_S T_{23}T_{s/c}I_{s/c} - \sqrt{\dfrac{2}{3}}n_{s/c}L_s\begin{bmatrix}cos\theta_{s/c}\\ sin\theta_{s/c}\end{bmatrix}\dot{I}_{s/c} \\ 0 = n_{s/c}R_S T_{s/c}^T T_{32}[I_S]_{\alpha\beta} + \sqrt{\dfrac{2}{3}}n_{s/c}L_s\left(T_{32}\begin{bmatrix}cos\theta_{s/c}\\ sin\theta_{s/c}\end{bmatrix}\right)^T T_{32}\left[\dot{I}_S\right]_{\alpha\beta} - n_{s/c}T_{s/c}^T T_{32}[E]_{\alpha\beta} \\ \qquad\qquad +n_{s/c}R_S I_{s/c} + \dfrac{2}{3}n_{s/c}^2 L_s\dot{I}_{s/c} \end{cases} \tag{6-12}$$

Where $L_s = \frac{3}{2}L_p$: Synchronous Inductance.

$$T_{23}T_{s/c} = \sqrt{\tfrac{2}{3}}\begin{bmatrix}cos\theta_{s/c}\\ sin\theta_{s/c}\end{bmatrix}$$

By posing $\left[I_{s/c}\right]_{\alpha\beta} = \begin{bmatrix}cos\theta_{s/c}\\ sin\theta_{s/c}\end{bmatrix}I_{s/c}$ and multiplying the second equation of (6-12) by $\begin{bmatrix}cos\theta_{s/c}\\ sin\theta_{s/c}\end{bmatrix}$ the equations (6-12) becomes:

$$\begin{cases} [V_S]_{\alpha\beta} = R_S[I_S]_{\alpha\beta} + L_S\left[\dot{I}_S\right]_{\alpha\beta} + [E]_{\alpha\beta} - \sqrt{\dfrac{2}{3}}n_{s/c}R_S\left[I_{s/c}\right]_{\alpha\beta} - \sqrt{\dfrac{2}{3}}n_{s/c}L_s\left[\dot{I}_{s/c}\right]_{\alpha\beta} \\ 0 = \sqrt{\dfrac{2}{3}}n_{s/c}R_S Q(\theta_{s/c})[I_S]_{\alpha\beta} + \sqrt{\dfrac{2}{3}}n_{s/c}L_s Q(\theta_{s/c})\left[\dot{I}_S\right]_{\alpha\beta} - \sqrt{\dfrac{2}{3}}n_{s/c}Q(\theta_{s/c})[E]_{\alpha\beta} \\ \qquad\qquad +n_{s/c}R_S\left[I_{s/c}\right]_{\alpha\beta} + \dfrac{2}{3}n_{s/c}^2 L_s\left[\dot{I}_{s/c}\right]_{\alpha\beta} \end{cases} \tag{6-13}$$

Where

$$Q(\theta_{s/c}) = \begin{bmatrix}cos(\theta_{s/c})\\ \sin(\theta_{s/c})\end{bmatrix}\begin{bmatrix}\cos(\theta_{s/c}) & \sin(\theta_{s/c})\end{bmatrix} = \begin{bmatrix}cos^2(\theta_{s/c}) & \cos(\theta_{s/c})\sin(\theta_{s/c})\\ \cos(\theta_{s/c})\sin(\theta_{s/c}) & sin^2(\theta_{s/c})\end{bmatrix}$$

By posing $\left[\vec{I}_{s/c}\right]_{\alpha\beta} = \sqrt{\frac{2}{3}}n_{s/c}R_S\left[I_{s/c}\right]_{\alpha\beta}$ the equations (6-13) are written:

$$\begin{cases} [V_S]_{\alpha\beta} = R_S\left[I_S - \tilde{T}_{s/c}\right]_{\alpha\beta} + L_S\left[\dot{I}_S - \dot{\tilde{I}}_{s/c}\right]_{\alpha\beta} + [E]_{\alpha\beta} \\ R_S\left[\tilde{T}_{s/c}\right]_{\alpha\beta} + \frac{2}{3}n_{s/c}L_s\left[\dot{\tilde{I}}_{s/c}\right]_{\alpha\beta} = \frac{2}{3}n_{s/c}Q(\theta_{s/c})\left(R_S[I_S]_{\alpha\beta} + L_S\left[\dot{I}_S - \dot{\tilde{I}}_{s/c}\right]_{\alpha\beta} + [E]_{\alpha\beta}\right) \end{cases} \quad (6\text{-}14)$$

Finally, by posing $[I'_S]_{\alpha\beta} = \left[I_S - \tilde{T}_{s/c}\right]_{\alpha\beta}$, the electrical equations relating to this model in the Concordia reference are expressed:

$$\begin{cases} [V_S]_{\alpha\beta} = R_S[I'_S]_{\alpha\beta} + L_S\left[\dot{I}'_S\right]_{\alpha\beta} + [E]_{\alpha\beta} \\ \left[\tilde{T}_{s/c}\right]_{\alpha\beta} = \frac{2n_{s/c}}{(3-2n_{s/c})R_S}Q(\theta_{s/c})[V_S]_{\alpha\beta} = \left[Y_{s/c}\right]_{\alpha\beta}[V_S]_{\alpha\beta} \end{cases} \quad (6\text{-}15)$$

Where

$$\left[Y_{s/c}\right]_{\alpha\beta} = \left[\frac{1}{Z_{s/c}}\right]_{\alpha\beta} = \frac{2n_{s/c}}{(3-2n_{s/c})R_S}Q(\theta_{s/c}) \quad (6\text{-}16)$$

By applying the Park transformation to (6-15), the electrical equations becomes:

$$\begin{cases} [V_S]_{dq} = R_S[I'_S]_{dq} + L_S\left[\dot{I}'_S\right]_{dq} + wL_S\begin{bmatrix} 0 & 1 \\ -1 & 0 \end{bmatrix}[I'_S]_{dq} + [E]_{dq} \\ \left[\tilde{T}_{s/c}\right]_{dq} = P(\theta_e)\frac{1}{\left[Z_{s/c}\right]_{dq}}P(\theta_e)^T[V_S]_{dq} = \left[Y_{s/c}\right]_{dq}[V_S]_{dq} \end{cases} \quad (6\text{-}17)$$

Where

$$\left[Y_{s/c}\right]_{dq} = \left[\frac{1}{Z_{s/c}}\right]_{dq} = \frac{2n_{s/c}}{(3-2n_{s/c})R_S}P(\theta_e)\,Q(\theta_{s/c})\,P(\theta_e)^T$$

Finally, the equations of state relating to this model in the Park referential are expressed:

$$\begin{cases} \left[\dot{I}'_S\right]_{dq} = \begin{bmatrix} -\frac{R_S}{L_S} & \omega \\ -\omega & -\frac{R_S}{L_S} \end{bmatrix}[I'_S]_{dq} - \frac{1}{L_S}[E]_{dq} + \frac{1}{L_S}[V_S]_{dq} \\ [I_S]_{dq} = [I'_S]_{dq} + \left[\tilde{T}_{s/c}\right]_{dq} = [I'_S]_{dq} + \left[Y_{s/c}\right]_{dq}[V_S]_{dq} \end{cases} \quad (6\text{-}18)$$

The system of equations (6-18), shown schematically in Figure 6-10, corresponds to the classical equation of a healthy PMSM considering $[I'_S]$ as the stator current, to which is added an output equation relative to the fault.

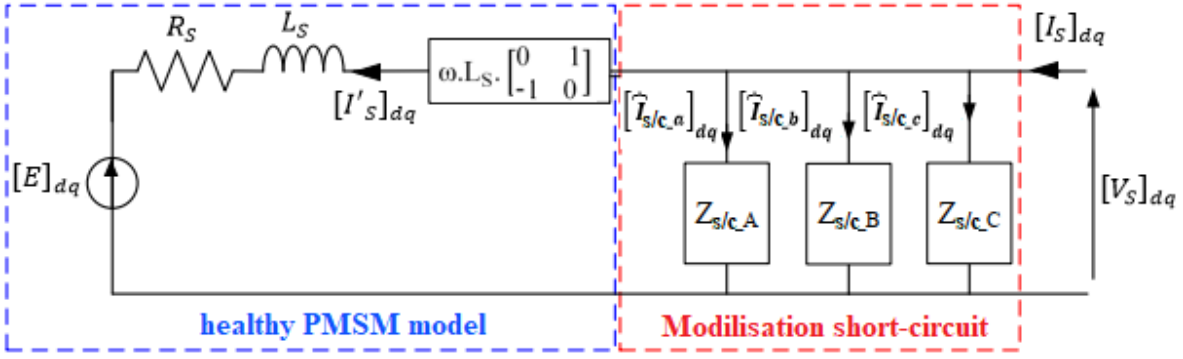

Figure 6.10 Faulty PMSM model in Park referential[28]

The short circuit current is characterized by an impedance $[Z_{s/c}]$ which deviate a part of the stator current when the fault occurs. This impedance depends on the location of the fault, because of the presence of $\theta_{s/c}$ in its expression. By applying this modeling principle to the three stator phases, by fixing the value of $\theta_{s/c}$ three fault impedances $[Z_{s/c\_A}]$, $[Z_{s/c\_B}]$ and $[Z_{s/c\_C}]$ are defined. They respectively correspond to localize the fault on the phase A ($\theta_{s/c} = 0$), B ($\theta_{s/c} = \frac{2\pi}{3}$), C ($\theta_{s/c} = \frac{4\pi}{3}$).

These impedances depend only on the percentages of turns in short-circuit n_{s/c_A}, n_{s/c_B} et n_{s/c_C} which will be the parameters estimated by the extended MVT observer.

The equations (6-18) of faulty model, can be written as state space form as follows:

$$\begin{cases}\dot{x}(t) = A(t)x(t) + Bu(t)\\ y(t) = Cx(t) + Du(t)\end{cases} \tag{6-19}$$

Where

$$x = \left[I'_{Sd}\ \ I'_{Sq}\ \ w\right]^T ;\quad u = \left[V_{Sd}\ \ V_{Sq}\ \ E_{Sd}\ \ E_{Sq}\right]^T$$

$$A = \begin{bmatrix} -\frac{R_S}{L_S} & w & 0\\ -w & -\frac{R_S}{L_S} & 0\\ 0 & 0 & 0\end{bmatrix} ; B = \begin{bmatrix} \frac{1}{L_S} & 0 & -\frac{1}{L_S} & 0\\ 0 & \frac{1}{L_S} & 0 & -\frac{1}{L_S}\\ 0 & 0 & 0 & 0\end{bmatrix} ;\ C = I_{3\times3} ;\ D = \begin{bmatrix}[Y_{s/c}]_{dq} & 0_{2\times2}\\ 0_{1\times2} & 0_{1\times2}\end{bmatrix}$$

6.5. Estimation of the extended MVT Observer on the identification models

6.5.1. Model based on a "healthy" MSAP structure

In order to estimate one of the parameters present in equation (6-8), the state vector must be extended. Thus, the state model is found in the Lipchitz form:

$$\begin{cases} \dot{x}_e(t) = A_e x_e(t) + B_e u(t) + \emptyset_e\big(x_e(t)\big) \\ y_e(t) = C_e x_e(t) \end{cases} \tag{6-20}$$

According to the estimated parameter, the extended state vector x_e and the output vector y_e are expressed:

- For the electric pulsation w:

$$\begin{cases} x_e = \begin{bmatrix} I_{sd} \\ I_{sq} \\ w \end{bmatrix} \\ y_e = \begin{bmatrix} I_{sd} \\ I_{sq} \end{bmatrix} \end{cases} \Longrightarrow \begin{cases} A_e = \begin{bmatrix} -\frac{R_S}{L_S} & 0 & 0 \\ 0 & -\frac{R_S}{L_S} & \frac{K_e}{L_S} \\ 0 & 0 & 0 \end{bmatrix};\ B_e = \begin{bmatrix} \frac{1}{L_S} & 0 \\ 0 & \frac{1}{L_S} \\ 0 & 0 \end{bmatrix};\ \emptyset_e = f_e(x_e) - A_e x_e \\ C = \begin{bmatrix} 1 & 0 & 0 \\ 0 & 1 & 0 \end{bmatrix} \end{cases} \tag{6-21}$$

- For stator resistance R_S:

$$\begin{cases} x_e = \begin{bmatrix} I_{sd} \\ I_{sq} \\ w \\ R_S \end{bmatrix} \\ y_e = \begin{bmatrix} I_{sd} \\ I_{sq} \end{bmatrix} \end{cases} \Longrightarrow \begin{cases} A_e = \begin{bmatrix} -\frac{R_S}{L_S} & 0 & 0 & 0 \\ 0 & -\frac{R_S}{L_S} & \frac{K_e}{L_S} & 0 \\ 0 & 0 & 0 & 0 \\ 0 & 0 & 0 & 0 \end{bmatrix};\ B_e = \begin{bmatrix} \frac{1}{L_S} & 0 \\ 0 & \frac{1}{L_S} \\ 0 & 0 \\ 0 & 0 \end{bmatrix};\ \emptyset_e = f_e(x_e) - A_e x_e \\ C = \begin{bmatrix} 1 & 0 & 0 & 0 \\ 0 & 1 & 0 & 0 \end{bmatrix} \end{cases} \tag{6-22}$$

For the estimation of the constant of fem K_e or of the inverse of the cyclic inductance $1/L_S$, the extended state model is the same as for that concerning the stator resistance by replacing R_S respectively by K_e or $1/L_S$ in the extended state vector x_e.

6.5.2. Model based on a "faulty" PMSM structure

As in the case of the healthy model, the estimation of the percentages of short-circuit turns ($n_{s/c\_A}, n_{s/c\_B}, n_{s/c\_C}$) passes per the extension of the state vector. According to equation (6-18), the resulting extended state system is written with:

$$\begin{cases} \dot{x}_e(t) = A_e x_e(t) + B_e u(t) \\ y_e(t) = C_e x_e(t) + \Psi_e\big(x_e(t)\big) \end{cases} \tag{6-23}$$

Where

$$\begin{cases} x_e = \begin{bmatrix} I_{Sd} \\ I_{Sq} \\ n_{s/c\_A} \\ n_{s/c\_B} \\ n_{s/c\_C} \end{bmatrix} \Longrightarrow \begin{cases} A_e = \begin{bmatrix} \begin{bmatrix} -\dfrac{R_S}{L_S} & w \\ -w & -\dfrac{R_S}{L_S} \end{bmatrix} & [\mathrm{O}_{2\times 3}] \\ [\mathrm{O}_{3\times 2}] & [\mathrm{O}_{3\times 3}] \end{bmatrix} \\ B_e = \begin{bmatrix} \begin{bmatrix} \dfrac{1}{L_S} & 0 & -\dfrac{1}{L_S} & 0 \\ 0 & \dfrac{1}{L_S} & 0 & -\dfrac{1}{L_S} \end{bmatrix} \\ [\mathrm{O}_{3\times 4}] \end{bmatrix} \\ C = \begin{bmatrix} 1 & 0 & 0 & 0 & 0 \\ 0 & 1 & 0 & 0 & 0 \end{bmatrix} \\ \Psi_e(x_e) = [[Y_{s/c\_A} \quad Y_{s/c\_B} \quad Y_{s/c\_C}]_{dq} \quad [\mathrm{O}_{2\times 2}]] \end{cases} \\ y_e = \begin{bmatrix} I_{Sd} \\ I_{Sq} \end{bmatrix} \end{cases} \tag{6-24}$$

Where $u(t) = \begin{bmatrix} V_{Sd} & V_{Sq} & E_{Sd} & E_{Sq} \end{bmatrix}^T$

In (6-24) the short-circuit admittances Y_{s/c_i} are expressed:

$$\big[Y_{s/c_i}\big]_{dq} = \frac{1}{R_S} k\big(n_{s/c_i}\big) M_i(\theta_e) \qquad for\ i = A, B, C \tag{6-25}$$

$$\begin{cases} k\big(n_{s/c_i}\big) = \dfrac{2n_{s/c_i}}{\big(3 - 2n_{s/c_i}\big)} \qquad for\ i = A, B, C \\ M_i(\theta_e) = P(\theta_e) Q\big(\theta_{s/c\_i}\big) P(\theta_e)^T \qquad with \begin{cases} \theta_{s/c\_A} = 0 \\ \theta_{s/c\_B} = \dfrac{2\pi}{3} \\ \theta_{s/c\_C} = \dfrac{4\pi}{3} \end{cases} \end{cases} \tag{6-26}$$

We can also notice the absence of w in the extended state vector x_e of (6-24). Indeed, in order to reduce the computational cost of the extended MVT observer algorithm applied to this model, we decided to limit this system to an order 5, considering the electric pulsation as slowly variable compared to the sampling period. Thus, no longer part of the state vector but still remains measured in order to update its value in the state matrix A_e. We verified by simulation that this order

reduction does not alter the estimation performance of the states and parameters of the system (6-24).

6.6. Construction and evaluation of indicators of presence of inter-turn short-circuits

6.6.1. Principle of construction of the indicators

In this part, the construction principle of the different inter-turn short-circuit presence indicators is presented. It is based on parameter estimation via the extended MVT observer from a "healthy" or "faulty" PMSM model. Firstly, the response of the estimated parameters during the appearance of an inter-turn short-circuit is presented. Then, the behavior of each parameter is studied in order to construct a relevant fault indicator.

6.6.1.1. Model “ healthy ”

In this chapter, we have shown that the application of the extended MVT observer on the "healthy" model of the PMSM, expressed in the Park coordinate system, makes it possible to estimate various parameters:

- The electric pulsation *w*
- The constant of fem *Ke*
- Stator resistance *Rs*
- The inverse of cyclic inductance *1/Ls*

These estimated parameters will be used to construct indicators of presence of inter-turn faults within the stator windings of the PMSM.

Figure 6-11 shows the evolution of each parameter estimated from the "healthy" PMSM model, when an inter-turn short-circuit of 15% of the turns appears on phase A at t = 0.5s. We can notice that each parameter is strongly impacted by the appearance of the faulty regime. Indeed, while it is estimated around its nominal value in healthy mode (for t <0.5s), a change in its average value and significant oscillations appear as soon as the fault occurs.

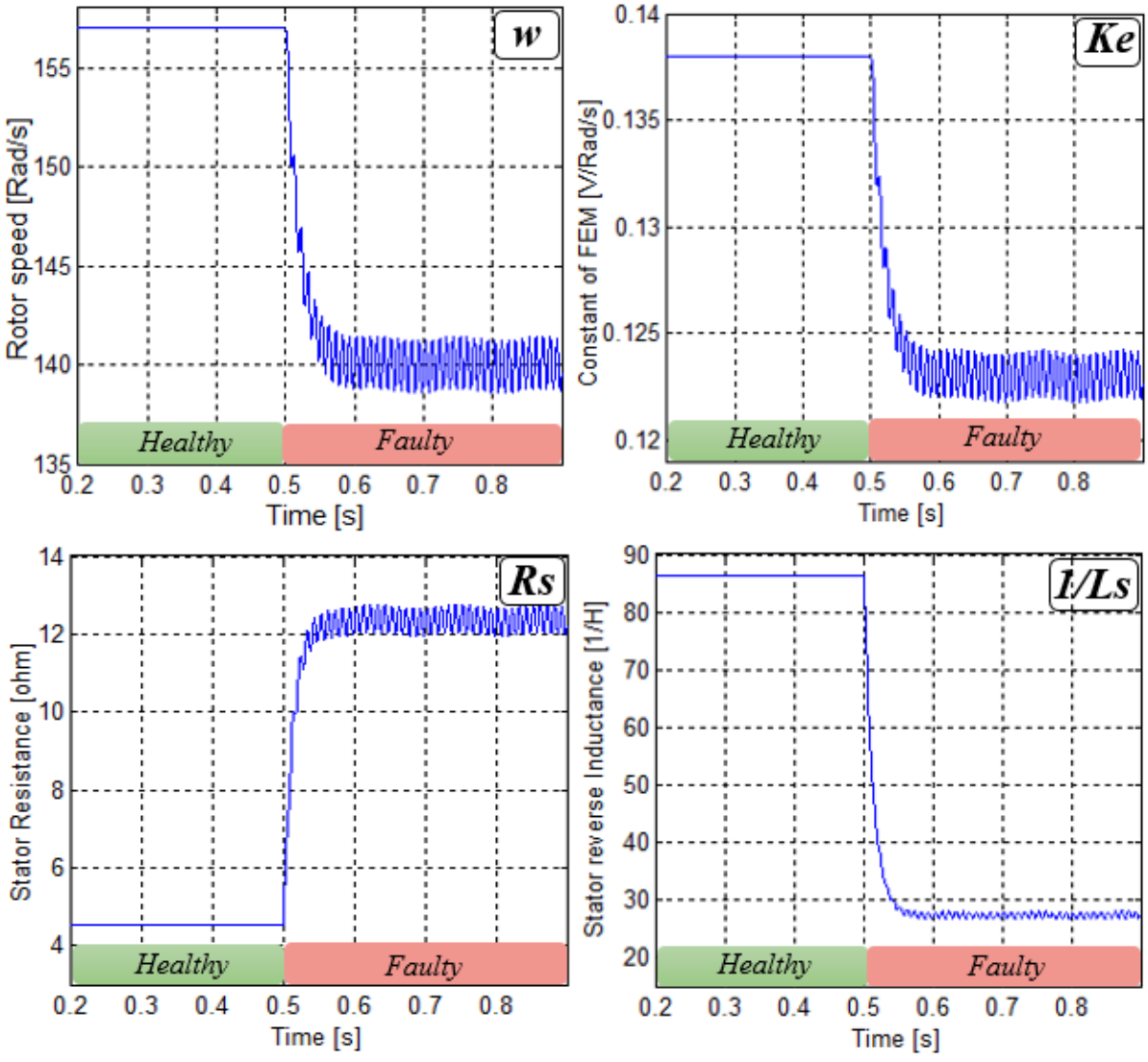

Figure 6.11 Evolution of the estimated parameters resulting from the "healthy" model of the PMSM during a short circuit of 15% of the turns on phase A (for $I_{Load} = 6A$ and $f = 50Hz$)

By focusing more particularly on the evolution of the estimate parameters when the short-circuit is established, we can see, in Figure 6-11, that the oscillations on the parameters estimation appear at 100 Hz, which corresponds to the 2.fs frequency. The presence of this frequency is consistent insofar as it is characteristic of an imbalance in a three phase system when the latter is represented in the Park reference system.

In order to limit the influence of the oscillations at 2. fs in the faulty mode, this estimation error is filtered. Finally, from the estimation of a parameter resulting from the "healthy" model of the

PMSM, the indicator used to detect the inter-turns short-circuits in the stator windings of the machine is expressed by:

$$Ind_{\lambda} = 100.\left\langle \left| \frac{\hat{\lambda} - \lambda_{ref}}{\lambda_{ref}} \right| \right\rangle \tag{6-27}$$

Where $\hat{\lambda}$ is the estimated parameter and λ_{ref} is the reference value of the parameter.

A. Indicator response for different numbers of turns in short circuit

Figure 6-12 shows the evolution of the indicators, constructed from the parameter estimation, for a healthy PMSM (t < 0.5s) and a default PMSM (t > 0.5s), with different numbers of turns in short circuit. In the healthy case, the value of the indicator remains close to zero, which reflects a good estimate of the parameters in relation to their nominal value. In the case of an inter-turn short circuit, the value of the indicator increases with the number of short-circuit turns. This confirms the fact that the detection of the fault is more delicate for a small number of short-circuited turns, whereas these same faults are nevertheless the most critical (values of the highest short-circuit currents). The more the number of turns in short-circuit franc increases, the more the imbalance between the healthy model and the faulty generator is perceptible, therefore more the parametric reaction will be important.

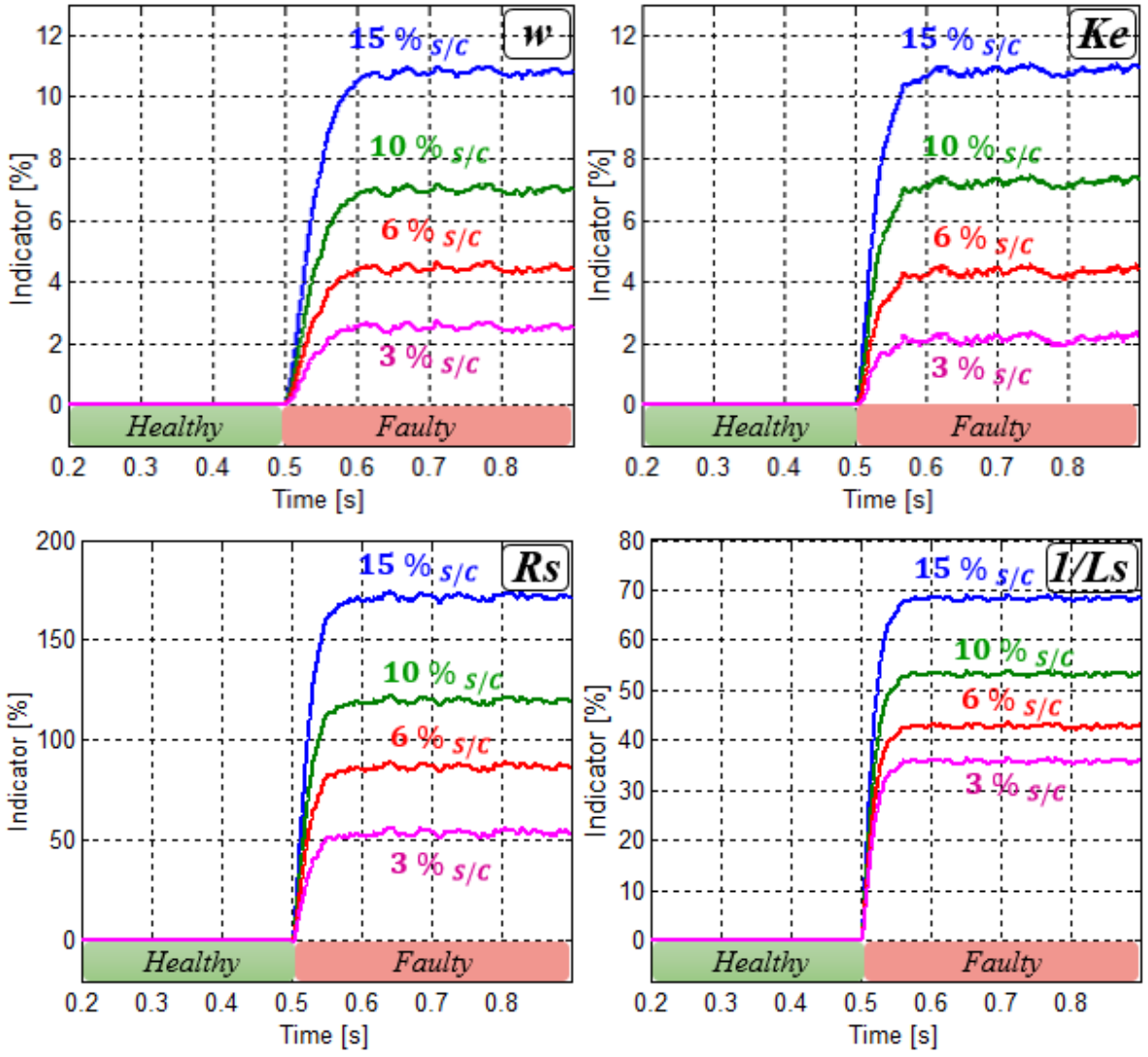

Figure 6.12 Evolution of the indicators constructed from the estimated parameters resulting from the "healthy" model of the PMSM for different numbers of turns in short-circuit (for $I_{Load} = 6A$ and $f=50Hz$)

The indicators proposed here are thus more an image of the imbalance generated by the fault rather than an indicator linked to the dangerousness of the fault.

However, if we compare the behavior of the indicators for a healthy PMSM and a faulty PMSM, we notice that a fast detection is possible even for a small number of shorted turns

6.6.1.2. Model " faulty "

The "faulty" PMSM model, expressed in the Park references (see Figure 6.10 and equation (6-18)), makes it possible to estimate the percentages of turns in short-circuit on the three phases of the PMSM. As in the case of the "healthy" model, the construction principle of the inter-turn fault indicator using the estimated parameters from the "faulty" model is detailed in this section.

A. Estimated Parameters Response

As shown in Figure 6.13, where a 15% inter-turn short-circuit is generated at t = 0.5 s on phase A, estimated parameters $n_{s/c}$ are impacted. Indeed, a modification of mean value and large oscillations at twice the electrical frequency appear as soon as the winding fault occurs. It is also noticeable that n_{s/c_A} is not the only estimated parameter sensitive to the short circuit. n_{s/c_B} and n_{s/c_C} are also modified in a lesser extent due to some simplifying assumptions about PMSM symmetry in the definition of the dq frame model. However, the fault can be clearly located on phase A in this test.

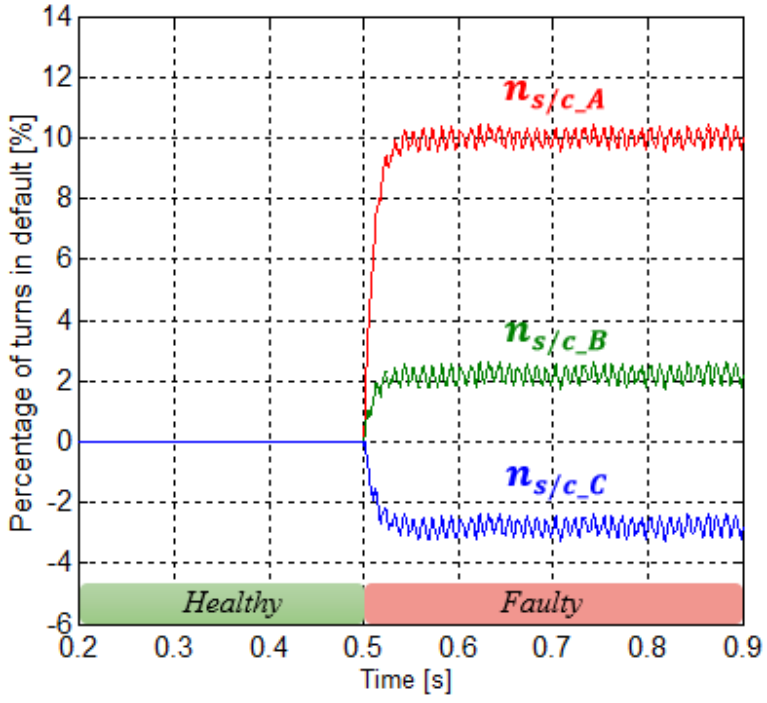

Figure 6.13 Evolution of the estimated parameters resulting from the "faulty" model of the PMSM during a short-circuit of 15% of the turns on phase A (for I_{Load} = 6A and f = 50Hz)

B. Construction of the indicator based on the parameters $n_{s/c}$

In Figure 6.13, we find that the oscillations on the percentages of turns in short-circuit also appear at 100Hz, which corresponds to the frequency 2.fs. Given the behavior of the parameters estimated during the fault, the indicator chosen to detect the presence of an inter-turn short-circuit is calculated from the sum of the absolute values of the percentages of turns in short-circuit on each phase. This sum is also filtered to minimize oscillations. Finally, the indicator constructed from the "faulty" model of the PMSM is expressed as:

$$Ind_{n_{s/c}} = 100. \sum_{i=A,B,C} \langle |n_{s/c\_i}| \rangle \tag{6-28}$$

C. Indicator response for different numbers of turns in short-circuit

Figure 6.14 shows the evolution of the indicator, constructed from the estimate of $n_{s/c}$, for a healthy PMSM (t < 0.5s) and a faulty PMSM (t > 0.5s), with different number of turns in short-circuit. If there is no fault, the value of the indicator remains close to zero. This indicates that the faulty part of the identification model has little influence; PMSM can therefore be considered healthy. In the case of an inter-turn short-circuit, the value of the indicator increases with the number of turns in short-circuit. In addition, during this simulation, this indicator also makes it easy to distinguish a healthy operation from a faulty operation, even for a small number of turns in short circuit. As before, the value of the indicator is not directly the image of the current in the short-circuit loop but an image of the imbalance generated by the fault.

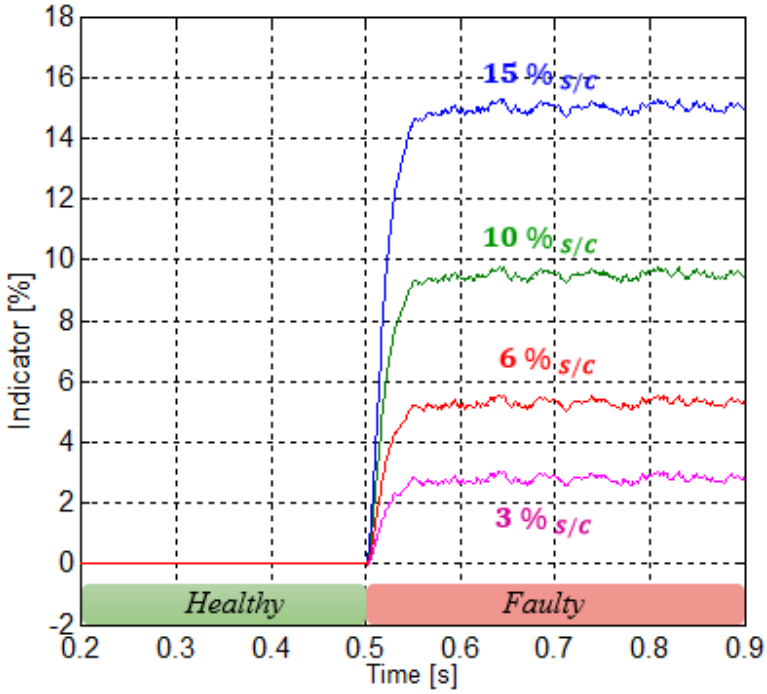

Figure 6.14 Evolution of the indicator constructed from the estimated parameters resulting from the "faulty" model of the PMSM for different numbers of turns in short-circuit (for $I_{Load} = 5A$ and $f = 50Hz$)

6.6.2. Evaluation of the indicators

In this part, the performance of the proposed indicators will be evaluated according to the criteria of robustness.

6.6.2.1. Robustness Analysis

In order to evaluate the robustness of the fault indicator to the inter-turn short-circuit diagnosis against electrical network variations, several tests based on simulation test bench have been made and are listed in the following.

Test 1: Frequency variation from 30 to 60 Hz with 10-Hz step and 6-A load current per phase.

Test 2: Power variation from 8- to 2-A load current per phase with 2 A step and 50-Hz electrical frequency.

A. Variation of the electric frequency

The purpose of this test is to study the behavior of the indicators for several operating frequencies.

Figure 6.15 shows the evolution of the indicator based on the estimate of ω for different operating frequencies. Figures for other indicators are available in Appendix B.

In failed mode, Figure 6.11-c shows that, for a given number of shorted turns, the value of the indicators increases with the operating frequency. This is due to the essentially resistive nature of the fault loop on the machine studied during a short circuit of a small number of turns. In the case of short-circuit and knowing the nature of the fault loop, the value of short-circuit current can then be expressed:

$$I_{s/c} = \frac{n_{s/c}\, V_s}{\left|R_{faulty} + jX_{faulty}\right|} \xrightarrow{R_{faulty} \gg L_{faulty}} \frac{V_s}{R_s} \tag{6-29}$$

The voltage of the PMSM is proportional to the rotational frequency of the rotor (neglecting voltage drops), we can deduct from (6-29) that the amplitude of the short-circuit current is also proportional to the frequency, given the resistive nature of the fault loop. This is verified by Figure 6.15-b. Thus, for high frequencies, the imbalance generated on the machine by an inter-turn short-circuit will be greater, which explains the increase in the value of the indicators.

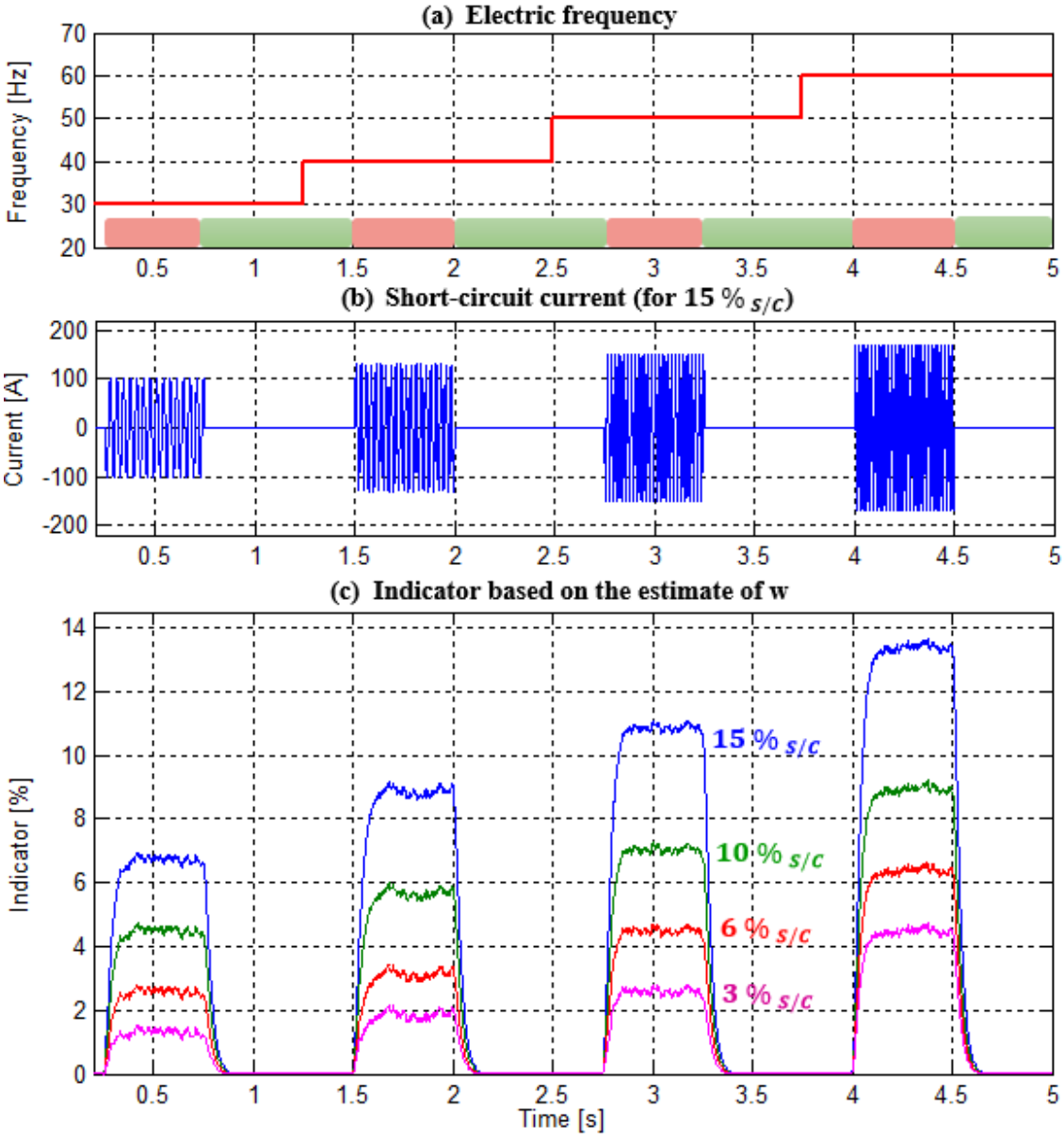

Figure 6.15 Response of the indicator based on the estimation of ***w*** for different operating frequencies

However, the distinction between a healthy PMSM and a faulty PMSM is possible with the proposed indicators, regardless of the operating frequency. This is confirmed by Table 6-1 where the least favorable values of the steady state indicators are reported, for a healthy operation (maximum value of the indicator) and for a faulty operation (minimum value of the indicator). The ratio between the healthy indicator value and the indicator in the failed mode is also indicated. Since the maximum value of the indicator for a healthy PMSM is always lower than its minimum value in the case of an inter-turn short-circuit, we can conclude that for a variable speed operation it is possible to detect a fault with these indicators even for a small number of turns in short circuit.

State of PMSM / Estimated parameters	Healthy	Fault 3 % s/c		Fault 6 % s/c		Fault 10 % s/c		Fault 15 % s/c	
		Ind.	ratio	Ind.	ratio	Ind.	ratio	Ind.	ratio
w	0.73 %	1.46%	2	2.58%	3.53	4.41%	6.04	6.82%	9.34
K_e	0.81 %	1.47%	1.81	2.55%	3.14	4.42%	5.45	6.81%	8.4
R_S	2.3 %	11.3%	4.91	31.4%	13.65	52.9%	23	82.4%	35.82
$1/L_S$	1.1 %	30%	27.2	37.5%	34.1	46.3%	42.1	57.5%	52.3
$n_{s/c}$	0.85 %	1.98%	2.32	4%	4.7	6.72%	7.9	10%	11.7

Table 6-1 Values for steady-state indicators for healthy or faulty PMSM in the frequency variation test

B. Variation of power

In this test, the behavior of the indicators is studied for different power levels. For this purpose, the simulation test consists in varying the load torque T_L in order to obtain a current ranging from 8 A to 2A in steps of 2 A, for an electrical frequency of 50 Hz (Figure 6.16-a). For each load current, an inter-turn short-circuit is generated for 500ms (Figure 6-16-b). We can notice that the amplitude of the short-circuit current depends little on the power demanded. This is due to the small voltage drop caused by the load current.

Figure 6.16-c shows the evolution of the indicator based on the estimate of *1/Ls*, for different power levels. Figures for other indicators are available in Appendix B.

In addition the value of the indicator in faulty mode increases when the charging current decreases. In fact, for same number of short-circuited turns, the variation of the parametric *Rs* or *1/Ls* estimation must be greater at low current in order to compensate the differences between the representation model of healthy machine and faulty machine.

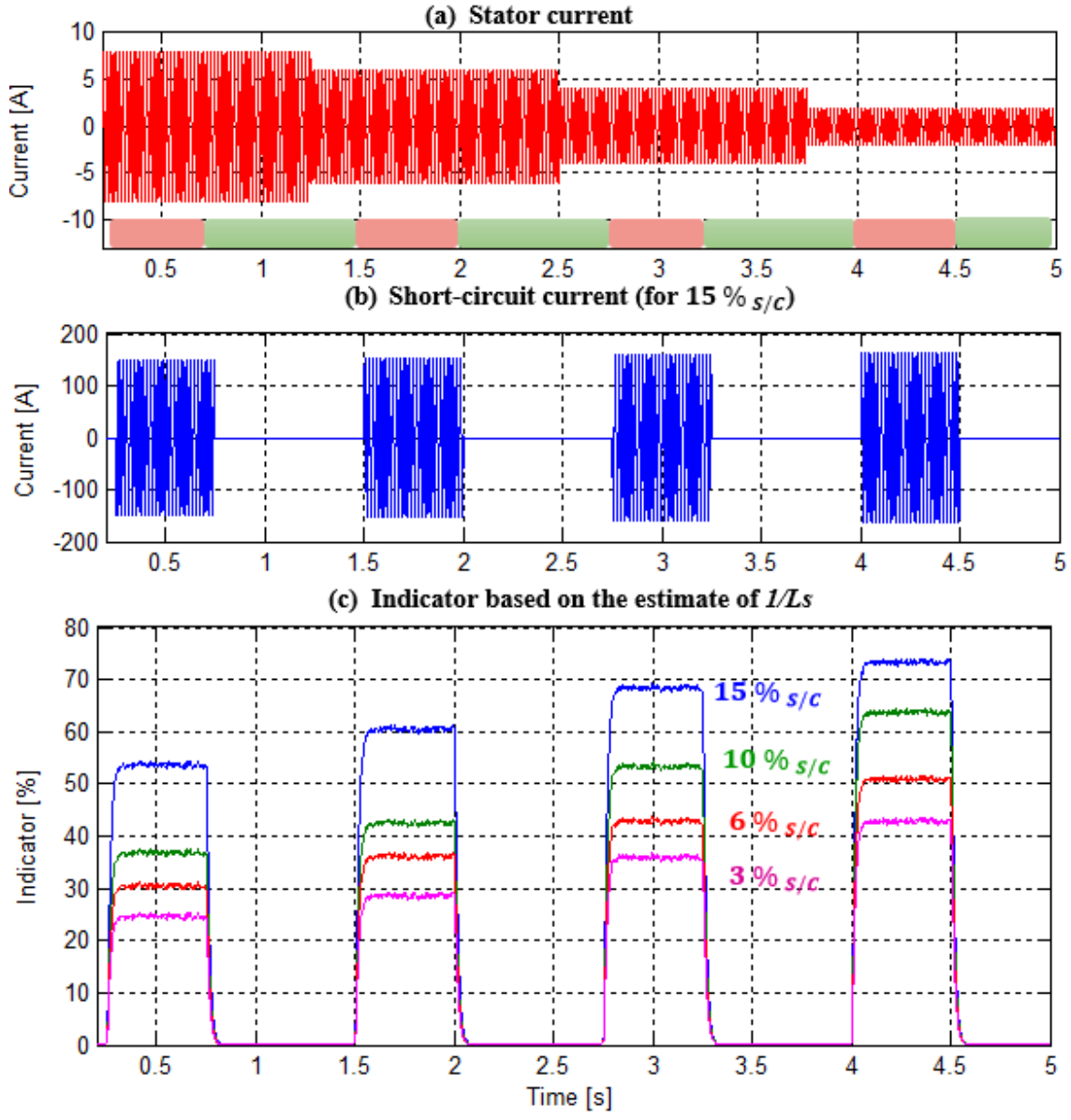

Figure 6.15 Response of the indicator based on the estimation of ***1/Ls*** for different power.

The indicators based on the estimate of ***w***, ***Ke*** and $n_{s/c}$ are little influenced by the power demanded by the load. Indeed, their values in healthy regime and faulty regime, for a given number of short-circuit turns, depend only very little on the current level.

Table 6-2 shows that these indicators make it possible to detect an inter-turn short-circuit of a small number of turns, for the different power levels demanded.

State of PMSM / Estimated parameters	Healthy	Fault 3 % s/c		Fault 6 % s/c		Fault 10 % s/c		Fault 15 % s/c	
		Ind.	ratio	Ind.	ratio	Ind.	ratio	Ind.	ratio
w	0.96%	2.05%	2.13	3.95%	4.11	6.3%	6.5	10.2%	10.6
K_e	0.77%	2.41%	3.11	4.2%	5.45	6.95%	9.02	10.7%	13.9
R_S	1.7%	12.1%	7.11	21.8%	12.8	30.6%	18	50.8%	29.9
$1/L_S$	1.15%	25.2%	25.1	30.5%	26.5	37.8%	32.9	53.6%	46.6
$n_{s/c}$	0.98%	2.75%	2.8	5.3%	5.3	9.42%	9.42	14.6%	14.9

Table 6-1 Values for steady-state indicators for healthy or faulty PMSM in the power variation test

6.7. Conclusion

In this chapter, we have firstly an introduction and general diagnosis of motor drive are presented, such as, we have given a deferent fault are exist in PMSM spicily, and we have given a deferent diagnostic methods, we have talk also about model based fault detection and diagnosis. Then we have modelized the PMSM machine in the presence of stator faults, finally, a simulation results through MATLAB/SIMILINK are presented.

These simulation tests confirm that the indicator based on the $1/L_s$ estimation is the most efficient for detecting the faults of a small number of turns for a resistive short circuit. Indicators based on K_e and $n_{s/c}$ estimation are also suitable for the detection of resistive short circuits. They have, moreover, the advantage of being little dependent on the point of operation of the machine at the moment when the fault occurs. Finally, the indicators based on the estimate of w and R_s are not sufficiently robust in terms of robustness to be used as reliable indicators of presence of short-circuit inter-turns. In the end, the obtained results mentioned above prove the effectiveness of this approach and confirm also the efficiency of the extended MVT Observer to estimate deferent prameters.

References of Chapter VI

[1] S. Nandi, H. A. Toliyat, and X. Li, "Condition monitoring and fault diagnosis of electrical motors—A review," *IEEE transactions on energy conversion*, vol. 20, pp. 719-729, 2005.

[2] M. E. H. Benbouzid, "A review of induction motors signature analysis as a medium for faults detection," *IEEE transactions on industrial electronics*, vol. 47, pp. 984-993, 2000.

[3] A. Siddique, G. Yadava, and B. Singh, "A review of stator fault monitoring techniques of induction motors," *IEEE transactions on energy conversion*, vol. 20, pp. 106-114, 2005.

[4] J. Penman and T. Tavner, *Condition monitoring of electrical machines*: Research Studies Press Ltd., Wiley, New York, 1989.

[5] C. Gerada, K. Bradley, and M. Summer, "Winding turn-to-turn faults in permanent magnet synchronous machine drives," in *Fourtieth IAS Annual Meeting. Conference Record of the 2005 Industry Applications Conference, 2005.*, 2005, pp. 1029-1036.

[6] J. Ahmed Farooq, T. Raminosoa, A. Djerdir, and A. Miraoui, "Modelling and simulation of stator winding inter-turn faults in permanent magnet synchronous motors," *COMPEL-The international journal for computation and mathematics in electrical and electronic engineering*, vol. 27, pp. 887-896, 2008.

[7] A. Khlaief, M. Boussak, and M. Gossa, "Open phase faults detection in PMSM drives based on current signature analysis," in *The XIX International Conference on Electrical Machines-ICEM 2010*, 2010, pp. 1-6.

[8] J. A. Rosero, L. Romeral, J. A. Ortega, and E. Rosero, "Short-circuit detection by means of empirical mode decomposition and Wigner–Ville distribution for PMSM running under dynamic condition," *IEEE Transactions on Industrial Electronics*, vol. 56, pp. 4534-4547, 2009.

[9] B. A. Welchko, T. M. Jahns, and S. Hiti, "IPM synchronous machine drive response to a single-phase open circuit fault," *IEEE Transactions on Power Electronics*, vol. 17, pp. 764-771, 2002.

[10] S. S. Moosavi, A. Djerdir, Y. Aït-Amirat, and D. A. Khaburi, "Fault detection in 3-phase traction motor using artificial neural networks," in *2012 IEEE Transportation Electrification Conference and Expo (ITEC)*, 2012, pp. 1-6.

[11] C.-Y. Lee, "Effects of unbalanced voltage on the operation performance of a three-phase induction motor," *IEEE Transactions on Energy Conversion*, vol. 14, pp. 202-208, 1999.

[12] S. S. Moosavi, A. Djerdir, Y. Aït-Amirat, and D. Kkuburi, "Artificial neural networks based fault detection in 3-Phase PMSM traction motor," in *2012 XXth International Conference on Electrical Machines*, 2012, pp. 1579-1585.

[13] S. Rajagopalan, W. le Roux, T. G. Habetler, and R. G. Harley, "Dynamic eccentricity and demagnetized rotor magnet detection in trapezoidal flux (brushless DC) motors operating

under different load conditions," *IEEE Transactions on Power Electronics,* vol. 22, pp. 2061-2069, 2007.

[14] C. Ruschetti, G. Bossio, C. De Angelo, and C. Verucchi, "Effects of partial rotor demagnetization on permanent magnet synchronous machines," in *2010 IEEE International Conference on Industrial Technology*, 2010, pp. 1233-1238.

[15] W. Le Roux, R. Harley, and T. Habetler, "Rotor fault analysis of a permanent magnet synchronous machine," in *Proc. 15th Int. Conf. Elect. Mach.(ICEM'02)*, 2002, pp. 25-28.

[16] J. Hong, S. Park, D. Hyun, T.-j. Kang, S. B. Lee, C. Kral, *et al.*, "Detection and classification of rotor demagnetization and eccentricity faults for PM synchronous motors," *IEEE Transactions on Industry Applications,* vol. 48, pp. 923-932, 2012.

[17] S. Ruoho and A. Arkkio, "Partial demagnetization of permanent magnets in electrical machines caused by an inclined field," *IEEE Transactions on Magnetics,* vol. 44, pp. 1773-1778, 2008.

[18] J. Hong, D. Hyun, S. B. Lee, J.-Y. Yoo, and K.-W. Lee, "Automated monitoring of magnet quality for permanent-magnet synchronous motors at standstill," *IEEE Transactions on Industry Applications,* vol. 46, pp. 1397-1405, 2010.

[19] J. Farooq, S. Srairi, A. Djerdir, and A. Miraoui, "Use of permeance network method in the demagnetization phenomenon modeling in a permanent magnet motor," *IEEE Transactions on Magnetics,* vol. 42, pp. 1295-1298, 2006.

[20] J. Rosero, L. Romeral, J. Cusido, and J. Ortega, "Fault detection by means of wavelet transform in a PMSMW under demagnetization," in *IECON 2007-33rd Annual Conference of the IEEE Industrial Electronics Society*, 2007, pp. 1149-1154.

[21] D. Torregrossa, A. Khoobroo, and B. Fahimi, "Prediction of acoustic noise and torque pulsation in PM synchronous machines with static eccentricity and partial demagnetization using field reconstruction method," *IEEE Transactions on Industrial Electronics,* vol. 59, pp. 934-944, 2012.

[22] H.-K. Kim, J. Hur, B.-W. Kim, and G.-H. Kang, "Characteristic analysis of IPM type BLDC motor considering the demagnetization of PM by stator turn fault," in *2010 IEEE Energy Conversion Congress and Exposition*, 2010, pp. 3063-3070.

[23] G.-H. Kang, J. Hur, H. Nam, J.-P. Hong, and G.-T. Kim, "Analysis of irreversible magnet demagnetization in line-start motors based on the finite-element method," *IEEE Transactions on Magnetics,* vol. 39, pp. 1488-1491, 2003.

[24] Y. Da, X. Shi, and M. Krishnamurthy, "Health monitoring, fault diagnosis and failure prognosis techniques for Brushless Permanent Magnet Machines," in *2011 IEEE Vehicle Power and Propulsion Conference*, 2011, pp. 1-7.

[25] J. Rosero, J. Cusido, A. Garcia, J. Ortega, and L. Romeral, "Broken bearings and eccentricity fault detection for a permanent magnet synchronous motor," in *IECON 2006-32nd Annual Conference on IEEE Industrial Electronics*, 2006, pp. 964-969.

[26] J. Cameron, W. Thomson, and A. Dow, "Vibration and current monitoring for detecting airgap eccentricity in large induction motors," in *IEE Proceedings B (Electric Power Applications)*, 1986, pp. 155-163.

[27] W. Le Roux, R. G. Harley, and T. G. Habetler, "Detecting rotor faults in low power permanent magnet synchronous machines," *IEEE Transactions on Power Electronics,* vol. 22, pp. 322-328, 2007.

[28] B. Aubert, "Détection des courts-circuits inter-spires dans les Générateurs Synchrones à Aimants Permanents : Méthodes basées modèles et fltre de Kalman étendu - Application à un canal de génération électrique en aéronautique," École Doctorale Génie Électrique, Électronique et Télécommunications: du …, 2014.

[29] R. K. Mehra and J. Peschon, "An innovations approach to fault detection and diagnosis in dynamic systems," *Automatica,* vol. 7, pp. 637-640, 1971.

[30] D. Lainiotis and S. Park, "On joint detection, estimation and system identification: discrete data case," *International Journal of Control,* vol. 17, pp. 609-633, 1973.

[31] A. S. Willsky, "A survey of design methods for failure detection in dynamic systems," *Automatica,* vol. 12, pp. 601-611, 1976.

[32] R. Isermann, "Process fault detection based on modeling and estimation methods—A survey," *automatica,* vol. 20, pp. 387-404, 1984.

[33] J. J. Gertler, "Survey of model-based failure detection and isolation in complex plants," *IEEE Control systems magazine,* vol. 8, pp. 3-11, 1988.

[34] M. Basseville, "Detecting changes in signals and systems—a survey," *Automatica,* vol. 24, pp. 309-326, 1988.

[35] P. M. Frank, "Fault diagnosis in dynamic systems using analytical and knowledge-based redundancy: A survey and some new results," *automatica,* vol. 26, pp. 459-474, 1990.

[36] P. M. Frank and B. Köppen-Seliger, "New developments using AI in fault diagnosis," *Engineering Applications of Artificial Intelligence,* vol. 10, pp. 3-14, 1997.

[37] E. A. Garcia and P. Frank, "Deterministic nonlinear observer-based approaches to fault diagnosis: a survey," *Control Engineering Practice,* vol. 5, pp. 663-670, 1997.

[38] E. Chow and A. Willsky, "Analytical redundancy and the design of robust failure detection systems," *IEEE Transactions on automatic control,* vol. 29, pp. 603-614, 1984.

[39] X.-C. Lou, A. S. Willsky, and G. C. Verghese, "Optimally robust redundancy relations for failure detection in uncertain systems," *Automatica,* vol. 22, pp. 333-344, 1986.

[40] J.-F. Magni and P. Mouyon, "On residual generation by observer and parity space approaches," *IEEE Transactions on Automatic Control,* vol. 39, pp. 441-447, 1994.

[41] R. N. Clark, "The dedicated observer approach to instrument failure detection," in *1979 18th IEEE Conference on Decision and Control including the Symposium on Adaptive Processes*, 1979, pp. 237-241.

[42] R. J. Patton and J. Chen, "Observer-based fault detection and isolation: Robustness and applications," *Control Engineering Practice,* vol. 5, pp. 671-682, 1997.

[43] R. Isermann, "Estimation of physical parameters for dynamic processes with application to an industrial robot," in *[1991 Proceedings] 6th Mediterranean Electrotechnical Conference*, 1991, pp. 12-17.

[44] J. Gertler, "Diagnosing parametric faults: from parameter estimation to parity relations," in *Proceedings of 1995 American Control Conference-ACC'95*, 1995, pp. 1615-1620.

[45] R. Isermann, "Model-based fault-detection and diagnosis–status and applications," *Annual Reviews in control,* vol. 29, pp. 71-85, 2005.

CHAPTER VII

7.1. General Conclusion

This thesis presented control, observer and diagnosis algorithms for PMSM drives that can be applied to a wide range of motor drives applications. Sensorless control of PMSM drives offers obvious advantages in terms of cost, size, and reliability and was explored extensively in this thesis. This algorithms are based on the MVT approach and sector non-linearity transformation must be used to the dynamics model of the nonlinear systems and to design stable and robust structures. The main goals in this work is: firstly, the development of control and observation methodologies based on the MVT approach essentially for a three-phase PMSM where the influence of the parameters uncertainties and disturbances on the performances command is taken into consideration . Secondly, a fault detection and diagnosis using an Extended MVT observer for the estimation of the parameters PMSM which used it as an indicators of faults.

The subsections which will be presented below summarize the conclusions of the different topics considered in this thesis.

Firstly an introduction of the T-S fuzzy model. Then a model-based fuzzy controller design utilizing the concept PDC was described. Moreover, it was shown in this chapter that the stability analysis and control design problems can be reduced to LMI problems. Secondly, the designs of observers and controllers based on MVT were presented, such that, we showed the basic mathematical tools used in the MVT and sector nonlinearity approaches. The stability analysis expressed also in term of LMIs.

The focus of chapter 4 was on the notion of an extended observer based-controller based on the MVT and sector nonlinearity approaches for the Lipchitz nonlinear PMSM model. Where the simulation results implemented in MATLAB/SIMULINK environment were confirmed and demonstrated the feasibility and effectiveness of the proposed approach, despite of its simple implementation. Chapter 5 was concentrated on the idea of the robust extended H_∞ observer and robust H_∞ controller based on the MVT essentially, applied to the PMSM drive, through an illustrative simulation implemented in MATLAB/SIMULINK, the simulation results were

confirmed and demonstrated the effectiveness of the proposed algorithms and ensured a minimum disturbance attenuation level to the estimation error or the control error.

The work presented in the last chapter dealt with the monitoring of permanent magnet synchronous machine (PMSM) with the aim of setting up, a function dedicated to the online detection of inter-turn short-circuits in PMSM. This monitoring function must be able to integrate within existing protections and be able to determine, automatically and in real time, an indicator of the state of health of the PMSM stator that can be operated by a supervisory system.

Due to the context of use of the PMSM and the properties of the fault to be detected, strong constraints in terms of robustness are imposed in the construction of this fault indicator. Given these constraints, the detection method based on the use of the Extended MVT observer, in order to estimate in real time the parameters of a PMSM model, was chosen. Five indicators of inter-turns short-circuit fault have been developed. The first four are based on the estimation of a parameter resulting from a representation of a "healthy" PMSM in the Park referential (*w*, *Ke*, *Rs* or *1/Ls*). The fifth is constructed from the estimation of percentages of turns in short-circuit (n_{s/c_A}, n_{s/c_B} and n_{s/c_C}) on a model of a "faulty" PMSM expressed specifically for the consideration of inter-turns short-circuits.

Two robustness tests were studied in simulation on the different indicators, one by variation of frequency and the second by variation of power. On the one hand, the indicator based on the estimate of *1/Ls* was appeared to be the most sensitive for detecting resistive short-circuits of low amperage. On the other hand, the indicator based on the estimation of $n_{s/c}$ is robust to variations in the operating point and appears to be sufficiently sensitive to detect resistive short circuits. In addition, depending on the topology of the machine, it could be used to locate the faulty phase.

7.2. Perspectives

Several study perspectives can be identified following this work. The first concerns the experimental validation of all the algorithms presented in this thesis on the PMSM drive. the second, the application of the proposed approach of the control and the observation used in this thesis to other types of the electrical systems (Asynchronous machines, double fed Induction Machine, photovoltaic system,…). Also, in the short term we intend to apply the tolerant fault control based on MVT theory to the PMSM drives.

Finally, permanent magnet machines can also be the source of other types of faults that we have not considered, such as mechanical faults or those related to the demagnetization of magnets. Many works already provide some solutions to diagnose these types of faults and it would be interesting to associate several indicators to achieve information cross.

APPENDIXES

Appendix A: Park and Clarke Transformation

A.1. Clarke transformation

The purpose of this transformation is that the stator current space vector is expressed in another reference frame with two orthogonal axes. Assuming that the axis "a" and the axis "α" are in the same direction then we have the following vector diagram.

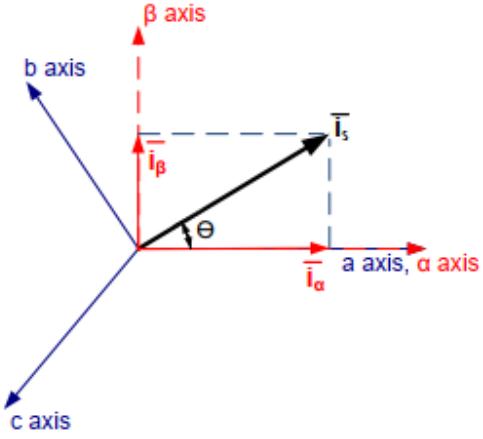

Figure A.1 Stator current representation in two co-ordinate stationary frame

The stator current space vector can be projected into two orthogonal axes. The real part of the stator current space vector is equal to the value of the direct-axis stator current component (i_α) and the imaginary part is equal to the quadrature-axis stator current component represented as (i_β) which are shown in Fig. A. 1. Then, the stator current space vector can be expressed in the reference frame as:

$$\overline{i_s} = i_\alpha + j i_\beta \tag{A-1}$$

The projection of the stator current space vector on the orthogonal α, β axes can be derived as the following:

$$i_\alpha = \left|\overline{i_s}\right| \cos(\theta) \tag{A-2}$$

$$= |k(i_a + \mathrm{a} i_b + \mathrm{a}^2 i_c)| \cos(\theta) \tag{A-3}$$

$$= k\left(i_a - i_b\cos(\frac{\pi}{3}) - i_c\cos(\frac{\pi}{3})\right) \quad \text{(A-4)}$$

Where $i_c = -i_a - i_b$ and

$$i_\alpha = k\left(\frac{3}{2}\right) i_a \quad \text{(A-5)}$$

k is the transformation constant, chosen as k = 2/3 to select $i_\alpha = i_a$

Similarly, i_β can be derived and found as the following:

$$i_\beta = \left|\overline{i_s}\right| \sin(\theta) \quad \text{(A-6)}$$

$$i_\beta = \frac{1}{\sqrt{3}} i_b - \frac{1}{\sqrt{3}} i_c \quad \text{(A-7)}$$

Then the matrix form of the stator current transformation can be written as:

$$[f_{\alpha\beta 0}] = [T_{\alpha\beta 0}][f_{abc}]$$

$$\begin{bmatrix} i_\alpha \\ i_\beta \\ i_0 \end{bmatrix} = \frac{2}{3}\begin{bmatrix} 1 & -\frac{1}{2} & -\frac{1}{2} \\ 0 & \sqrt{\frac{3}{2}} & -\sqrt{\frac{3}{2}} \\ \frac{1}{2} & \frac{1}{2} & \frac{1}{2} \end{bmatrix}\begin{bmatrix} i_a \\ i_b \\ i_c \end{bmatrix} \quad \text{(A-8)}$$

$$[T_{\alpha\beta 0}] = \begin{bmatrix} 1 & -\frac{1}{2} & -\frac{1}{2} \\ 0 & \sqrt{\frac{3}{2}} & -\sqrt{\frac{3}{2}} \\ \frac{1}{2} & \frac{1}{2} & \frac{1}{2} \end{bmatrix} \quad \text{(A-9)}$$

$[T_{\alpha\beta 0}]$ is the transformation matrix.

Zero sequence component i_0 stated in the equation (A-8) is equal to zero for balanced three phase loads. The each phase of three phase balanced stator windings is displaced with $\frac{2\pi}{3}$ radians phase shifts in space shown in Fig. A. 2(a). And its two axes equivalent has two orthogonal windings as

shown in Fig. A. 2(b). Orthogonal windings guarantee that there is no interaction between perpendicular windings.

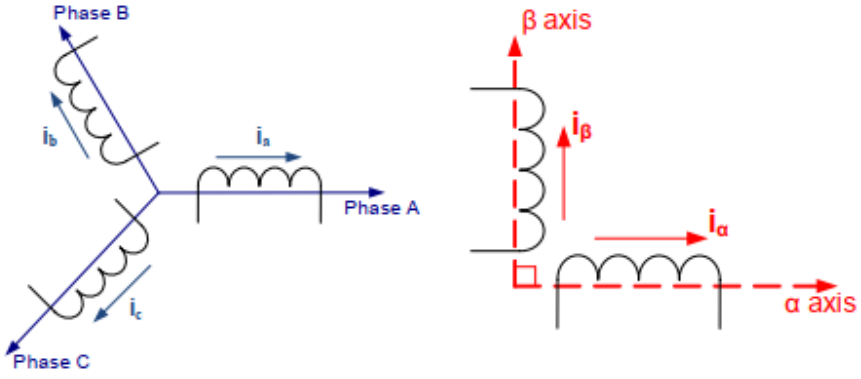

(a) (b)

Figure A.2 (a) Three-phase balanced windings and (b) its two axes equivalent

After this transformation the torque equation is still dependent on the position of the rotor flux. In order to remove the dependency, second transformation called as Park Transformation must be applied.

A.2. Park transformation

This transformation modifies the stationary two-phase orthogonal system α, β in the d, q rotating reference frame where d-axis is aligned with the rotor flux. In this frame, the torque expression is independent from the position of the rotor flux. Hence, working on this rotating reference frame makes the control easy. The next figure shows the relationship between the two reference frames.

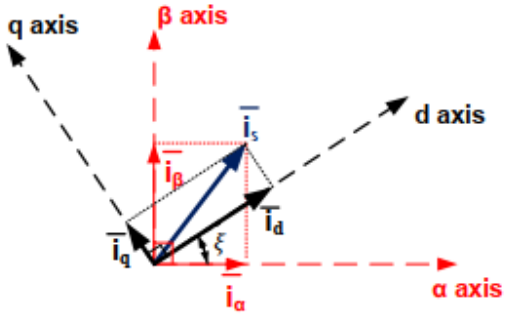

Figure A.3 d, q rotating reference frame

ξ is the instantaneous angle between the d axis and α axis.

The projection of the direct-axis stator current component (i_α) and the quadrature-axis stator current component (i_β) on the rotating d, q axes can be derived as the following:

$$i_d = i_\alpha \cos(\xi) + i_\beta \sin(\xi) \tag{A-10}$$

$$i_q = -i_\alpha \sin(\xi) + i_\beta \cos(\xi) \tag{A-11}$$

The matrix form of the Park Transformation can be written as:

$$\begin{bmatrix} i_d \\ i_q \end{bmatrix} = \begin{bmatrix} \cos(\xi) & \sin(\xi) \\ -\sin(\xi) & \cos(\xi) \end{bmatrix} \begin{bmatrix} i_\alpha \\ i_\beta \end{bmatrix} \tag{A-12}$$

Also i_d and i_q are obtained directly from i_a, i_b and i_c.

$$\begin{bmatrix} i_d \\ i_q \end{bmatrix} = \begin{bmatrix} \cos(\xi) & \sin(\xi) \\ -\sin(\xi) & \cos(\xi) \end{bmatrix} \frac{2}{3} \begin{bmatrix} 1 & -\frac{1}{2} & -\frac{1}{2} \\ 0 & \sqrt{\frac{3}{2}} & -\sqrt{\frac{3}{2}} \end{bmatrix} \begin{bmatrix} i_a \\ i_b \\ i_c \end{bmatrix} \tag{A-13}$$

$$\begin{bmatrix} i_d \\ i_q \end{bmatrix} = \frac{2}{3} \begin{bmatrix} \cos(\xi) & \cos(\xi - \frac{2\pi}{3}) & \cos(\xi + \frac{2\pi}{3}) \\ -\sin(\xi) & -\sin(\xi - \frac{2\pi}{3}) & -\sin(\xi + \frac{2\pi}{3}) \end{bmatrix} \begin{bmatrix} i_a \\ i_b \\ i_c \end{bmatrix} \tag{A-14}$$

And inverse park transformation has the following equations:

$$\begin{bmatrix} i_\alpha \\ i_\beta \end{bmatrix} = \begin{bmatrix} \cos(\xi) & -\sin(\xi) \\ \sin(\xi) & \cos(\xi) \end{bmatrix} \begin{bmatrix} i_d \\ i_q \end{bmatrix} \tag{A-15}$$

Appendix B: Evaluation of Indicators

The results presented in this Appendix are complements to the robustness of the indicators presented in section 4.3.1. For each indicator developed, the curves of the two tests simulated for the evaluation of the robustness of the indicator (frequency variation, power variation).

B.1. Indicator based on the estimation of *w*

❖ **Variation of frequency**

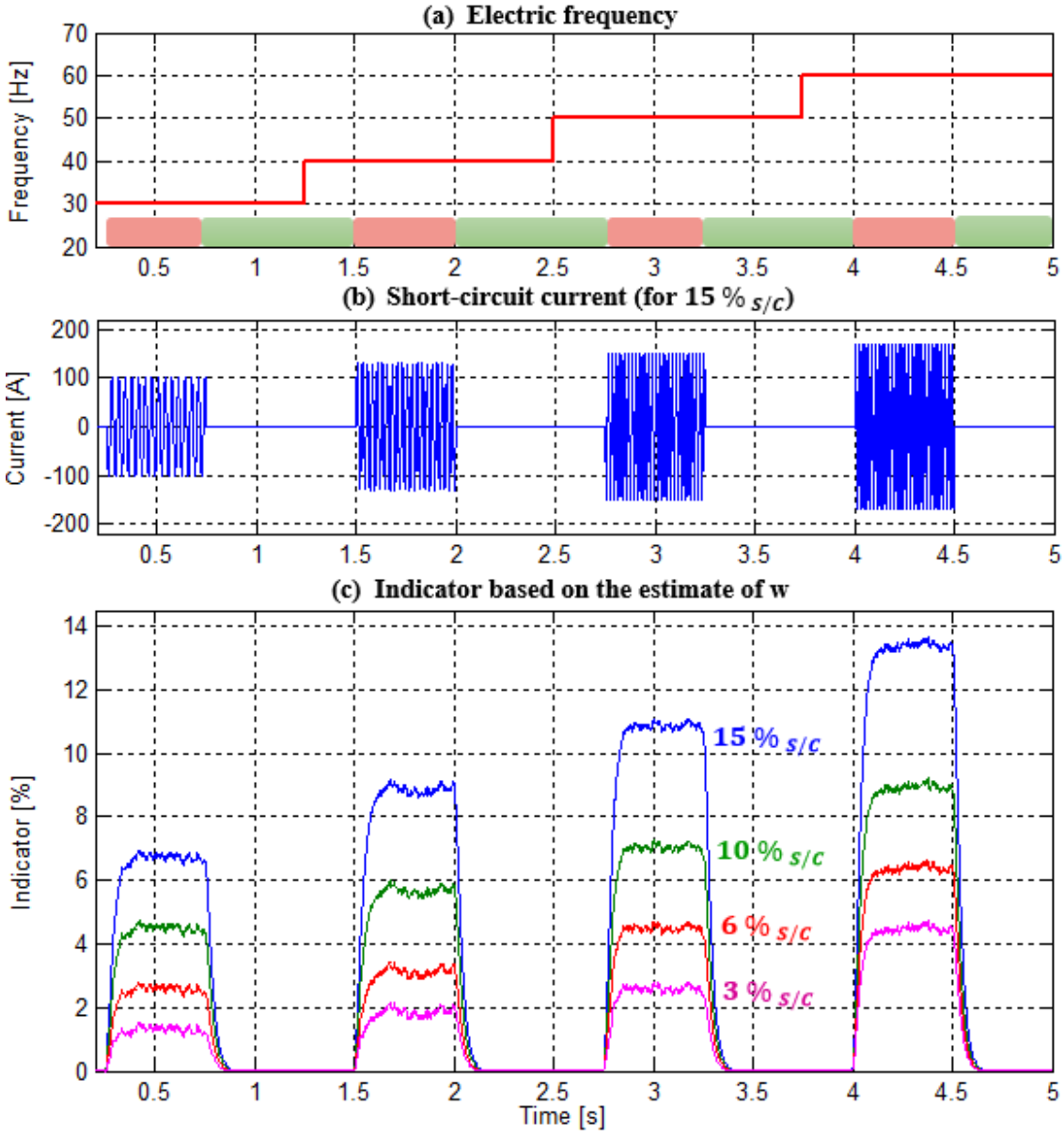

Figure B.1 Response of the indicator based on the estimation of ***w*** for different frequency

❖ **Variation of power**

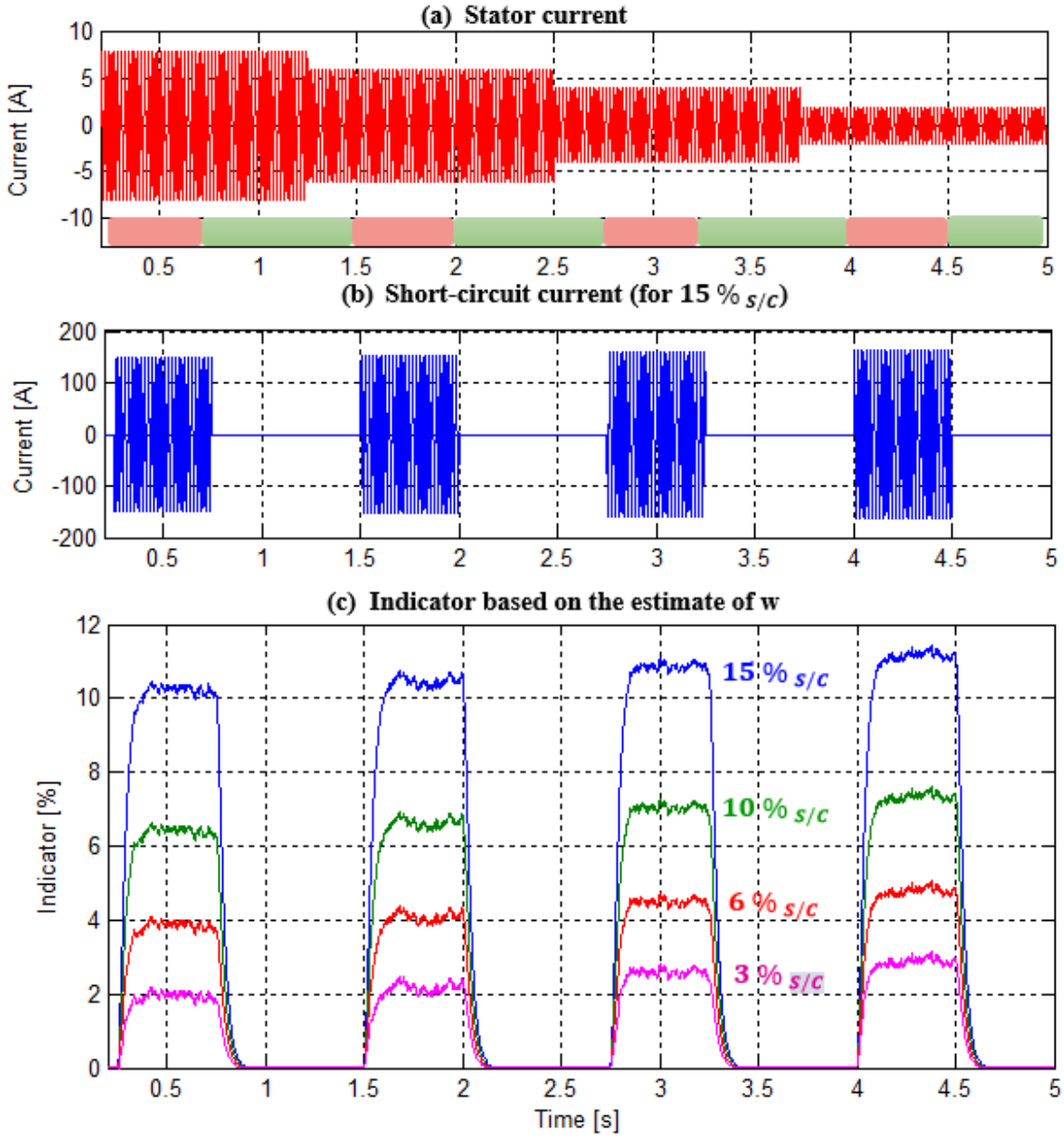

Figure B.2 Response of the indicator based on the estimation of ***w*** for different power

B.2. Indicator based on the estimation of *Ke*

❖ **Variation of frequency**

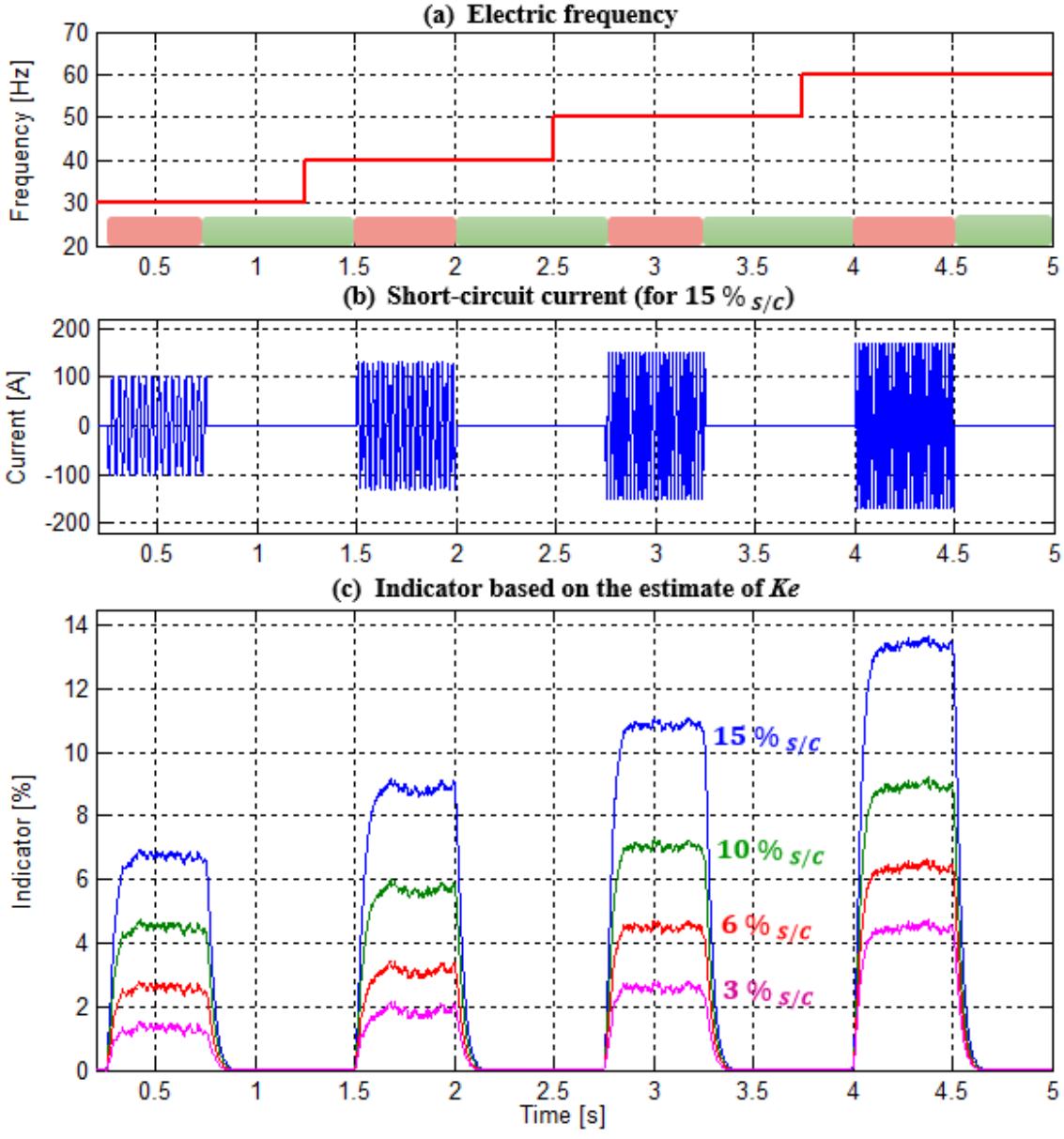

Figure B.3 Response of the indicator based on the estimation of ***Ke*** for different frequency

❖ **Variation of power**

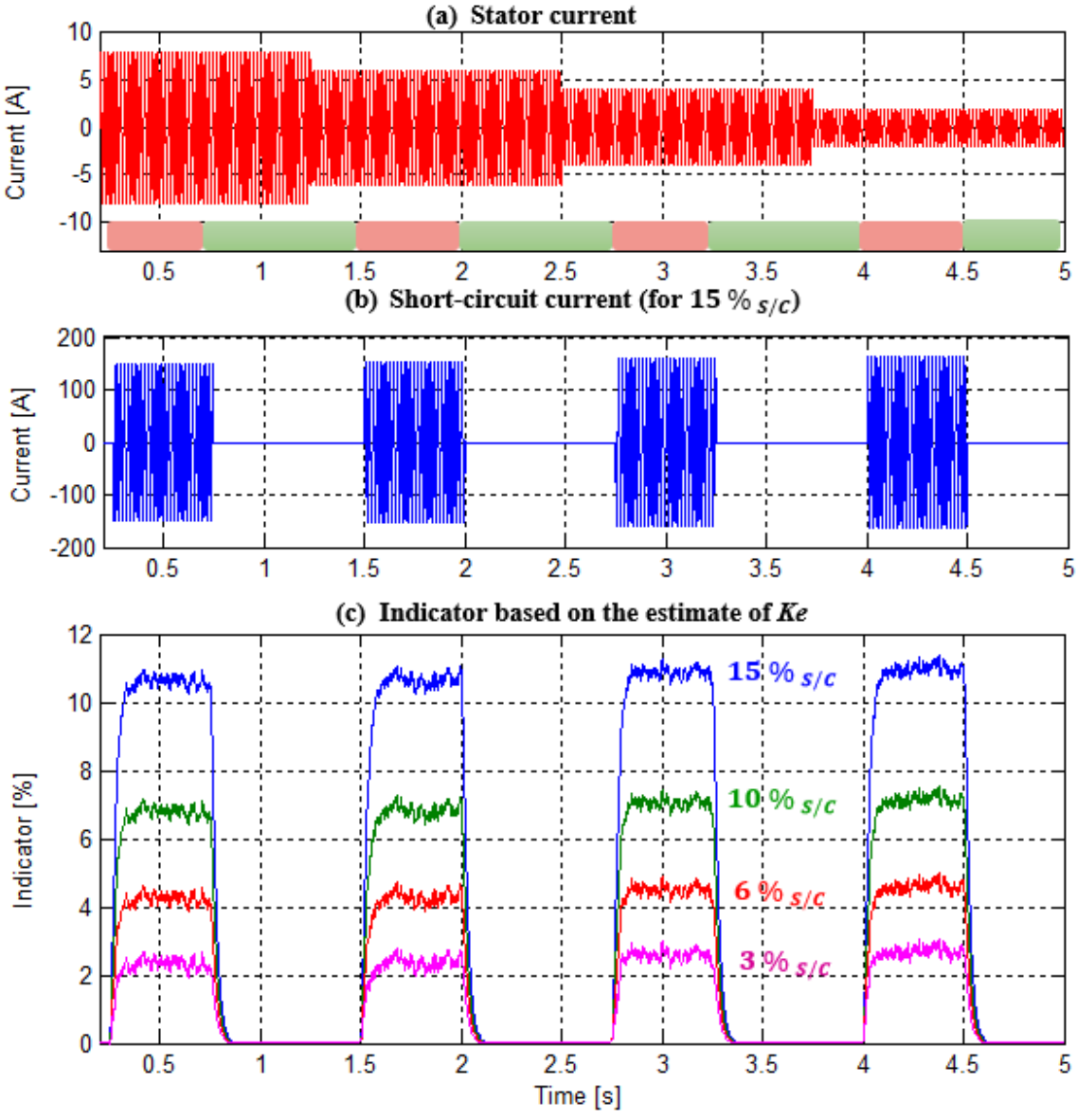

Figure B.4 Response of the indicator based on the estimation of ***Ke*** for different power

B.3. Indicator based on the estimation of *Rs*

❖ **Variation of frequency**

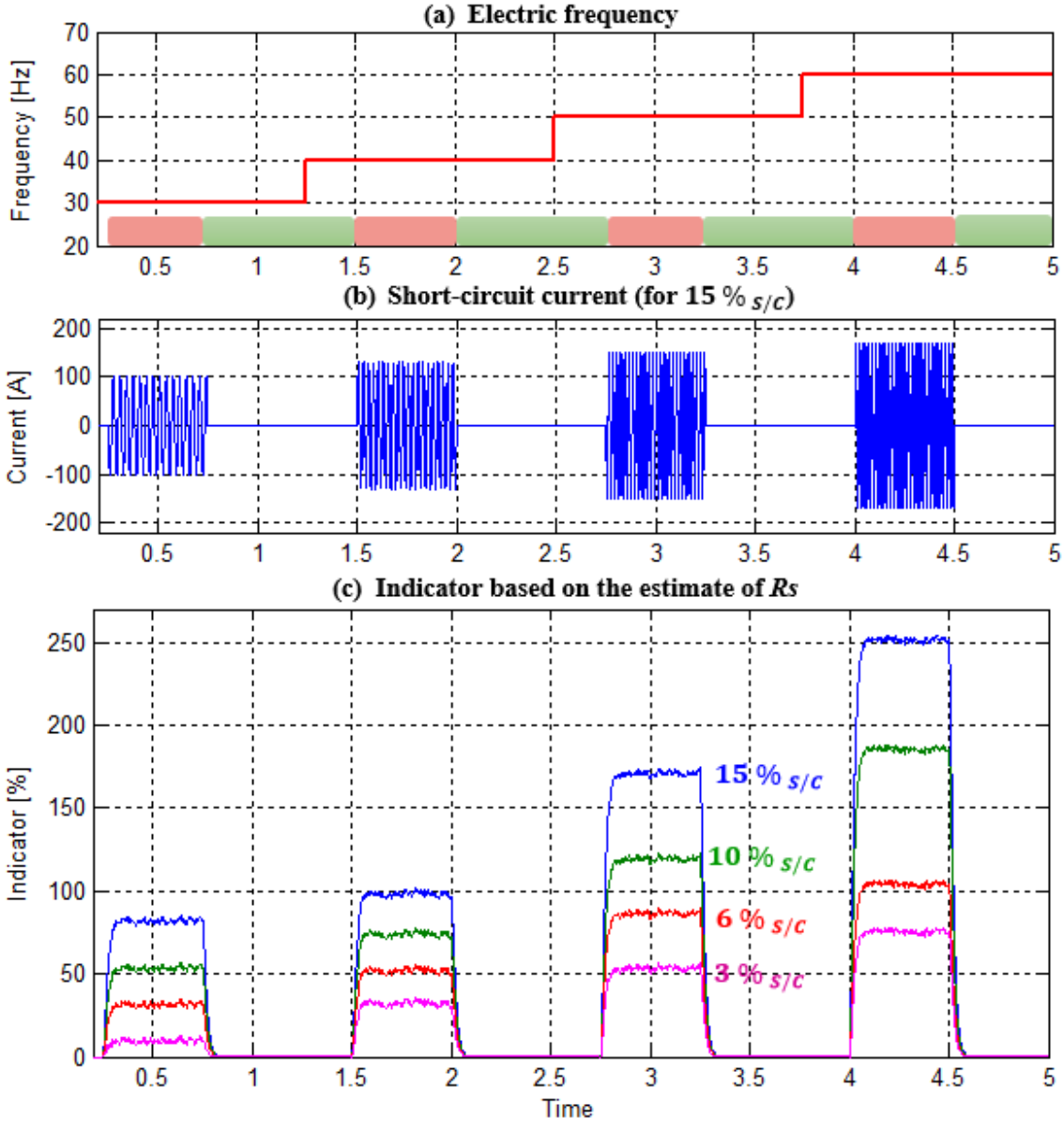

Figure B.5 Response of the indicator based on the estimation of ***Rs*** for different frequency

❖ **Variation of power**

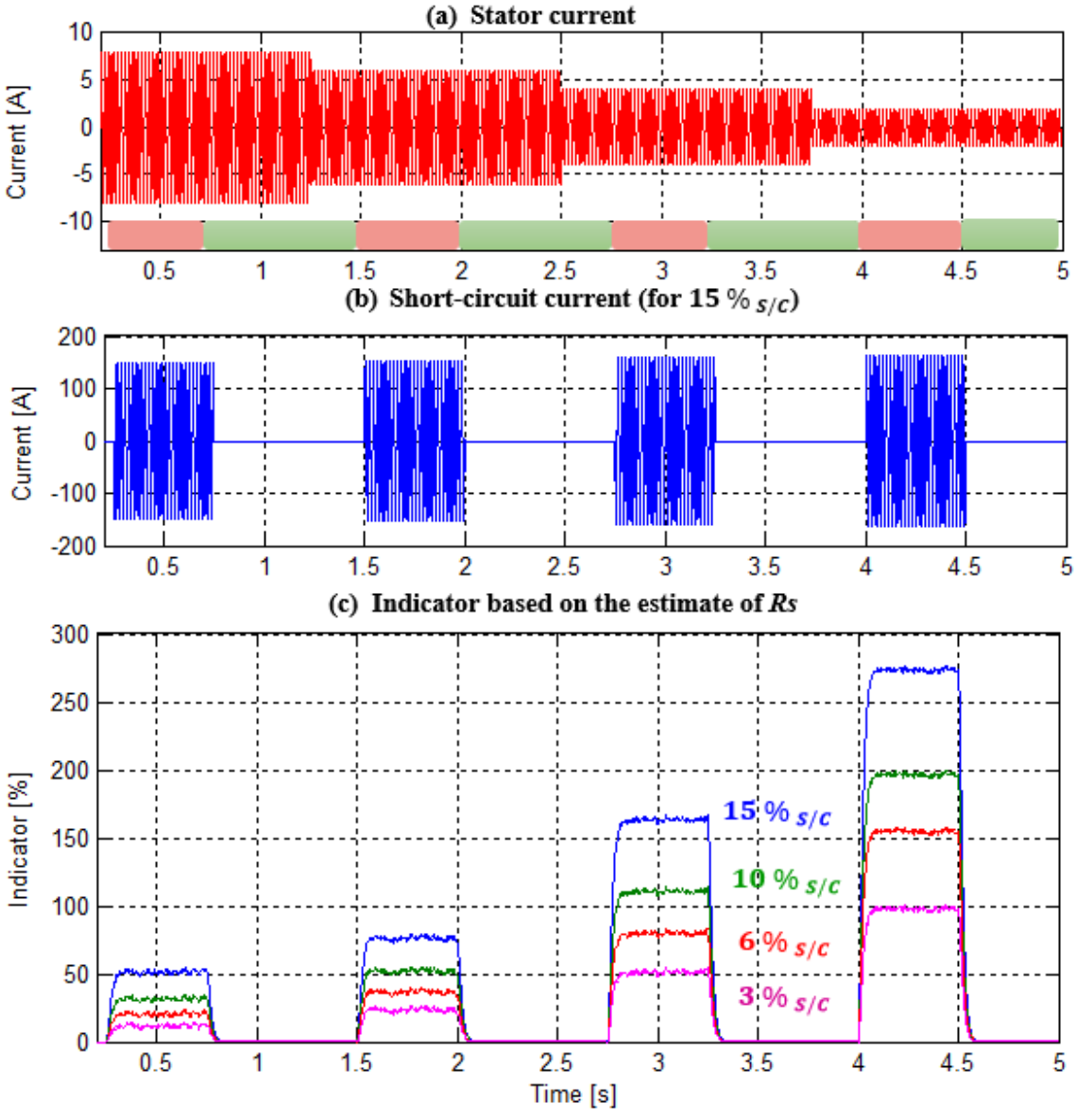

Figure B.6 Response of the indicator based on the estimation of ***Rs*** for different power

B.4. Indicator based on the estimation of *1/Ls*

❖ **Variation of frequency**

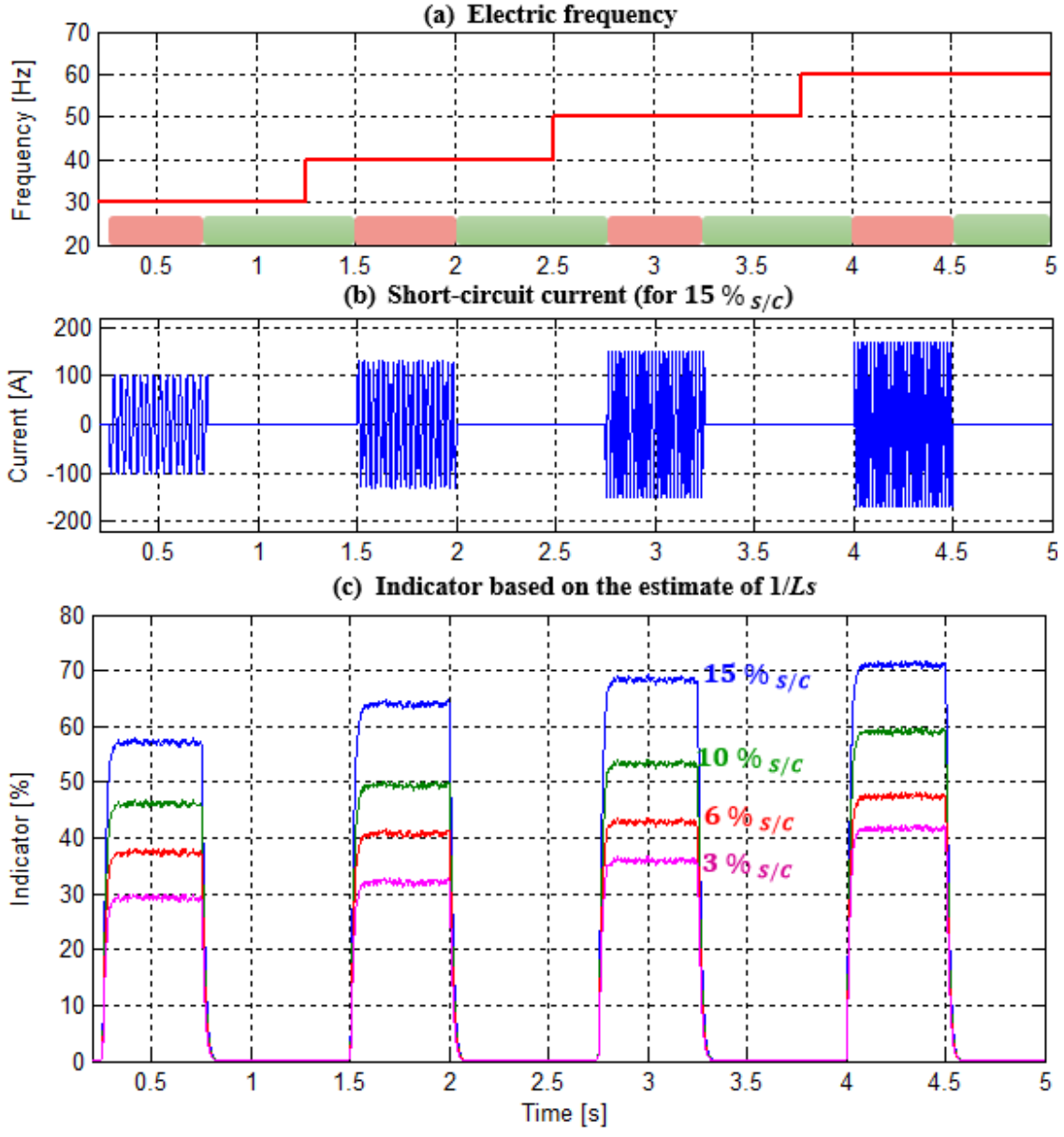

Figure B.7 Response of the indicator based on the estimation of ***1/Ls*** for different frequency

❖ **Variation of power**

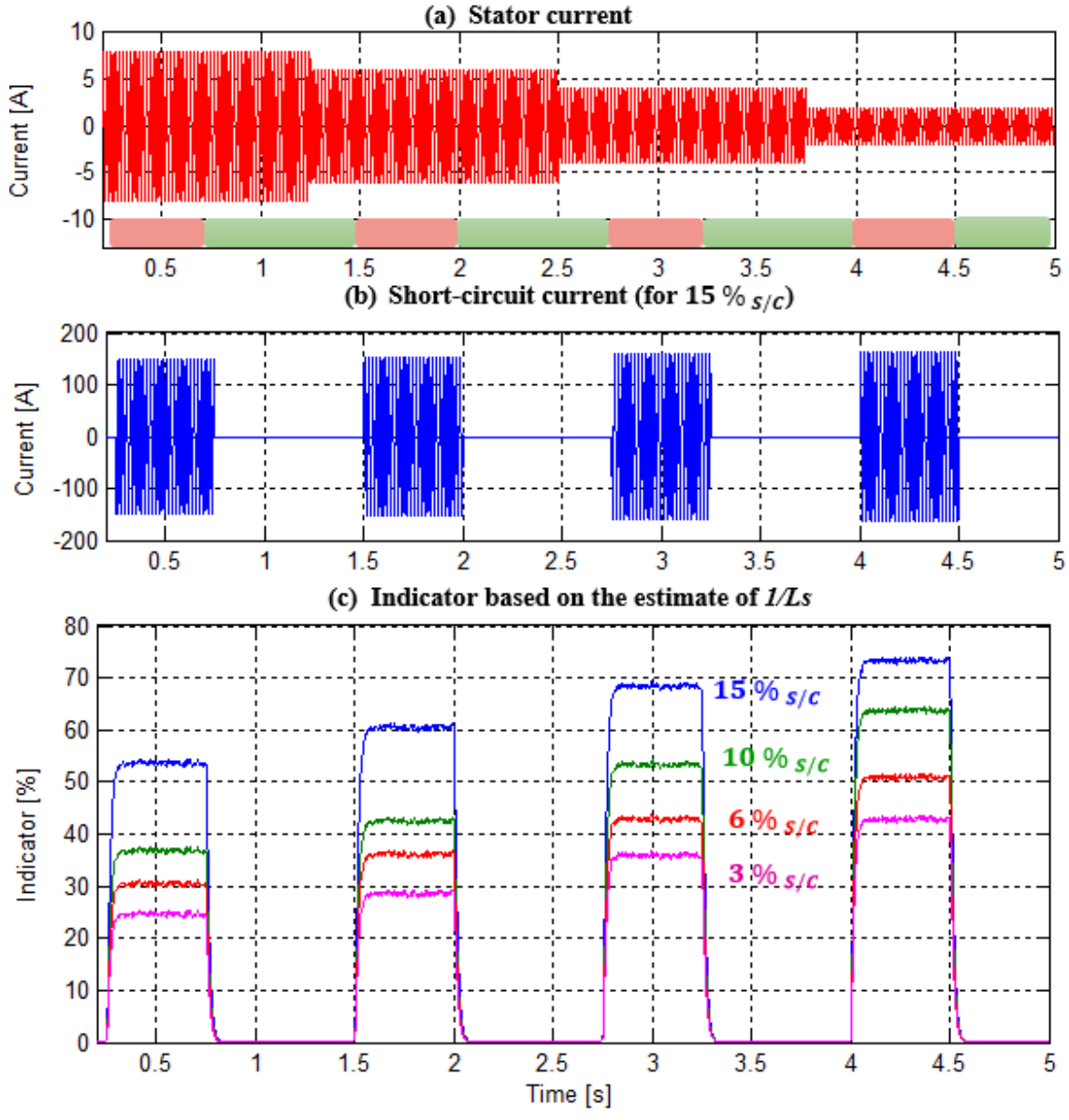

Figure B.8 Response of the indicator based on the estimation of ***1/Ls*** for different power

B.5. Indicator based on the estimation of $n_{s/c}$

❖ **Variation of frequency**

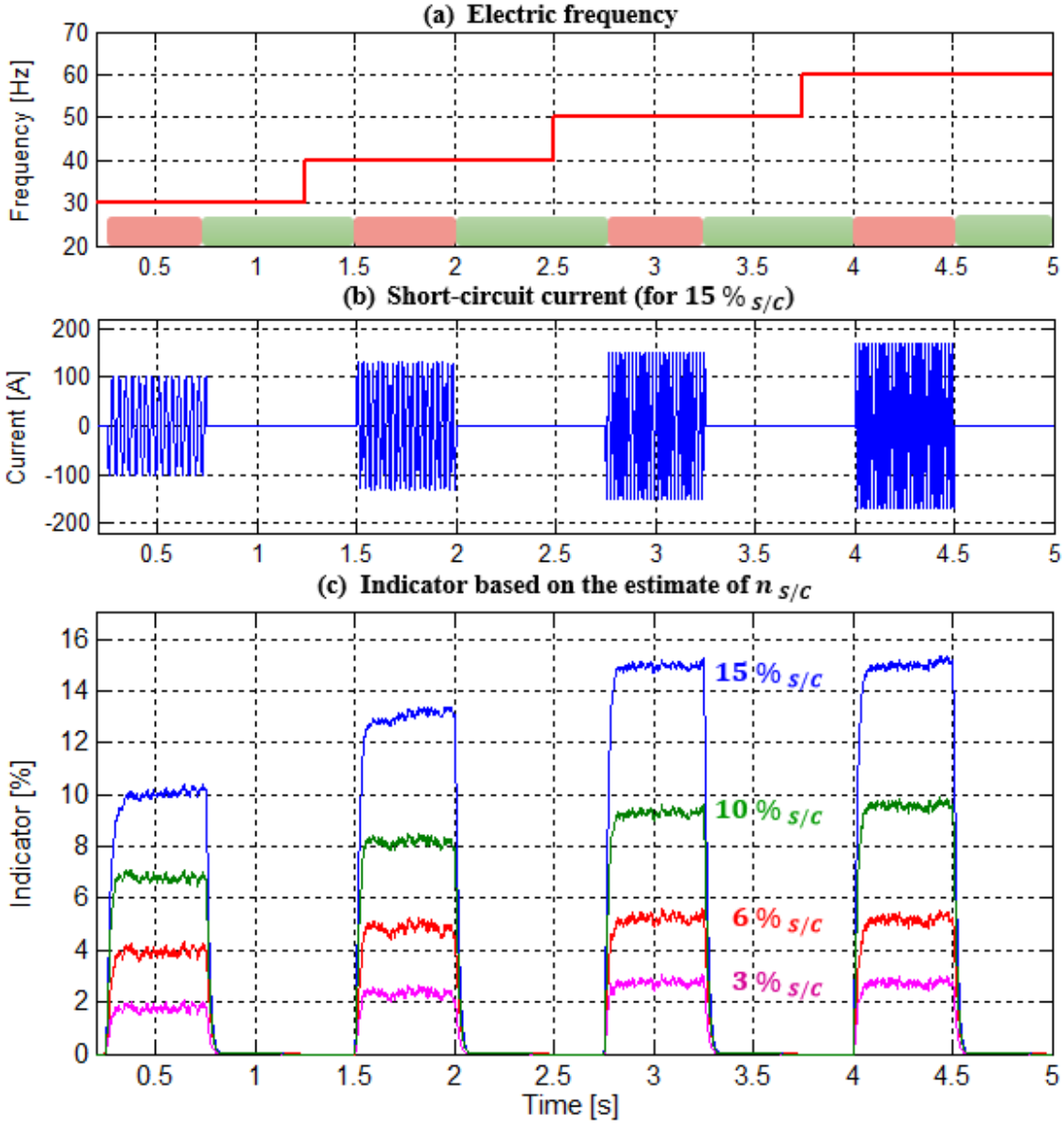

Figure B.9 Response of the indicator based on the estimation of $n_{s/c}$ for different frequency

❖ **Variation of power**

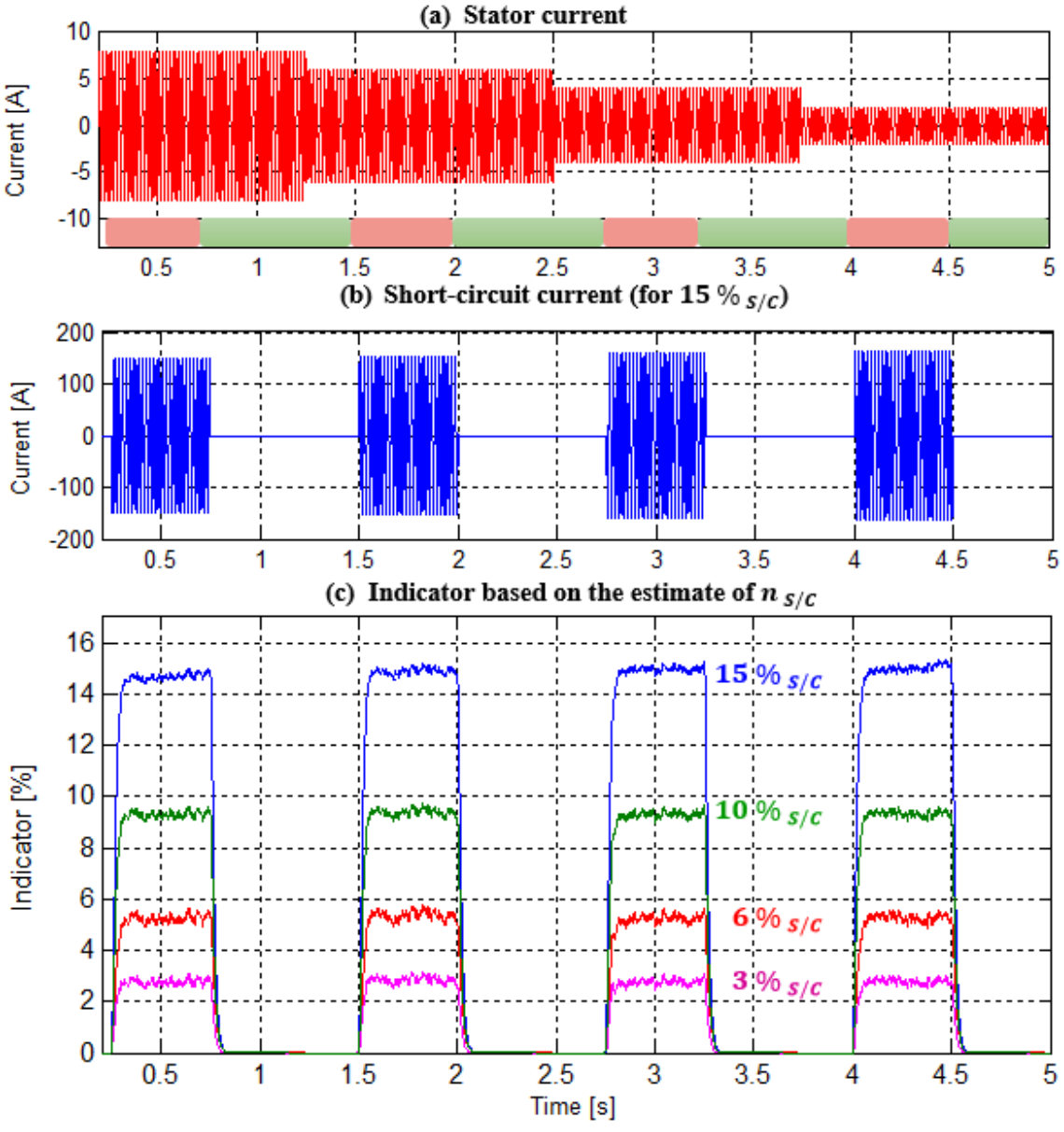

Figure B.10 Response of the indicator based on the estimation of $n_{s/c}$ for different power

Appendix C: The PMSM Parameters

❖ Used in the simulations results

Parameter	*Symbol*	*Value*	*Unit*
Stator Resistance	R_s	4.55	*Ohm*
Stator Inductance	L_s	0.0116	*Henry*
Moment of inertia	J	$6.36 * 10^{-4}$	$Kg.m^2$
Permanent Magnets Flux	Φ_f	0.317	*Wb*
Friction Factor	f	0.00611	*Nm/Rad/s*
Pole Pair	p	2	/
Power	P_n	1.1	*Kw*

❖ Used in the experimental results

Parameter	*Symbol*	*Value*	*Unit*
Stator Resistance	R_s	4	*Ohm*
Stator Inductance	L_s	0.043	*Henry*
Moment of inertia	J	$5 * 10^{-4}$	$Kg.m^2$
Permanent Magnets Flux	Φ_f	0.274	*Wb*
Friction Factor	f	$8 * 10^{-5}$	*Nm/Rad/s*
Pole Pair	p	2	/
Power	P_n	0.415	*Kw*